

UNIVERSITY OF TURIN

Ph.D. School in life and Health Sciences

Molecular Medicine

XXXII Cycle

Academic Years: 2016-2020



Patient Derived Models Prove the Actionability of PIK3R1^{W624R} Mutation in High Grade Serous Ovarian Carcinoma

Tutor

Prof.ssa Maria Flavia Di Renzo

Candidata

Concetta D'Ambrosio

Coordinatore

Prof. Francesco Novelli

*“The future belongs to those who believe
in the beauty of their dreams”*

(Eleanor Roosevelt)

TABLE OF CONTENTS

• LIST OF ABBREVIATIONS.....	5
• ABSTRACT.....	6
• GRAPHICAL ABSTRACT.....	7
• 1. INTRODUCTION.....	8
- 1.1 Ovarian Cancer	8
- 1.2 High Grade Serous Ovarian Cancer (HGS-EOC)	11
- 1.3 Ovarian Cancer Therapeutic Strategies	14
- 1.4 Ovarian Cancer Models	19
- 1.5 PIK3R1 as an Actionable Target in Cancer	22
• 2. AIM OF THE WORK.....	30
• 3. MATERIALS & METHODS.....	32
- 3.1 Cell Lines	32
- 3.2 Patient Derived Xenografts (PDXs) Platform and Mice Treatment	32
- 3.3 Immunohistochemistry	34
- 3.4 PDX Derived Tumor Cells (PDTCs) Culture Derivation	36
- 3.5 PDTCs Quality Assessment and Viability Assays	37
- 3.5.1 CellTiter-Glo® Viability Assays	38
- 3.5.2 Crystal Violet Cytotoxic/ Cytostatic Assays	38
- 3.5.3 Tumorigenicity Assessment	39
- 3.6 Western Blot Analysis	39
- 3.7 Crystal Structure Analysis	40
- 3.8 WES and CAN Analysis	40
- 3.9 Pyrosequencing Analysis	41
• 4. RESULTS	43
- 4.1 Characterization of PDX Lines from HGS-EOCs	43
- 4.2 WES and CNAs Analyses of Selected PDX Lines	49
- 4.3 Identification of Possible Driver and Actionable Mutations	53
- 4.4 Study of PIK3R1 ^{W624R} Mutation Outcome: Structure-based Approach	56
- 4.5 PIK3R1 ^{W624R} Results in the Activation of the PI3K Pathway	58

- 4.6 PIK3R1 ^{W624R} is a Trunk Mutation in the #475 PDX Line and in the ST	59
- 4.7 <i>Ex Vivo</i> Assays of PIK3R1 ^{W624R} as a Driver and Actionable Mutation	62
- 4.7.1 Establishment and Quality Assessment of PDTCs as Ex Vivo Model	
Part 1: Carboplatin Sensitivity	62
- 4.7.2 Establishment and Quality Assessment of PDTCs as Ex Vivo Model	
Part 2: Tumorigenicity of PDTCs	65
- 4.7.3 <i>Ex Vivo</i> Assays of PI3K Pathway Inhibitors on #475 PDTCs	65
- 4.7.4 CellTiter-Glo® Viability Assays of PI3K Pathway Inhibitors	
on #475 PDTCs	67
- 4.7.5 Crystal Violet Cytotoxic/ Cytostatic Assays of PI3K Pathway	
Inhibitor on #475 PDTCs	72
- 4.8 <i>In Vivo</i> Assays of PIK3R1 ^{W624R} Actionability	74
• 5. DISCUSSION	79
• REFERENCES	83
• ACKNOWLEDGMENTS	97

LIST OF ABBREVIATIONS

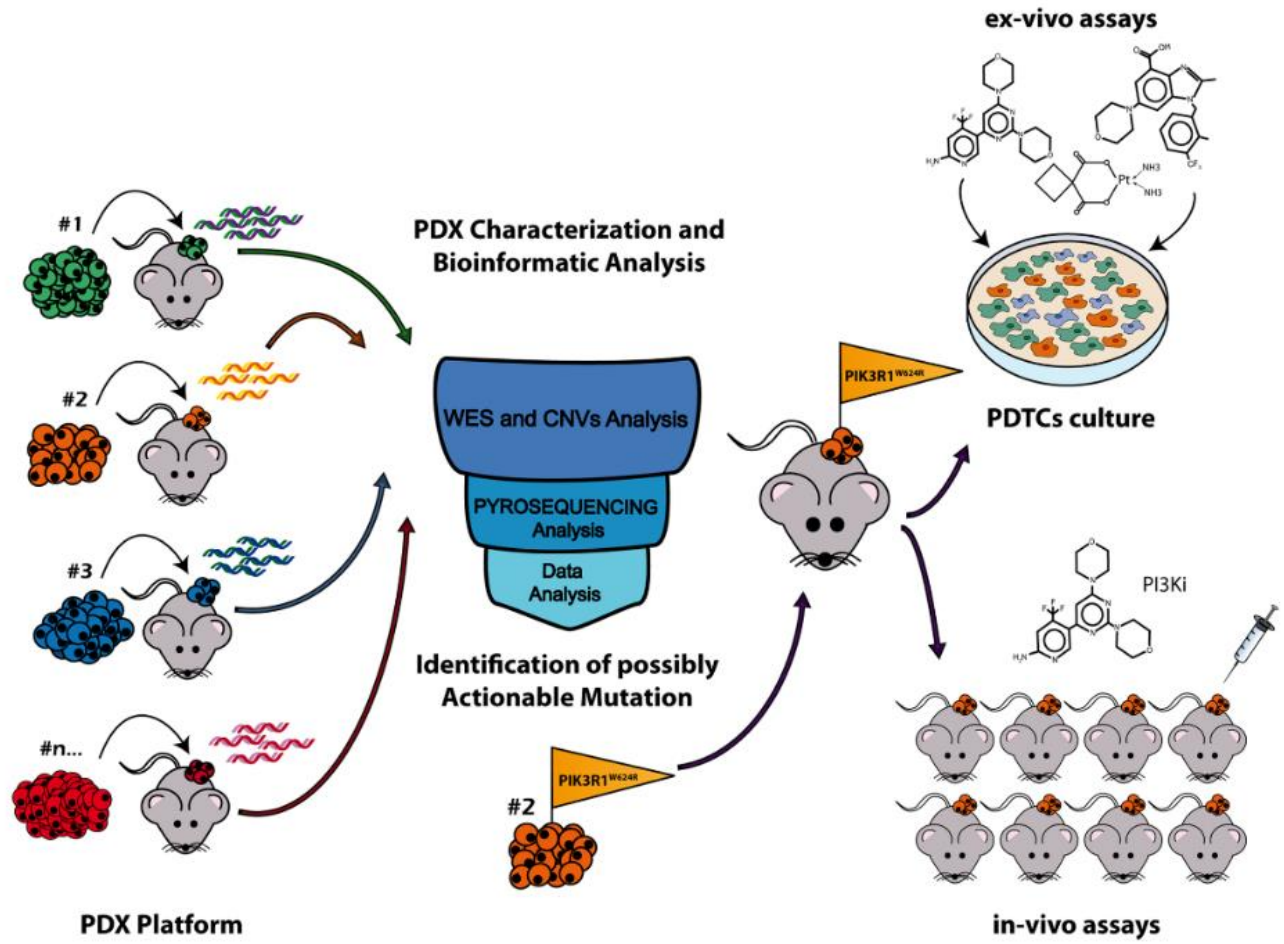
AF: Allele Frequency	PDTCs: PDX-Derived Tumor Cells
ATP: Adenosine Triphosphate	PDTOs: Patient-Derived Tumor Organoids
BERs: Base Excision Repair	PDXs: Patient-Derived Xenografts
BRCA: Breast Related Cancer Antigen	PFI: Platinum-Free Interval
CICs: Cortical Inclusion Cysts	PFS: Progression-Free Survival
CK7: Cytokeratin 7	PI3K: Phosphatidylinositol 3-Kinase
CNAs: Copy Number Alterations	PI3Ki: PI3K inhibitor
COSMIC: Catalogue of Somatic Mutations in Cancer	PROS: <i>PIK3CA</i> -Related Overgrowth Spectrum
DNA: Deoxyribonucleic Acid	RD: Residual Disease
DSBs: Double Strand Breaks	RTKs: Tyrosine Kinases Receptors
EMA: European Medicine Agency	SC: Subcutaneously
EOC: Epithelial Ovarian Cancer	SET: Solid pseudo-Endometrioid and/or Transitional carcinomas
FBS: Foetal Bovine Serum	SNVs: Single Nucleotide Variants
FDA: Food and Drug Administration	SSBs: Single Strand Breaks
GPCRs: G Protein-Coupled Receptors	ST: Source of Tumor
GR: Growth Rate	STICs: Serous Tubal Intraepithelial Carcinomas
HE: Haematoxylin and Eosin	TCGA: The Cancer Genome Atlas
HGS-EOC: High Grade Serous- Epithelial Ovarian Cancer	TMA: Tissue Macro Array
HR: Homologous Recombination	T-NGS: Targeted Next Generation Sequencing
IHC: Immunohistochemistry	TP53: Tumor Protein 53
IP: Intra-Peritoneum	WB: Western Blot
LOH: Loss of Heterozygosity	WES: Whole Exome Sequence
NA-CHT: Neoadjuvant-Chemotherapy	WHO: World Health Organization
NSCLC: Non-Small Cell Lung Carcinoma	WT1: Wilms' Tumor protein
OC: Ovarian Cancer	
OS: Overall Survival	
OSE: Ovary Surface Epithelium	
PAF: Paraformaldehyde	
PARP: Poly(ADP-Ribose) Polymerase	
PARPi: PARP Inhibitors	
PAX8: Paired-box gene 8	
PDASs: Patient-Derived Ascitic Spheroids	
PDMs: Patient-Derived Models	

ABSTRACT

Patients with epithelial ovarian cancer (EOC) have experienced little improvement in overall survival, despite short term good response to standard treatments. The development of target therapies did not revolutionize EOC treatment, as only targeted anti-PARP1 therapies has shown effectiveness in EOC subgroups ¹⁻³. Genomic analysis of EOC samples have demonstrated a profound genetic instability with a great number of copy number alterations (CNAs) ^{4,5}. Conversely, EOC is characterized ⁴ by few recurrent mutations and the so-called “long tail” distribution of low-frequency mutations in cancer-related genes. The role of these infrequent mutations in EOC is still unclear and needs to be investigated ^{1,6}.

In order to validate low frequency mutations as biomarkers for target therapy, we used patient derived models. We have developed a patient-derived xenograft (PDX) platform collecting and implanting EOCs samples in NOD/shi-scid/IL-2R γ null mice and from a number of PDX lines we derived short term cultures (PDX Derived Tumor Cells, PDTCs). All PDX lines were characterized using targeted NGS and immunohistochemistry. Subsequently WES and CNA analyses were performed on 12 PDX lines derived from naïve high-grade serous (HGS)-EOCs, which are the most frequent and lethal EOCs. Using bioinformatics tools, we found a possible driver mutation in the *PIK3R1* gene in one line (#475), which resulted in activation of the PI3K pathway. *PIK3R1*^{W624R} had an allele frequency in both passages PDX and the source tumor that suggested its possible role as a trunk mutation. The functional relevance of this mutation was investigated using PDTCs for *ex-vivo* drugs screening of a number of inhibitors of the PI3K/AKT/mTOR pathway. Once tested on PDTc lines, the most promising drug was tested *in vivo* in the #475 PDX line. Data demonstrated that Patient Derived models are invaluable tools to unveil actionable pathways for the treatment of advanced/metastatic HGS-EOC.

GRAPHICAL ABSTRACT



1. INTRODUCTION

1.1 Ovarian Cancer

Ovarian cancer (OC) is the seventh most commonly diagnosed cancer among women in the world and the fourth commonest cause of gynecological cancer-associated death^{7,8}. Among the risk factors related with the occurrence of OC there are ageing, with a peak around 50-60 year, and numbers of ovulations, whereas parity reduces risk⁹.

The main cause of the OC high mortality is delayed diagnosis: approximately 70% of cases are diagnosed at advanced stage, when cancer has invaded tissues beyond ovaries and the peritoneal cavity^{10,11}.

Almost the totality of both benign and malignant ovarian neoplasms derive from one of the three main cell subtypes in ovaries: Germ cells 2-3%, Specialized gonadal stromal cells 5-6% and Epithelial cells 90%^{12,13}.

Epithelial ovarian cancer (EOC) is the most common and the most lethal ovarian cancer type. It is a heterogeneous disease with five major histologic subtypes: serous (60-70%), endometrioid (10-20%), mucinous (5-20%), clear cells (3-10%) and undifferentiated (1%), which differ for cell of origins, clinic-pathologic features, treatment response and genetic- molecular characteristics^{7,14}.

Historically, pathologists classified ovarian cancers based on microscopic aspects, assuming that all epithelial ovarian carcinomas developed from the ovarian surface epithelium: primarily because the bigger masses were often found in the ovaries and secondly because precursor lesions were scarce and hard to identify^{15,16}. The comprehension of the dynamics of pathogenesis has a great importance in the era of personalized medicine in order to find the best fitting therapeutic approach. This explains why lot of efforts have been made in the study of ovarian carcinogenesis by clinicians and researchers.

In the last two decades, the introduction of molecular biology and new methodologies for tissue sampling revolutionized the EOC knowledge, especially regarding tumor onset.

In 2004 Kurman and Shih in order to better classify and understand the pathogenesis of EOC proposed the “Dualistic model of ovarian carcinogenesis” [4]. This model has been supported by several studies ¹⁸⁻²⁷. In particular, the “Dualistic model” aims at: 1) unraveling of the molecular genetic pathways involved in the pathogenesis of primary ovarian carcinoma; 2) finding a correlation between these pathways and the histopathologic classification. Following this model, the diverse types of EOC should not be classified only for their morphology but also for their molecular and genetic characteristics ^{14,28}.

In 2014 the World Health Organization (WHO) recognized the “Dualistic model” and updated the histopathologic classification of ovarian tumors, highlighting specific characteristics for each subtype ²⁹. Therefore, based on histopathology and molecular-genetic alterations, EOC is currently regarded as a disease composed by the aforementioned five histologic subtypes, which are in turn divided in two broad categories: type I and type II. The main difference between the two types is the striking genetic instability of type II EOC compared to type I. Type I tumors include clear cell carcinomas, low grade endometrioid, low grade serous, mucinous carcinomas and Brenner tumors. At diagnosis, these tumors may be large, but generally unilateral, indolent and confined in the ovary. Type II ovarian cancers include high grade serous carcinoma, malignant mixed mesodermal tumors (carcinosarcomas) and undifferentiated carcinomas. Their behavior is aggressive with a rapid progression and high invasiveness. At diagnosis, type II EOCs are generally in late stage, frequently involve both ovaries and as a consequence are associated with a low survival rate. Women with type II tumors often have also an extensive extra-ovarian disease with ascites and metastasis derived from dissemination of tumor cells into the peritoneum. From a genetic point of view, in addition to the previously mentioned genetic instability, the majority of these tumors are characterized by the inactivation of TP53 ^{12,14,17}. Both Type I and Type II have been proposed to have an extra-ovarian origin. In particular, clear cell and mucinous EOC are supposed to derive

from an endometrial stem cell, and likely associated to endometriosis; high-grade serous carcinomas are thought to originate from fallopian tube epithelium ^{12,15,17,18,30} (Fig 1.1).

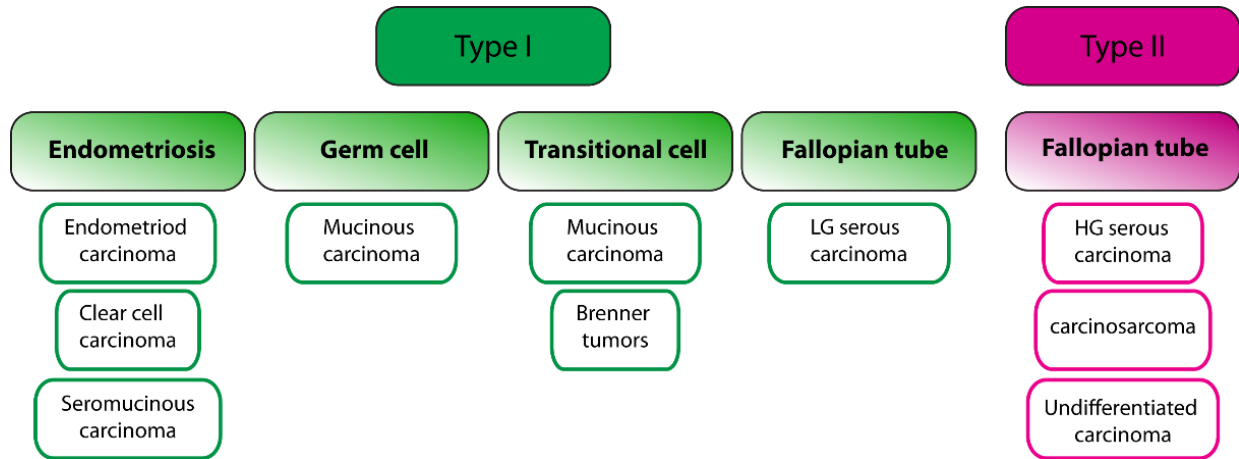


Fig1.1: Dualistic model for epithelial ovarian cancers. Adapted from: Kurman R.J. and Shih I. 2016 ¹⁷

In addition to the TP53 mutations, in type II tumors germline or somatic molecular alterations in *BRCA1/2* genes are quite common, with a reported occurrence of 20-40% in HGS-EOCs ^{12,14}. Indeed, among the several risk factors for ovarian cancer -such as: diet, parity and lactation- the strongest one is a family history of breast or ovarian cancer and the presence of germline mutations in *BRCA1* and *BRCA2*. The latter expose women to a lifetime risk of 30-50% to develop OC ^{14,31,32}. *BRCA1/2* are both tumor suppressor genes encoding for proteins involved in the homologous recombination (HR) process ³¹. Inactivation of *BRCA1/2* genes usually occurs by mutations in the gene sequence or by promoter methylation ¹. The development of genetic screening methods is providing important tools to anticipate the diagnosis in high risk individuals. Currently, the possibility to detect somatic or germline alterations in *BRCA1/2* genes in ovarian or breast cancer has proven to be effective not only in primary (healthy lifestyle) and secondary (early diagnosis) prevention of ovarian cancer, but also to apply molecular targeted therapies (see below) ^{1,2}.

1.2 High Grade Serous Ovarian Cancer (HGS-EOC)

Among the epithelial ovarian cancer subtypes, high grade serous carcinoma (HGS-EOC) is the most common, accounting roughly for 60-70% of EOC cases [7]. This tumor type is mostly associated with a bad prognosis due to its high aggressiveness and relapse after treatment, with a 5-year survival rate of about 30-40% ^{2,12,29}. The main cause of the high lethality is the diagnosis at late stage when tumor has already spread in peritoneal cavity. Indeed, the disease diagnosed at early stages, when it is only locally spread, has a 5-year relative survival rate of 93% ^{3,12}.

From a morphological point of view, H&E staining of HGS-EOC tissue sections shows solid masses of cells with slit-like fenestrations; tumor cells have an intermediate size, hyperchromatic and pleomorphic giant nuclei and prominent eosinophilic nucleoli ^{1,17,29,30}. After Ki67 staining, these cells usually show a high mitotic index with many and partly atypical mitoses ²⁹.

Besides genetic alterations, a panel of markers are used in immunohistochemistry to distinguish HGS-EOC from other ovarian cancer subtypes ^{14,16,17}, as follows:

- P53, that is encoded by the *TP53* tumor suppressor gene involved in cell cycle progression and proliferation. About 96% of HGS-EOCs carry *TP53* mutation. Nearly all HGS-EOC cells have a strong positive staining for p53 protein due to gene missense mutations. Indeed, most mutations cause the production of an aberrant protein which is not recognized by the proteasome and accumulates in cells ^{1,2,17,29}. The occurrence of nonsense mutations in *TP53* sequence has also been reported in cases where protein staining in tumors is almost totally negative ¹⁷. Since *TP53* inactivation occurs in the majority of HGS-EOCs it could be one of the earliest event in carcinogenesis, suggesting that *TP53* disruption could play the role of a trunk mutation in HGS-EOC ^{1,33,34}.

- Wilms' tumor protein (WT1) is a transcription factor involved in the development of urogenital system. It has been reported that WT1 is overexpressed in several malignancies such as breast and ovarian cancers ^{17,30,35-37}.
- Cytokeratin 7 (CK7) is an epithelial marker, which is expressed in healthy and tumor cells of epithelial origin ³⁸.
- Paired-box gene 8 (PAX8) is a member of the PAX family of transcription factors. PAX8 is involved in the embryological development of several tissues such as the Müllerian systems, but more interestingly it is implicated in the regulation of WT1 expression. In ovarian cancer and in others cells of Müllerian origin, PAX8 is expressed at high level ^{39,40}.
- P16 is a protein encoded by the *CDKN2A* tumor suppressor gene. The p16 protein performs an important role in cell cycle regulation by decelerating cell progression from G1 to S phase. Approximately 60%–80% of HGS-EOCs show diffuse p16 staining ⁴¹⁻⁴⁴.
- P63 is a p53 homologue gene, encoding different transcripts that may display diverse effects on p53 activation and apoptosis. Some studies have shown that p63 expression may occur in serous carcinomas of the ovary bound to undergo malignant progression ^{45,46}.

Mutations in Breast Related Cancer Antigens 1/2 (*BRCA1/2*) genes, as previously described, are used as genetic HGS-EOC markers. The IHC detection of the loss of either protein has given conflicting results and is not routinely assayed ⁴⁷. The majority of HGS-EOCs phenotypically resemble the architecture of fallopian tubes epithelium surface. However, there are some rare cases that morphologically relate with other EOCs subtypes. Albeit the expression markers of these HGS-EOCs are comparable to that of “classic” HGS-EOCs, phenotypically they display many areas with the aspect of endometrioid or transitional cell carcinomas ^{1,29,48}. The phenotypical differences of this subset of HGS-EOCs arose many perplexities about the origin of high grade serous carcinomas. In order to highlight the differences between the two HGS-

EOC types, researchers refer to this alternative kind of HGS-EOCs as “SET”: solid pseudo-endometrioid and/or transitional carcinomas ^{1,2,22}.

As already mentioned, in the past the ovary surface epithelium (OSE) was regarded as the tissue precursor of all epithelial ovarian tumors. It was speculated that the constant cycle of repairs and regenerations of OSE, as a result of ovulation, was at the base of HGS-EOCs onset. The ovulatory process creates invaginations in OSE, forming cortical inclusion cysts (CICs). According to this hypothesis in the pro-inflammatory and pro-oxidative environment of ovaries, CICs could act as precancerous lesions ⁴⁹. Two decades ago, Piek and coworkers described the presence of small areas of dysplastic lesions in distal fallopian tubes of women with *BRCA1* or *BRCA2* mutations ¹⁹. This evidence laid the groundwork for the formulation of a new hypothesis according to which HGS-EOCs derive from early lesions called serous tubal intraepithelial carcinomas (STICs) ^{2,18,19,22}. The presence in STICs and in the corresponding HGSs of the identical *TP53* mutation and copy number gain in *CCNE*, provided some evidence supporting this hypothesis ^{33,50,51}. STICs can be identified in $\approx 50\%$ of HGSs in advanced stages and in up to 80% of early stage but not in all HGS-EOCs cases ².

In 2011 The cancer genome atlas (TCGA) showed whole exome sequencing (WES) of 316 tissue samples of HGS-EOC patients, providing a milestone in understanding the genetic of this kind of tumor ⁴. In TCGA the genetic landscape of HGS-EOCs is characterized by a profound genetic instability, associated to inactivation of *TP53*, which occurs in 96% of cases, and of HR-related proteins ¹². *BRCA1* mutations affect 12.5% of HGS-EOCs (9% germline and 3.5% somatic mutations), while *BRCA2* mutations were found in 11.5% (8% germline and 3.3% somatic mutations). Interestingly, besides the above described mutations, in HGS-EOCs only a handful of other cancer genes are altered at high frequency. Most putative cancer-related genes have been found mutated at much lower frequency ($\approx 1\%$) showing the so called “long-tail” distribution (Fig 1.2) ^{1,6}. The role in carcinogenesis of the genes located in this tail of distribution is still unclear ^{6,52}. The TCGA screening has also shown that rather than specific recurrent mutations, the genomic instability of HGS-EOCs results in a substantial alteration in gene copy

number. For example, amplifications have been found in genes such as *CCNE1*, *PIK3CA* and *MYC* ¹.

In summary, the presence of the “long tail” in mutation distribution underlines the increasing need for the identification of new oncogenic drivers exploitable as therapeutic targets for HGS-EOC treatment ^{3,5}.

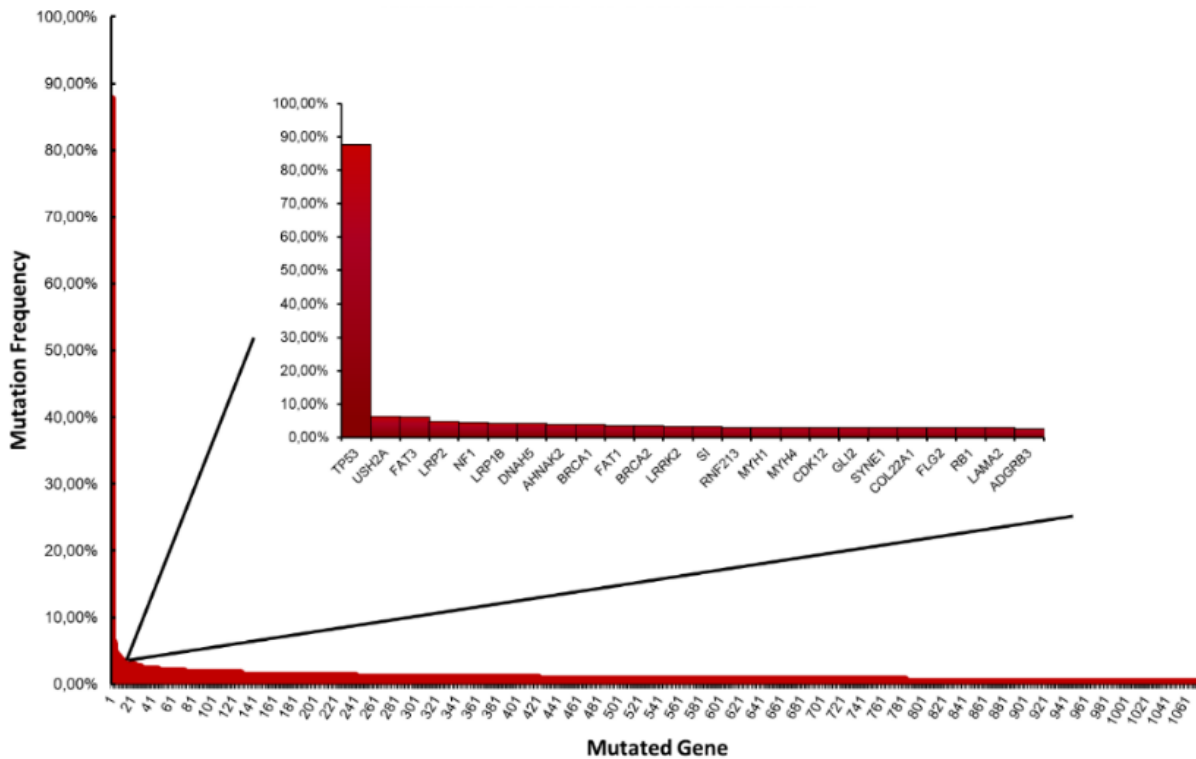


Fig 1.2: Long tail distribution of cancer-related genes in ovarian cancer. Data reported by TCGA show that in ovarian cancer only a handful of cancer related genes is mutated at high frequency, whereas the great part is mutated at much lower frequency ($\approx 1\%$). In the inset: graph with the first 25 genes in the list of cancer-related genes mutated in ovarian cancer. Graphs are obtained from TCGA data elaboration ⁹.

1.3 Ovarian Cancer Therapeutic Strategies

The primary treatment for women with newly diagnosed ovarian cancer is cytoreductive, also known as “debulking” surgery, which is used as therapeutic approach but is also necessary, when possible, for histopathological diagnosis and tumor staging.

The main goal of the surgical approach is to achieve removal of all visible tumor mass(es) ^{2,53}. Patients with an advanced stage of HGS-EOC have less probabilities of surgical complete debulking, due to tumor dissemination in peritoneal cavity and to the formation of metastatic foci ¹.

The level of primary cytoreduction achieved is the most important prognostic factor, influencing both progression-free survival (PFS) and overall survival (OS) of patients ²⁹.

Generally, the surgical approach is satisfying when the residual disease (RD) is less than 1 cm. After surgery, patients with Stage IIb or higher disease level are treated with adjuvant chemotherapy consisting in the administration of Carboplatin alone or in combination with Paclitaxel ^{1,2}. Patients not suitable for a complete cytoreduction at presentation are treated with 3-6 cycles of neo-adjuvant chemotherapy in order to reduce tumor size, also consisting in platinum-based chemotherapy alone or in combination with paclitaxel ^{2,53}.

The carboplatin-paclitaxel combination has been the standard of care for ovarian cancers treatment for the last 20 years. Alternatives to this approach have been extensively studied, but no chemotherapeutic regimen has been conclusively demonstrated as being superior ^{1,2,53}. With the advances in target therapy, in 2011 the administration of Bevacizumab in the first line chemotherapy regimens has been approved. Bevacizumab is a humanized antibody anti VEGF-A and together with carboplatin-paclitaxel combination seems to improve PFS, as shown by two different clinical trials: GOG218 and ICON7 ^{54,55}.

Although more than 70% of patients with advanced disease positively respond to first-line treatment, approximately 80% undergo relapse. When platinum-free interval (PFI), i.e. the time lapse between the initial response to chemotherapy and the appearance of relapse, is equal or greater than 6-12 months, tumors are regarded as platinum partially sensitive or platinum-sensitive, respectively. Conversely when PFI is shorter than 6 months tumors are considered platinum-refractory ⁵⁶.

The second-line treatment of relapsing HGS-EOCs is mainly based on the platinum response during the first line treatment and on the entity of relapsing disease ^{2,53}. Despite rare exceptions,

recurrent ovarian cancers are generally incurable. Thus the main goals of the second-line treatment are to prolong the survival, improve the quality of life, and postpone disease progression and symptoms manifestation ^{2,53}.

For platinum-sensitive tumors the second-line treatment would be again platinum-based chemotherapy, alone or in combination with other agents, albeit there is a progressively decrease in PFS for every administration of chemotherapy. Many trials have shown that the combination of platinum-based chemotherapy with paclitaxel, gemcitabine, trabectedin, pegylated liposomal doxorubicin and bevacizumab improves outcomes compared with the single agent. ^{2,57-60}. After treatment with several cycles of platinum-based chemotherapy, acquired resistance phenomena can occur, causing the failure in treatment response of tumors that were previously platinum-sensitive ^{2,56}. Acquired resistance is an issue of the majority of cancer types and is widely studied by researchers. Regarding HGS-EOCs it has been supposed that the main cause of acquired resistance could be its heterogeneity. In particular, according to the hypothesis of the evolutionary nature of cancers, in each tumor there are multiple cell populations with different genetic traits. These cell subsets evolve over time, following a pattern of Darwinian evolution. In this context chemotherapy can act as a selective pressure event, killing some cell subpopulations but favoring at the same time the increase of others ⁶¹⁻⁶³.

In platinum-refractory patients the second-line therapy consists in Bevacizumab administration in combination with paclitaxel, pegylated liposomal doxorubicin or topotecan. Moreover, other single agents that can be used in platinum-refractory cases are gemcitabine, trabectedin and etoposide. However, in platinum-refractory patients the overall average response to these therapies is quite poor accounting only about 10-15% with a PFS of 3-4 months ^{1,2,53}.

Unlike other cancer types the development of target therapies did not completely change the therapeutic approach in ovarian cancer; this is mainly caused by the molecular and genetic features of this cancer type. In particular, as already described, in HGS-EOC there are few

recurrent mutations in cancer-related genes. The majority of mutations have a low frequency and their possibility to be actionable is still undergoing investigations ^{1,2,53}. The most important targeted approach regards a class of compounds known as Poly(ADP-ribose) polymerase (PARP) inhibitors. PARP1 and PARP2 are enzymes involved in DNA single-strand break (SSBs) ⁶⁴.

The mechanism of action of PARP inhibitors (PARPi) is based on the principle of synthetic lethality (Fig 1.3): the loss of function in one gene can be tolerated by cells but could be lethal when combined with the loss of an additional gene product or pathway ⁶⁵. PARP inhibitors block the catalytic activity of PARP preventing repair of SSBs and leading to the development of DSBs at the replication fork, which are toxic for cells ⁶⁴. In cells in which there is already the inactivation of one mechanism of DNA damage repair such as HR, the additional inhibition of PARP results in a block of DNA replication followed by apoptosis ^{1,64,66}.

As mentioned above, HGS-EOC is characterized by a widespread genomic instability and the majority of patients possess some deficiency in DNA repair pathways (somatic or germline), especially in proteins involved in HR such as BRCA1/2. In this context PARP inhibitors were expected to be highly effective ^{64,66}. The first PARP inhibitor tested on patients was Olaparib. Many trials have been carried out on patients with *BRCA1/2* mutation (somatic or germline) to explore the therapeutic potential of Olaparib alone or in combination with chemotherapy ^{8,53,66-71}. Given the significant improvement in PFS, Olaparib was approved for treatment or maintenance therapy in *BRCA* mutant patients, with platinum-sensitive recurrent HGS-EOC, who have already positively responded to platinum ^{1,2,11,53,66}.

The high genomic instability of HGS-EOCs, even in the absence of *BRCA1/2* mutation, has brought the scientists to speculate on the possibility to use PARPi also on patients with *BRCA1/2* wild-type. The promising results of several trials prompted the recent approval of two others PARPi: Niraparib and Rucaparib, also for the treatment of *BRCA* wild-type HGS-EOC patients, with platinum-sensitive recurrent tumors ^{72,73}. Like for platinum-based chemotherapy, even during PARP inhibitors treatment acquired resistance may occur. The

mechanism underlying the appearance of resistance can again involve the heterogeneity of HGS-EOC. As described above, in a context of several clonal subpopulations genetically and molecularly different, pharmacologic treatment with PARPi could act as a selection agent, favoring the spread of clonal subpopulations which are not PARPi sensitive ^{3,11,53,56,64,66}. Moreover, the occurrence of a secondary somatic mutations that restore BRCA1/2 in carcinomas from women with germline *BRCA1/2* mutations affects PARPi response ⁷⁴.

Besides PARPi, another group of drugs has been explored for application in ovarian cancer therapy: the immune check-point inhibitors. In recent years the application of immunotherapy approaches has shown promising results in the treatment of different tumor types. However, in ovarian cancer the therapeutic application of this drug category has progressed slowly. In 2008 Tothill and coworkers, proposed the stratification of high grade serous ovarian cancers in five clusters (C1-C5) ⁷⁵. This classification is based on the expression of specific markers and correlates molecular and genetic features with patient outcome. Particularly, cluster C2 is characterized by a high number of tumor infiltrating CD3⁺ T-lymphocyte and by a gene-expression signature with the up-regulation of many genes involved in immune cells activation. This phenotype has been called immunoreactive and is regarded a positive prognostic factor for the high 5-years survival rate. Given the elevated number of immune cells in tumors, it has been hypothesized that patients with immunoreactive phenotype could take advantages by treatment with immune check-point blockade. Currently, many trials are ongoing in order to explore the possibilities to use anti PD-1/PD-L1 and anti CTLA-4 agents alone or in combination with PARPi or chemotherapy for ovarian cancers treatment. Though the many efforts aimed in this field no immune check-point inhibitor has yet been approved for the use in clinic ^{11,75-78}.

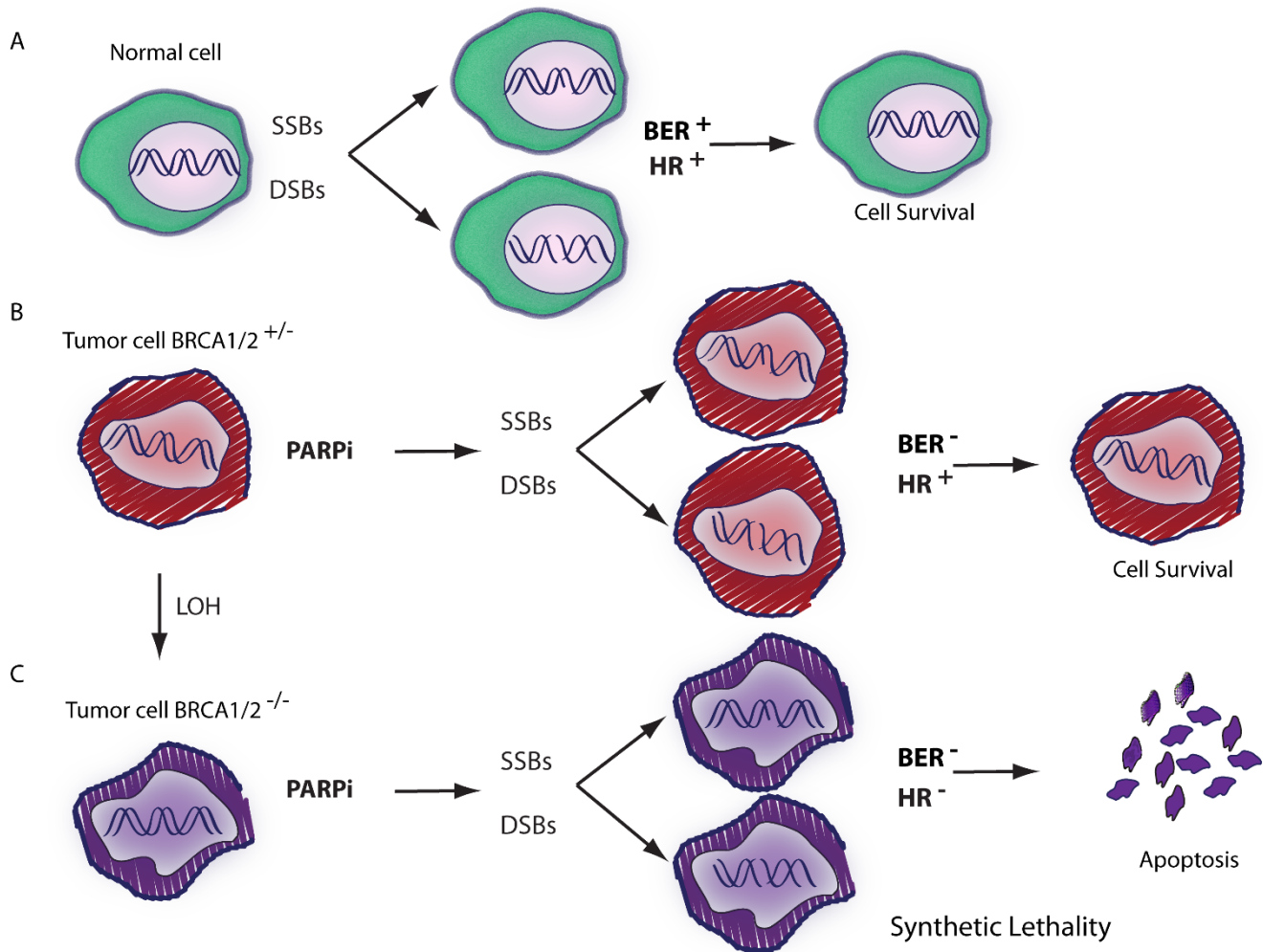


Fig 1.3: Schematic representation of synthetic lethality. (A) Normal cell, after SSBs and DSBs, DNA repair machineries repair damages restoring genomic integrity; (B) Tumor cell HR proficient, inhibition of BER exerted by PARPi does not affect genomic integrity; (C) After LOH occurrence in *BRCA1/2* and under the effect of PARPi, tumor cells HR deficient are not able to repair DNA damages and undergo apoptosis led by synthetic lethality.

1.4 Ovarian Cancer Models

The therapeutic approaches to ovarian cancer (as highlighted in the paragraph 1.3) are mainly based on cytoreductive surgery and platinum-taxane chemotherapy. The introduction of target therapy has modestly ameliorated patients' outcome. Moreover, the presence of the "long tail" of somatic mutations of unknown significance, did not allow the application of target therapies, which are currently limited to the use of PARPi and anti-VEGF agents (for references see

paragraph 1.3). Therefore, the identification of oncogenic drivers is essential to extend the list of available therapeutic options.

For efficient drug discovery, experimental preclinical models which accurately mimic biological properties of *in vivo* human tumors are required. In this context, *in vitro* and *in vivo* patient-derived models have assumed a great importance in predicting patients' drug response (for a review see ⁷⁹).

For many years in preclinical studies cancer cell lines represented the standard start-point for drug discovery process. More than 50 cell lines derived from ovarian cancers are currently available for research. Unfortunately, results of several studies have suggested that the most widely used cell lines do not correctly represent HSG-EOCs. In particular, the comparison of the genetic and molecular profiles between established cell lines and HGS-EOC tumors have shown that the majority of the commercially available ones do not represent HGS-EOCs ⁸⁰⁻⁸².

In this scenario, patient-derived models take on greater importance, especially because they represent for researchers the chance to work in an experimental context as similar as possible to that the human disease (for a review see ⁷⁹). In this thesis section patient-derived models are briefly described in their pros and cons, focusing on patient derived xenografts used in the presented experimental work.

Patient-derived xenografts (PDXs) of ovarian cancer can be obtained by the engraftment of human pieces of tumor (surgical resections or biopsy samples) or by injection of ascites or pleural fluid in immunocompromised mice. The engraftment can be orthotopic (in the ovary of mice) or heterotopic. The latter is mostly performed by sample engraftment in the flank of mice subcutaneously, or by the inoculation in peritoneal cavity ⁸³. The use of PDXs provide several advantages in preclinical research. First of all, they retain the principal histologic and genetic characteristics of their donor tumors, maintaining the heterogeneity of the samples along serial passages. Moreover, a high correlation between therapeutic efficacy in PDXs model and patient drug response it has been also shown, placing PDXs as reliable and reproducible

experimental models ⁸³⁻⁸⁷. Unlike other cancer types, the derivation of PDXs from ovarian cancer has a longer time of latency and a lower take rate (roughly of 30%) ⁸⁴. A great limitation of this preclinical model consists in the loss of human stroma along passages, that is replaced by murine stroma possibly altering tumor microenvironment ⁸⁸.

Patient-derived tumor cells could represent an important tool, especially for functional assays ⁸⁹⁻⁹². Primary cultures can be obtained by direct digestion of human samples. Although in several studies these models have shown a good correlation in their drug response compared to the correspondent patient's tumor, they remain a limitedly exploited model. There are several issues. First of all, the low efficiency of the establishment protocols and the difficulties in finding the right culture medium, the loss of tumor stroma along passages. Moreover, with the exceptions of rare cases in which the primary cultures are immortalized, another great limitation is that primary cells incur rapidly in multiplicative senescence, so they should be used as short-term cultures ⁹³. In this work, I will show the use and the characteristics of PDX derived tumor cells (PDTCs) obtained by digestion of a PDX derived tumor piece ⁹⁴.

Unlike the other cancer types, only recently 3D models for ovarian cancer studies have been developed. These are patient-derived ascitic spheroids (PDASs), patient-derived tumor organoids (PDTOs) and other 3D organotypic models (for a review see ⁷⁹).

Spheroids are sphere-like aggregates of cells, which are cultured as floating 3D structures and used for genetic and molecular studies but also for *in vitro* drug testing. As already described in the paragraph 1.1, in advanced stages of HGS-EOCs, tumor cells invade peritoneum and disseminate as malignant ascites fluid. In ascites, tumor cells can aggregate between each other but also with other cell subtypes, as immune cells and fibroblasts, forming highly heterogeneous 3D structures. After paracentesis or thoracentesis, ascites or pleural effusion, respectively, can be cultured and the PDASs can be used as a preclinical model to study dynamics of advanced stages of HGS-EOCs. More importantly, it has been hypothesized that these cell aggregates in ascites play the role of metastatic units, which can also be responsible for disease recurrence and therapy resistance. Due to their direct patient's

derivation, spheroids might retain molecular and genetic characteristics of source tumors. Overall, the greatest advantage of PDASs is that they form or detach spontaneously and preserve also tumor microenvironmental cells ^{95,96}.

Only a few studies have documented the development of organoid platforms for ovarian cancer similar to those developed from other cancer histotypes. D'Andrea's and Clevers' groups were the first to use this model in preclinical research ^{97,98}. Patient-derived tumor organoids (PDTOs) can be generated from single tumor cells or small pieces of tumors directly from patients. In both instances, PDTOs consisted of only tumor epithelial cells cultured and propagated as 3D structures in growth factor-enriched media. PDTOs have been used to study the molecular and genetic characteristics of tumors and are envisaged as a model to predict clinical response of patients to drugs. However, they lack tumor stroma and immune microenvironment which is a limitation (for a review see ⁷⁹).

Another 3D model used in ovarian cancer research is the one proposed by Jenkins and co-workers, i.e. an organotypic tumor model obtained by growing tumor fragments directly derived from patients in microfluidic cells ⁹⁹. These 3D cultures recap the molecular and genetic features of correspondent tumors and show the presence of tumor microenvironment, possibly solving a critical issue in tumor biology studies but also in the evaluation of drug response. In their studies Jenkins and colleagues exploited this model to examine the mechanisms underlying attachment and invasion of ovarian cancer and also the tumor response to immune-checkpoint inhibitors ^{99,100}.

1.5 PI3K as an Actionable Target in Cancer

Phosphatidylinositol 3-kinases (PI3Ks) are a family of lipid kinases that integrate signals from growth factors, cytokines and other environmental cues, translating them into intracellular signals that regulate multiple signaling pathways (for reviews see ¹⁰¹⁻¹⁰⁶). PI3Ks family were described for the first time in 1988 by Cantley and co-workers, who identified a group of

proteins responsible for the phosphorylation of phosphatidylinositol (PtdIns), making an active metabolite with the role of second-messenger in cells ^{101,102,104}. PI3K was mostly regarded as an enzyme associated with tyrosine kinases receptors (RTKs). Evidence collected afterward, made clearer the role of this group of proteins as important mediators in several cell processes including cell proliferation, migration, differentiation and metabolism, paving the way for subsequent studies aimed to improve the knowledge of the PI3K family ^{105,107}. Nowadays much more insights have been achieved on the PI3K pathway (Fig 1.4) and on its implications in human pathologies. It comes as no surprises that drug discovery research is extensively engaged on the study of PI3K pathway and on its inhibition using target therapy (for reviews see ¹⁰⁷⁻¹¹⁰).

According to their structural characteristics and substrate specificity in human cells PI3Ks are divided in three classes: Class I PI3Ks, class II PI3K-C2 kinases and class III ¹⁰⁵.

Class I PI3K are heterodimeric molecules composed of a regulatory subunit and a catalytic one. The latter acts in the enzymatic transformation of PtdIns(4,5)P₂ in PtdIns(3,4,5)P₃, whereas the regulatory subunit interacts with and regulates the catalytic subunit. Relatively little is known about class II PI3Ks. These proteins consist of monomeric lipid kinases without a regulatory subunit. The preferred substrate of this class is PtdIns(4)P, which is converted in PtdIns(3,4)P₂. The physiological role of class II PI3Ks is not fully understood, but it seems that they are important in diverse cellular contexts, including primary cilium formation and functions, migration, recycling, and metabolic pathways activation ¹¹¹. Class III PI3Ks consist of a single catalytic subunit VPS34 which converts the PtdIns in PtdIns(3)P, an important second messenger involved in intracellular trafficking and autophagy ¹⁰³.

Among the three different classes of PI3Ks the most studied is class I. Based on the activating receptor type, class I PI3Ks are further divided in:

- Class IA activated by receptors tyrosine kinases (RTKs), G protein-coupled receptors (GPCRs) and small G protein
- Class IB exclusively activated by GPCRs

Classes IA and IB differ from each other for the isoforms of regulatory and catalytic subunit composing the heterodimer. Class IA regulatory subunits can be p85 α (and its splicing variants p55 α and p50 α), p85 β and p55 γ , encoded by *PIK3R1*, *PIK3R2* and *PIK3R3* genes, respectively. The catalytic subunits can be p110 α , p110 β (which are ubiquitously expressed) and p110 δ (more abundant in hematopoietic cells), encoded by *PIK3CA*, *PIK3CB* and *PIK3CD* genes, respectively. Class IB is composed by only one isoform of catalytic subunit p110 γ encoded by *PIK3CG* gene –mainly expressed in immune cells– and three possible regulatory subunits p101, p84 and p87 (encoded by *PIK3R5* and *PIK3R6*). The latter directly interact with the G $\beta\gamma$ subunit of trimeric G protein, leading the activation of the catalytic subunit ^{103,105,107–109,112}.

The mechanism of action of class I PI3Ks is a multistep process which starts with the activation of cell surface receptors. In the absence of activating signals, p85 interacts with p110 and inhibits p110 kinase activity. Following RTKs or GPCRs activation, class I PI3Ks are recruited to the plasma membrane, where p85 inhibition of p110 is relieved and p110 phosphorylates PtdIns(4,5)P₂, to generate PtdIns(3,4,5)P₃. This lipid product acts as a second messenger, activating in turn other proteins by binding their pleckstrin homology domain (PH). In particular, PtdIns(3,4,5)P₃ rise in cells triggers the translocation of AKT in the inner plasma membrane. PtdIns(3,4,5)P₃ activates PDK1 by binding its PH domain; once activated PDK1 phosphorylates AKT in position T308. A second phosphorylation in position S473 leads to the full activation of AKT which stimulates cell survival, metabolism and migration through phosphorylation of other proteins. The cellular levels of PtdIns(3,4,5)P₃ are tightly regulated by the opposing activity of PTEN. PTEN is an important tumor suppressor which antagonizes the PI3K activity removing the 3' phosphate from PtdIns(3,4,5)P₃ through its intrinsic activity of lipid phosphatase ^{105,107,108,113–118}.

In this scenario it is clear the reason why alterations of the PI3K signalling pathway are often involved in tumorigenesis, cancer progression and metastasis. In cancers, PI3K pathway can be aberrantly activated through multiple mechanisms including cross-talk with other signaling pathways or intrinsic hyper-activation due to genomic aberrations. Common genomic

aberrations across cancer types in the PI3K pathway include aberrations in genes that among the most mutated in cancer, such as loss of the negative regulator PTEN, activating mutations or gene amplification in *PIK3CA* and mutations of *PIK3R1* that encodes the regulatory subunit of the PI3K ^{112,119,120}.

In particular, *PIK3CA* is the 2nd most frequently mutated gene across 12 cancer types sequenced by TCGA ¹²¹. Data reported by the “Catalogue of somatic mutations in cancers” (COSMIC) show that the majority of mutations in *PIK3CA* are missense substitutions ¹²². Eighty % of genetic alterations affecting this gene are mainly clustered in two ‘hotspot’ regions of the *PIK3CA* coding sequence. Particularly, the most frequent mutations are the substitutions E542K and E545K in the helical domain, and H1047R in the kinase domain. These missense mutations lead to the constitutive activation of p110 α by affecting the binding site for p85 α or through a stabilization of this protein to the plasma membrane, leading the continuous activation of AKT ^{103,107,108,112}. COSMIC data show that *PIK3CA* mutations have a high frequency in many cancer types especially in breast, prostate, colon and endometrial carcinomas. Although in ovarian cancer the frequency of *PIK3CA* point mutation is quite low, the alteration in copy number (>7 fold) is frequent among all the histologic subtypes and is associated with a poor prognosis ¹²³. In a genomic screening which involved about 200 ovarian cancers *PIK3CA* mutations or gene amplifications were detected in about 30% of all EOCs and 45% of endometrioid and clear cell subtypes ¹²⁴. Although p110 β involvement in tumorigenesis is still controversial, many studies show the possible implication of *PIK3CB* aberrations in cancer ¹⁰⁷.

Mutations affecting genes encoding the p85 α regulatory subunit have also been reported. TCGA data reported that the encoding gene *PIK3R1* is the 12th most commonly mutated across cancer lineages, and several mutations in hotspot regions have been detected ¹¹². COSMIC data report that 30% of these mutations consist in missense substitutions ¹²⁵. As mentioned above, p85 α plays a critical role in the stabilization and recruitment of p110 α to the plasma membrane. Therefore, somatic mutations affecting the binding site for p110 α disrupt the inhibitory action of the regulatory subunit, leading to aberrant PI3K pathway activation ¹²⁶.

Mutations generally involve the nSH2 and iSH2 domains of p85 α which are required for the binding with the catalytic subunit. However, approximately one third of mutations in *PIK3R1* occur in other domains, which are not involved in the interaction with the catalytic subunit. It is likely that this set of mutations are involved in p85 α function independently of its binding with p110. Recent studies have revealed that in some cell contexts p85 α is in excess over p110 and can be found either as monomer or as homodimer. These two additional conformations are supposed to negatively regulate PI3K pathway. When p85 α is monomeric, it might compete with p85-p110 dimers for binding to tyrosine-phosphorylated IRS-1, blocking the activation of downstream proteins^{112,127}. On the other hand, according to the homodimer model, the SH3 domains of two p85 α can interact between each other, constituting a major homodimerization interface and promoting the formation of an homodimeric complex. This complex competes with the WWP2 (the cell mediators for proteasomal degradation of PTEN), preventing the degradation of PTEN. Moreover, the p85 α homodimeric complex can also improve the phosphatase activity of PTEN and thus indirectly inhibit the PI3K pathway. Given that mutations in *PIK3R1* gene affect the interaction between p85 α and IRS-1 or the formation of the homodimeric complex, the final result is an aberrant activation of the PI3K pathway. However, one of the most exciting discovery of the studies on p85 α functions is the identification of a neomorphic set of mutations which confer to p85 α the capability to activate the MAPK pathway. These mutations cause the production of a truncated p85 α which misses one of the domain for the p110 binding but acquires the capability to activate the MAPK pathway^{112,126-131}.

TCGA data report that mutations in *PIK3R1* gene occur at high frequency in endometrial, colon, breast cancers and in glioblastomas. In ovarian cancers, aberration in *PIK3R1* gene mainly regard alteration in copy number, while mutations in gene sequence account only for about 3%^{125,128,132,133}.

Besides implication in cancer, PI3K pathway alterations are related with the occurrence of other human disease. Dysfunctional PI3K/AKT-mediated glucose transport and glycogen synthesis

are involved in the onset of metabolic diseases such as type 2 diabetes and obesity ¹³⁴. Mutations specifically involving *PIK3CA* are also the main cause of the *PIK3CA*-Related Overgrowth Spectrum (PROS) which is a group of diseases characterized by localized overgrowth, for example of a digit, to severe, extensive, and life-threatening overgrowth affecting major vessels and/or critical organs ¹³⁵⁻¹³⁷. In addition, germline mutations in heterozygosity, located in cSH2 domain of *PIK3R1* are responsible for the SHORT syndrome, characterized by developmental defect and historically defined by its acronym: short stature (S), hyper-extensibility of joints and/or inguinal hernia (H), ocular depression (O), Rieger abnormality (R) and teething delay (T). Molecular studies have shown that *PIK3R1* mutations associated to SHORT syndrome result in defects and not in activation the PI3K pathway ¹³⁸.

Given the great number of pathologic conditions related to PI3K pathway alterations, it is not surprising that efforts in target therapy research have been focused on this signaling pathway. Several PI3K inhibitors are currently tested or in development for clinical applications. Based on pharmacokinetic properties and isoform selectivity for ATP binding site, PI3K inhibitors have been classified into different groups:

- Pan-PI3K inhibitors able to bind all class I PI3Ks (*PI3K α* , *PI3K β* , *PI3K γ* and *PI3K δ*). The first two inhibitors of this category were Wortmaninn and LY294002, for a long time used in research to study PI3K, but not suitable for application in humans. Generally, this class of inhibitors displays cytostatic effects with consequent G1 phase arrest *in vitro* and favorable anti-cancer activity *in vivo* in experimental models. However, several clinical trials explored the efficacy of other pan-inhibitors alone or in combination with other anti-cancer agents, but did not show promising results in the treatment of both solid and hematologic malignancies ^{109,116,139,140}. Among this set of inhibitors one of the most tested is NVP-BKM120 (Buparlisib). NVP-BKM120 reversibly binds the ATP-binding site of the lipid kinase domain displaying a potent activity against all class I PI3K isoforms with high selectivity ^{105,109,139,141,142}.

- Specific isoform inhibitors act against only one isoform of PI3K and now appears more promising. Generally, these are ATP-competitors and have been developed with the aim of targeting specific alterations, avoiding the cumulative toxicity related with the inhibition of PI3K multiple isoforms ^{109,110}. The most effective and rapidly approved have been the inhibitors of the p110 δ for the treatment of hematological malignancies ¹¹⁶. Drugs specific for p110 α and p110 β , such as NVP-BYL719 (Alpelisib) and GSK2636771, respectively, have been or are under evaluation. In particular, NVP-BYL719 has shown a potent anti-cancer effect in patients with *PIK3CA* mutations either as a single or a multi-drug approach and it has recently been approved by FDA for the treatment of metastatic breast cancer in combination with Fulvestrant ^{110,143-146}. GSK2636771, specific for the p110 β subunit, is under evaluation for treatment of malignancies with PTEN loss ^{110,147,148}.
- Dual mTOR/PI3K inhibitors block the activities of both PI3Ks and mTOR kinases by competitively binding to the ATP binding sites. Since mTOR is structurally related to PI3Ks, ATP-competitive compounds inhibit these two kinases with equivalent potency. NVP-BEZ235 (Dactolisib) belongs to this set of drugs and is under evaluation in preclinical and clinical studies. NVP-BEZ235 suppresses cell proliferation inducing G1 cell cycle arrest and promoting autophagy. The major problem related to this dual inhibitors is the toxicity derived from their action on multiple targets ^{109,110,139, 147}.

Overall these molecules display promising results as anti-cancer drugs but they all cause important side effects such as hyperglycemia and metabolic alterations strictly related to the role of PI3K in many different cell processes and, in particular, in metabolism.

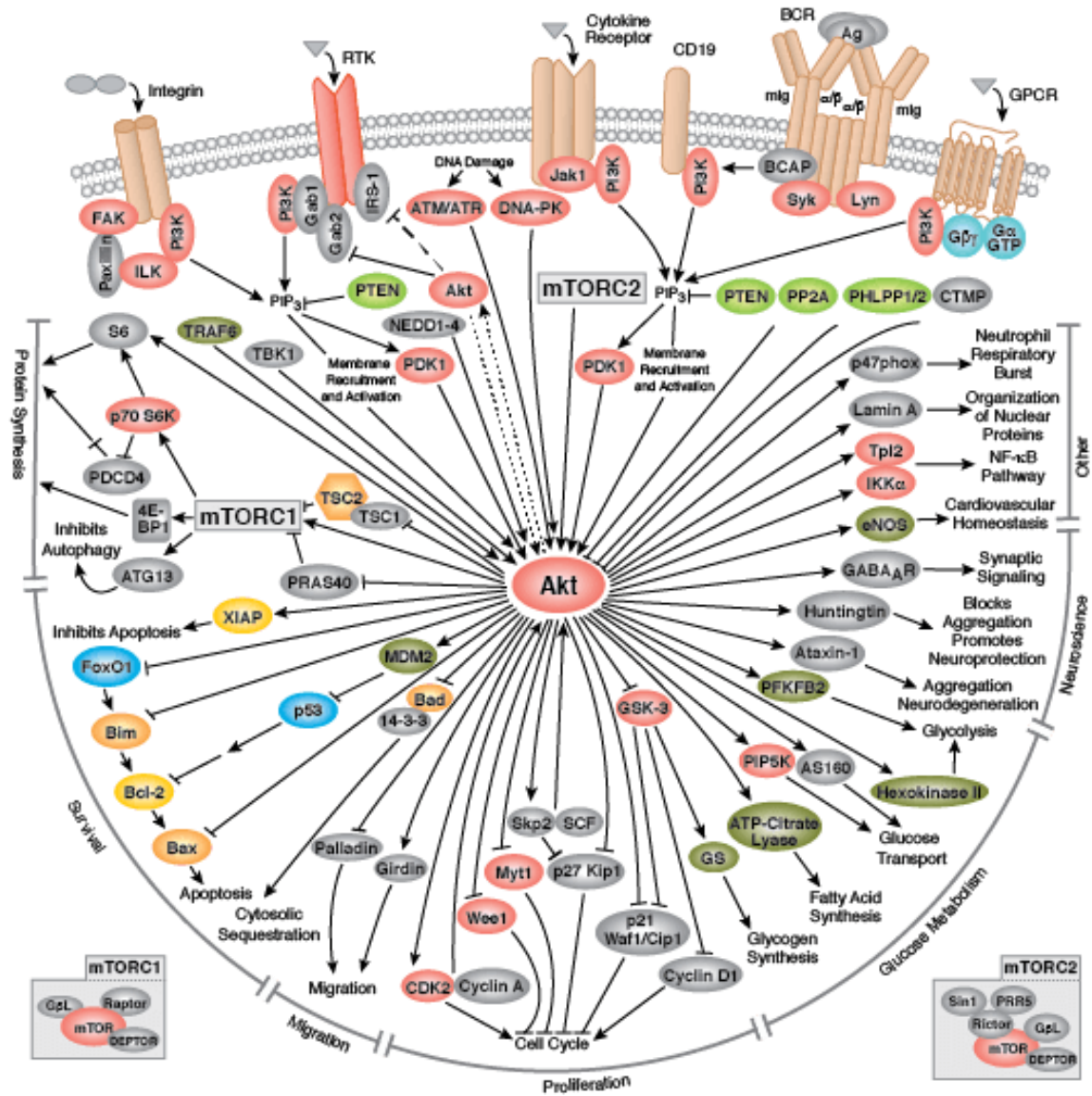


Fig 1.4: Schematic representation of PI3K/AKT/mTOR pathway. Adapted from Cell Signaling Technology: "https://www.cellsignal.com /contents/science/cst-pathways".

2. AIM OF THE WORK

Patients with high grade serous epithelial ovarian cancer (HGS-EOC) at advanced stage have experienced little improvement in overall survival, despite short term good response to standard treatments mainly based on cytoreductive surgery and platinum based-chemotherapy. The majority of patients with HGS-EOC present with advanced stage disease, when tumor has already spread to the peritoneum and invaded tissues beyond ovaries, with metastatic foci formation ^{2,3}. Unlike other cancer types, the development of target therapy did not completely change the therapeutic approaches in ovarian cancer which has remained unchanged in the past 20 years ^{1,2}. Molecular and genetic studies performed on HGS-EOC have demonstrated that its main characteristic is the inactivation of *TP53* which occurs in 96% of cases, which is currently not druggable. Only aberrations in homologous recombination (HR) pathway especially in *BRCA1/2* genes are quite common (approx. 20% of cases), and are biomarker for targeted treatment with PARP1 inhibitors ². Genomic analysis of EOC samples have demonstrated a profound genetic instability with a great number of copy number alterations (CNAs) ^{4,5}. Conversely, EOC is characterized by few recurrent mutations and the so-called “long tail” distribution of low-frequency mutations in cancer-related genes. ^{4,5}. The role in carcinogenesis of genes located in this tail of distribution is still unclear and needs to be investigated in order to understand the potential clinical impact of rare mutations as useful biomarkers of response to targeted therapies ^{1,6}.

Therefore, the main goal of this Ph. D. project is the identification of putative drivers and actionable cancer-genes in HGS-EOCs using patient-derived models, such as Patient Derived Xenografts (PDXs) and PDX derived tumor cells (PDTCs). We envisioned that the weakness of PDXs and PDTCs, i.e. lack of human stromal and immune cells, might be instrumental to identify mutations in human cancer cells and to associate mutations to treatments as clinically exploitable tumor biomarkers using experimental models. Thus, in this thesis project, PDXs

and PDXs have been extensively used to first identify and secondly validate the clinical importance of the mutations found following the pipeline shown in figure 2.1.

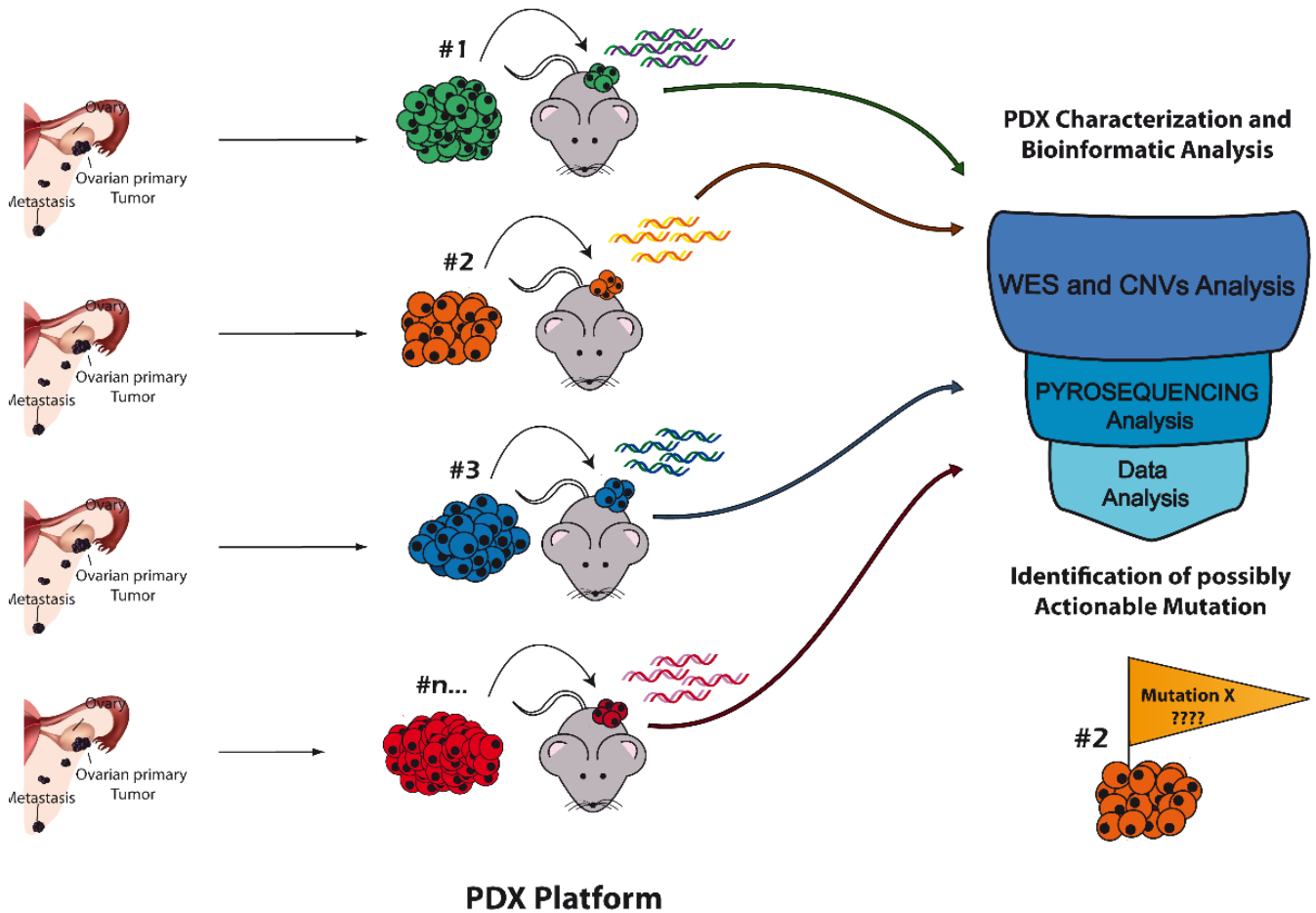


Fig 2.1: Representative image of the pipeline followed in this thesis work for the identification of putative drivers and actionable mutations in cancer-related genes. Human tumor samples were implanted in severely immunocompromised mice. Afterwards PDXs were histologically and genomically characterized. Subsequently WES, CNAs and bioinformatics analyses were performed in order to identify putative drivers and actionable cancer genes.

3. MATERIALS & METHODS

3.1 Cell Lines

A2780 (NCI-DTP, Cat# A2780, RRID: CVCL_0134) human, epithelial, adherent ovarian carcinoma cell lines and LNCaP (CLS, Cat# 300265/p761_LNCaP, RRID: CVCL_0395) human, epithelial, adherent prostate carcinoma cell line were purchased from American Type Culture Collection (ATCC, RRID: SCR_001672) and cultured in RPMI-1640 with 10% FBS (Fetal Bovine Serum). The OVCAR-8 (NCI-DTP Cat# OVCAR-8, RRID: CVCL_1629) human, epithelial, adherent ovarian carcinoma cell lines was obtained from the NCI-DCTP repository and cultured in RPMI-1640 with 10% FBS. Culture media were complemented with Glutamine 2mM (Cat# G7513) and Penicillin/Streptomycin mix 0.1mg/ml (Cat# P0781) both purchased by Sigma-Aldrich (St. Louis, MI, USA) All the cell lines, except for LNCaP, are certified as HGS-EOC.

3.2 Patient Derived Xenografts (PDXs) Platform and Mice Treatment

Between 2012 and 2016 a collection of 167 separate clinical samples of epithelial ovarian cancers was undertaken with the consent of each patient according to the PROFILING protocol and with the approval first of the ethical committee of Regione Piemonte and then after the foundation, of the FPO-IRCCS. For the development of PDX platform samples quality was assessed by pathologists. Human tumors were taken either at laparoscopy or at surgery from Candiolo Cancer Institute (FPO-IRCCS) and Sant'Anna gynecological hospital and implanted in mice either subcutaneously or intra peritoneum. In particular, tumors were grafted in anesthetized mice (gas anesthesia made of 2% isoflurane obtained from Zoetis U.K., in oxygen and nitrous oxide 2:1). After the implant, mice are monitored until the end of anesthesia effect. All surgical procedures in mice were performed in sterile conditions under laminar flow, using

mice of approximately 20 gr. A total of 65 PDX lines successfully grew with a take rate of approximately 40%. After the first implant and growth tumors were propagated subcutaneously for at least three passages for further experiments (e.g. PDX characterization, PDTCs derivation and *in vivo* drug treatments).

For the development of PDXs platform and *in vivo* experiments only severely immunocompromised NOD/shi-scid/IL-2R γ null female mice were used, purchased from Charles River Laboratories Italy. Once received mice did not undergo to any further modification. Mice have been housed in autoclaved and sterilized cages in group of 5-7 animals per cage. All cages have been separately located in mouse housing system where they receive filtered ventilation and where they are kept at 20 to 22 °C on a 12:12-h light:dark cycle. Mice were kept in cages with highly absorbing and sterilized bedding material which have been changed every week by mice facility team. Mice were fed *ad libitum* with commercial, sterile pelleted diet and water. All the procedures with animals have been approved by the local Ethical Commission and by the Italian Ministry of Health in accordance with EU Directive 2010/63/EU for animal experiments; a first authorization was obtained on 12/7/2012 and, following subsequent regulations, approved again on 14/01/2016 (no. 16/2016-PR) and extended for two additional years on 17/9/2018. All animal procedures comply with the “3R” principles.

For *in vivo* drug treatment experiments the PDX lines of interest were propagated in 18-20 mice in order to get PDX cohorts. When tumor volumes reached approximately 100mm³ mice were blindly and individually randomized in treated or control animal groups to obtain at least 6 animals/group using Laboratory Assistant Suite (LAS)¹⁴⁹. *In vivo* studies of the PDX line #475, were carried out as follows. For treatment with Buparlisib (purchased from Cayman Chem, Ann Arbor, MI) solution was freshly prepared every day by diluting in N-Methyl-2-pyrrolidinone and PEG 10/90 v/v to a final volume of 100 μ l, both purchased from Sigma Aldrich, (St. Louis, MO, USA). Buparlisib was administered by oral gavage every day (5 days/week) for 3 weeks (see Results Fig. 4.8.1), in sterile conditions. Buparlisib was

administered at the dose of 20 mg/Kg whereas control animals were treated with vehicle alone. Treated mice were monitored for tumor take and growth twice a week. Tumor volumes were measured with a digital caliper. When tumor size reached 2000 mm³ mice were sacrificed under gas anesthesia by cervical dislocation. Tumors derived from sacrificed mice were processed in different ways based on their further utilization in experiments: from each tumor one big piece was embedded in formalin and included in paraffin for immunohistochemistry (IHC) experiments, another piece was snap frozen for protein extraction and another part was frozen in vital condition for further implants.

3.3 Immunohistochemistry

Immunohistochemistry was carried out on tissue microarrays (TMA) or directly onto single FFPE blocks. TMAs preparation was described for the first time by Kononen and coworkers¹⁵⁰. This methodology allows combining tens to hundreds of paraffin-embedded tissue specimens into a single paraffin block providing an important tool to study genes and proteins expression simultaneously in several specimens. TMAs used in this thesis project were prepared by pathology facility of Candiolo Cancer Institute (FPO-IRCCS) starting from PDXs paraffin-embedded tissues following the protocol described by Sapino and coworkers¹⁵¹. Briefly, PDXs paraffin blocks (donor blocks) were examined to select two tumor areas from each block. Using the advanced tissue arrayer (mod. ATA-100, Chemicon International, Tamecula, CA, USA), tissue cylinders with a diameter of 1 mm were punched under the stereomicroscope from the specific areas of the donor block and brought into the “recipient” paraffin block. In each recipient block three control tissues were also inserted: 1) liver tissue; 2) lymphatic tissue; 3) human ovarian tissue.

Once assembled recipient blocks were incubated in an oven at 45°C for 20' to allow complete embedding of the grafted tissue cylinders in the paraffin, and then stored at 4°C until

microtome sectioning. Before the staining slices of 3.5 μ m thick were cut from the blocks of interest and fixed on slides.

For PDXs characterization, TMA slides were stained in the Ventana automated immunostainer (BenchMark AutoStainer, Ventana Medical Systems, Tucson, AZ, USA) using the following antibodies by Ventana Medical Systems: α WT1 (Cat# 760-4397), α TP53 (Cat# 790-2912), α EPCAM (Cat# 760-4383), α Cytokeratin 7 (Cat# 790-4462) and α CD20 (Cat# 760-2531). The latter antibody was used to rule out the growth of lymphoma in PDXs, which occurred in 10–20% of cases, as also reported by others ¹⁵².

Evaluation of phospho-S6 and S6 expression was detected with α pS6 rabbit monoclonal antibody (Cat# 4858) and α S6 rabbit monoclonal antibody (Cat# 2217), both purchased by Cell Signalling Technology (Denvers, MA, USA). In particular, TMA slides were deparaffinized and hydrated, then the antigen unmasking was carried out using citrate buffer for 1 hour at sub-boiling temperature (95-98°C). Antigen detection was performed incubating TMA slides overnight (O.N.) at 4°C with the specific antibodies diluted in blocking solution (TBS, 0.3% Triton x-100 0.3%, 0.1% Tween-20 and 5% normal goat serum). Subsequently were carried out the secondary antibody ad DAB reactions for signal revelation. Lastly, sections were dehydrated and slides mounted with cover slips.

At the end of the *in vivo* experiments tumors derived from control and treated PDX cohorts were sectioned and a piece of each tumor embedded in formalin and included in paraffin. Tissue sections of 3.5 μ m were obtained by cutting with a microtome. Immunostaining for Ki67, phospho-S6 and S6 expression in control and treated tumors was then performed on these slices. For the staining α Ki67 mouse monoclonal (clone MIB-1, Dako; Agilent, Santa Clara, CA, USA) and α pS6 rabbit monoclonal antibodies were used following the protocol described above.

Stained slides were analyzed under light microscope and for each PDX sample, 20-30 separate fields were taken. Quantifications of phospho-S6 and Ki67 positive cells were carried

out using the Color Deconvolution plug-in in ImageJ (RRID: SCR_003070). In particular, quantification of percentage of Ki67⁺ nuclei area in control and treated mice, was calculated performing the ratio between percentage of Ki67⁺ nuclei area on the percentage of total nuclei area for each field of each PDX in the experiment (see formula below); then only the averages of %Ki67⁺ nuclei area for each sample were taken in account and used to calculate the statistical significance.

$$\%Ki67^{+}nuclei\ area = \frac{\%Ki67^{+}nuclei\ area}{\%Ki67^{+}total\ nuclei\ area}$$

Quantification of phospho-S6⁺ cells areas in samples from control and treated mice, was calculated as above but instead of nuclei area, the percentage of total cells area stained with phospho-S6 cytoplasmic staining (see formula below) was taken in account.

$$\%pS6^{+}cells\ area = \frac{\%pS6^{+}cells\ area}{\%pS6^{+}total\ cells\ area}$$

Statistical analysis was carried out using Student-t test with Welch's correction in GraphPad Prism7 software (RRID: SCR_002798) on data of Ki67⁺ nuclei areas and phospho-S6⁺ cells areas, calculated as above. Statistical significance was defined as p-value < 0.05 (95% confidence interval). Graphical representation was elaborated using GraphPad Prism7.

3.4 PDX Derived Tumor Cells (PDTCs) Culture Derivation

To obtain PDTCs, when one or more PDXs reach the size of 2000 mm³, mice are sacrificed and xenograft processed. Before digestion, PDXs are incubated O.N. in 1:1 mixture of MCDB 131 and DMEM F12 with 10% FBS, and Penicillin /Streptomycin mix (0.1 mg/ml) at 4°C. After the incubation, xenografts are mechanically chopped and digested with Human Tumor Dissociation Kit (Cat# 130-095-929) in combination with GentleMacs dissociators (Cat# 130-093-

235) both purchased from Miltenyi Biotec (Bergisch Gladbach, Germany) following the protocol provided by manufacturer. Human tumor cells are isolated from murine stroma using Mouse Cell Depletion Kit (Cat# 130-108-339) Miltenyi Biotec. Subsequently PDTCs are plated in culture dishes for 24-48 hours in 1:1 mixture of MCDB 131 and DMEM F12 with 10% FBS and maintained in a 37°C in hypoxic condition. In order to assess the quality of cultures before the experiments, 5-6 images of each PDTCs culture are taken with a bright field microscope.

3.5 PDTCs Quality Assessment and Viability Assays

For viability assay, PDTCs 24-48 hours after derivation, and control cell line are trypsinized and 5000-8000 cells were plated in Costar® 96-multiwell plates (Corning NY, USA). PDTCs and control cell lines were treated with dose escalation drugs or vehicle (DMSO) for 72 hours and cell drug responses was evaluated with two different kind of viability assays: CellTiter-Go Promega (Madison, WI, USA) viability assay and Crystal Violet assays (see sections 3.6.1 and 3.6.2 for a detailed description of assays). For drug screening on PDTCs, Carboplatin was provided by hospital pharmacy at Candiolo Cancer institute (FPO-IRCCS) and used at decreasing concentration starting from 80µM to 0.3125µM (450mg/ml, Lot#W73346;) purchased by Pfizer (Milano, Italy) PI3K/AKT/MTOR inhibitors were purchased from Selleck Chemicals (Houston, TX, USA) and used as follows:

- NVP-BKM120, Buparlisib (Cat# S2247) powder was dissolved in DMSO at 10mM and used in experiments at decreasing concentration starting from 80µM to 0.005µM.
- NVP-BYL719, Alpelisib (Cat# S2814) powder was dissolved in DMSO at 100mM and used in experiments at decreasing concentration starting from 320µM to 0.020µM.
- NVP-BEZ235, Dactolisib (Cat# S1009) powder was dissolved in DMF at 10mM and used in experiments at decreasing concentration starting from 100µM to 0.0001µM.
- GSK2636771 (Cat# S8002) powder was dissolved in DMSO at 100mM and used in experiments at decreasing concentration starting from 160µM to 0.005µM.

- PKI587 (Cat# S2628) powder was dissolved in DMSO at 10mM and used in experiments at decreasing concentration starting from 100µM to 0.0001µM.

Results were analyzed with GR metrics, which normalizes cell drug response on cell doubling along the experiments as reported by Hafner and coworkers^{153,154}. GR values have been calculated for each drug concentration using the formula indicated below; data obtained by GR analyses were plotted using GraphPad Prism7 (RRID: SCR_002798).

$$GR(c) = 2^{\left(\frac{\log_2(x(c)/x_0)}{\log_2(x(ctrl)/x_0)}\right)} - 1$$

GR calculator formula. The GR value was calculated for each point of the dose-response curve GR(c). In this formula x(c) stand for viability value of treated cells at 72h at the dose of interest; x0 is the value of cell viability at the beginning of the experiment; x(ctrl) is the viability of control cells at 72h.

- *3.5.1 CellTiter-Glo® Viability Assays*

CellTiter-Glo® viability assays were performed according to the manufacturer 's protocol. Briefly: cells were incubated for 12 minutes (2 min of shaking incubation and 10 min of stand incubation) with CellTiter-Glo® (Cat# G755B) Promega (Madison, WI, USA) solution (1:8 in PBS). After incubation luminescent signal was measured using microplate reader BioTek Synergy HTX (Winooski, VT, USA).

- *3.5.2 Crystal Violet Cytotoxic/ Cytostatic Assays*

For this assay, at the end of experiments cells were fixed with 2% paraformaldehyde (PAF) in PBS for 40 min. Plates were washed 2 times with PBS and cells were stained with Crystal violet (10% crystal violet in 20% methanol in ddH₂O) for 40 min. Subsequently plates were washed extensively with ddH₂O and air-dried. Representative images of crystal violet staining of PDTs were taken with a PC scanner and then crystal violet was dissolved incubating with 10% acetic acid for 20 min on shaker. Crystal violet absorbance signal was measured at 595nm with the microplate reader BioTek Synergy HTX (Winooski, VT, USA).

- *3.5.3 Tumorigenicity Assessment*

Once derived, PDTCs were cultured for 48 hours, then 3×10^6 PDTCs cells were suspended 1:1 PBS and Matrigel (Cat# 356237) purchased by Corning (Corning, NY, USA) in a final volume of 100-200 μ l and injected subcutaneously in NOD/shi-scid/IL-2R γ null female mice. After tumor growth (2-3 months) mice were sacrificed and xenografts were included in paraffin for the subsequent Hematoxylin and Eosin (HE) staining.

3.6 Western Blot Analysis

For Western blot analysis, PDTCs were treated in a serum free medium for 24 hours with the indicated drug or vehicle 24 hours after plating. Proteins were extracted in ice cold elution buffer (TrisHCl pH 7.4, containing EDTA, 1% Triton x-100, 10% glycerol), protease inhibitors cocktail (1:1000), sodium orthovanadate (1:100) and phenylmethylsulfonyl fluoride (1:100) all purchased by Sigma-Aldrich (St. Louis, MI, USA), freshly added to lysis buffer. The extracted proteins were fractionated by SDS-PAGE and blotted onto nitrocellulose membrane using Trans-Blot Turbo Transfer System (BioRad, Hercules, CA). The membranes were decorated O.N. at 4°C with the following antibodies: rabbit polyclonal α AKT (Cat# 9272), rabbit monoclonal α pAKT^{Ser473} (Cat#4060), rabbit monoclonal α pS6 (Cat# 4858) and rabbit monoclonal α S6 (Cat# 2217) purchased from Cell Signalling Technology (Denvers, MA, USA) and goat polyclonal α Vinculin N-19 (Cat# sc-7649) purchased from Santa Cruz Biotechnology (Dallas, TX, USA), all antibodies were diluted 1:1000 as indicated in manufacturer 's protocols. Membranes were then incubated with HRP conjugated secondary antibodies (1:10000) and the chemo-luminescent signals have been revealed with ECL (Cat# 32106; Thermo Fisher Scientific; Waltham, MA, USA) using the ChemiDoc Touch Imaging System BioRad. For snap frozen PDX tissues, protein extraction was carry out in ice cold elution buffer (see details above) in combination with GentleMacs dissociators (Cat# 130-093-235) using M tubes (Cat# 130-094-392)

both purchased from Miltenyi Biotec (Bergisch Gladbach, Germany). Protein samples for western blot analysis were processed as described above.

3.7 Crystal Structure Analysis

The position of W624 residue in the structure of human p85 α encoded by PIK3R1 was predicted through sequence alignments and structure superimposition. Sequence alignments and domain assignment were performed using PSI-Blast (NCBI BLAST), whereas structure superimposition was performed using UCSF Chimera.

3.8 WES and CNA Analysis

Exome library preparation was performed using the Nextera Rapid Capture Enrichment kit from Illumina (San Diego, CA, USA). Genomic DNAs were quantified using the Qubit system Invitrogen (Carlsbad, CA, USA) and 50 ng were used as input material for library preparation. Pools of 12-plex libraries (500 ng each library) were hybridized with capture probes (coding exomes oligos) twice: a first hybridization step for 2 h and a second for 18 h. After elution and clean up, enriched DNA libraries were amplified with 10-cycle PCR. PCR products were then purified, loaded on a bioanalyser using DNA 1000 chip for quality control and quantified with Qubit. Samples were sequenced using the NextSeq 500 platform Illumina as paired 150 bp reads, using the NextSeq 500/550 High Output Kit v2, loading 1.4 pM DNA and obtaining as cluster density an average of 200 K/mm² clusters. Microarray HumanCytoSNP for CNA analysis was performed by Genomix4life S.R.L. (Baronissi, Salerno, Italy), using 200 ng of each DNA hybridized for 18 h at 48°C on HumanCytoSNP-12 v2.1 BeadChip, according to the manufacturer's instructions, and analyzed with an Illumina iSCAN. WES and SNP data analyses were performed using the pipeline shown in the figure below (Fig. 3.8.1), using each patient's germline DNA as reference.

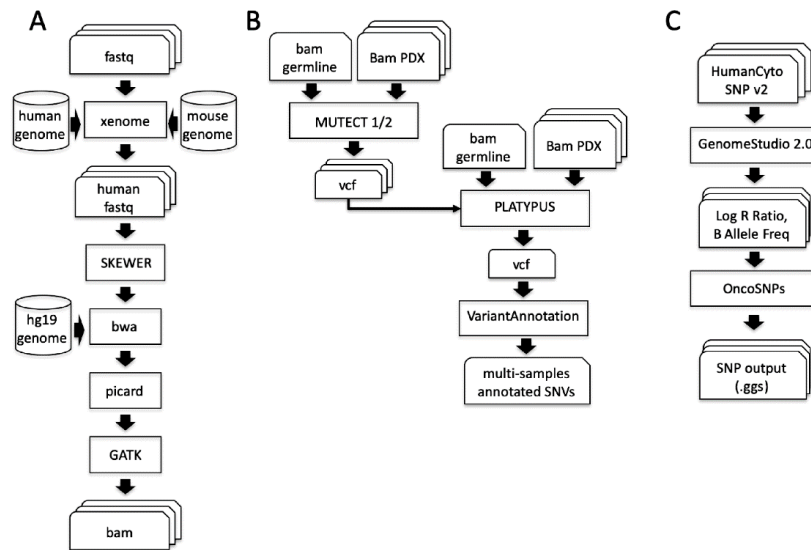


Fig. 3.8.1: Pipeline of WES and SNP array data analyses for the detection of SNV and CAN. (A) In order to exclude contaminating mouse read information in our analyses, WES reads derived from PDXs containing a mixture of human and mouse reads were separated using Xenome (version 1.0.0). Adaptor trimming was performed on human fastq files using skewer (version 0.2.2). Then human reads were mapped with BWA (version 0.7.12) onto the Human Reference Genome (hg19). Duplicated reads were removed with Picard suite (version 1.133). Indel realignment and quality recalibration was done with the Genome Analysis Toolkit (version 3.7-0-gcfe6b67). (B) SNVs and small insertion-deletions (indels) were called using MuTect1 (version 1.1.7), to increase sensitivity for somatic mutations. The somatic mutations identified were analyzed together to ensure comparable calls at every locus. Reads with mapping quality <30 and base quality <20 were discarded. Variants were only kept if they passed the standard Platypus filtering criteria, with the exceptions of variants showing allele bias and badreads to increase sensitivity. Variants were annotated using Variant Annotation Bioconductor package. (C) To estimate CAN, Log R ratio and B allele frequencies were calculated using Illumina GenomeStudio (version 2.0). OncoSNP (version 1.4) was then used.

3.9 Pyrosequencing Analysis

The presence and allele frequency of *TP53* and *PIK3R1* mutations in source tumors of any PDX line were assessed using pyrosequencing QIAGEN (Hilden, Germany). Briefly, sample DNAs were amplified, and the PCR products were subjected to the ‘sequence by synthesis’ pyrosequencing method following the manufacturer’s instructions, using the primers and conditions reported in table below (Tab. 3.9.1). Results were analyzed with the PSQ24 software (QIAGEN) for allelic quantification.

PRIMER	SEQUENCE 5'-3'	SIZE	PCR CONDITIONS
TP53 EX5 F	GGCCATCTACAAGCAGTCACA	90 bp	95°C 30 sec
TP53 EX5 R	(BIO)AGCTGCTCACCATCGCTATCT		58°C 30 sec
TP53 EX5 SEQ	GCACATGACGGAGGTT		72°C 45 sec
			95°C 3 min
			30 Cycles
			72°C 3 min
TP53 EX7 F	(BIO)CTCTGACTGTACCACCATCCACTA	115 bp	95°C 30 sec
TP53 EX7 R	GGCTCCTGACCTGGACTCTT		60°C 30 sec
TP53 EX7 R	GGTTCATGCCGCCCA		72°C 45 sec
			95°C 3 min
			30 Cycles
			72°C 3 min
PIK3R1 F	CTGGTGGAAGATGATGAAGATTTG	121 bp	95°C 30 sec
PIK3R1 F	(BIO)GGACAAGAAAAGTGCAATCTCG		60°C 30 sec
PIK3R1 SEQ	CCCATCATGATGAGAAG		72°C 45 sec
			95°C 3 min
			30 Cycles
			72°C 3 min

Tab. 3.9.1: Primers and PCR condition for pyrosequencing analyses

4. RESULTS

4.1 Characterization of PDX Lines from HGS-EOCs

Between 2012 and 2016 in the laboratory of Cancer Genetics, where I started my PhD in 2016, a PDX platform of ovarian carcinomas had been developed, collecting EOC samples at laparoscopy or at surgery, at the Candiolo Cancer Institute and the Sant'Anna gynecological Hospital of the "Città della Salute e della Scienza di Torino". Fresh samples, examined and selected by the pathologists, were implanted either subcutaneously or intra-peritoneum in severely immunocompromised NOD/shi-scid/IL-2R γ null female mice (see Methods section). Forty-three PDX lines derived from EOC samples were fully characterized, according to the minimal information standard for reporting PDX data, including clinical and pathological attributes of the patient's tumor, the processes of implantation and passaging in the host mouse strain and quality assurance by means of genotypic and phenotypic characterization¹⁵⁵. Quality assessment of samples and the clinical information were provided by the pathologists and are reported in table 4.1.1. This table reports also numbering of PDX lines derived from each tumor sample. Histological characterization was performed in order to classify tumor histotype and to compare the phenotype of the PDX to that of the corresponding source tumor (ST) (Fig. 4.1.2 and Tab. 4.1.3). This characterization was carried out using immunohistochemistry (IHC) on TMA sections and targeted next generation sequencing (T-NGS). For each sample the expression of CK7, EPCAM TP53, WT1, PAX8 as epithelial and tumor markers for HGS-EOC was evaluated. Expression of CD20 was also scrutinized to rule out the growth of lymphoma in PDXs, which occurs in 10–20% of cases¹⁵². The results obtained with IHC analyses confirmed the diagnosis of high-grade serous histology of 25 EOC-derived PDXs out of 43 successfully propagated and are reported in figure 4.1.2 and in table 4.1.3.

Patient Clinical information						PDX Information	
PATIENT ID (PROFILING)	AGE	CONSENT TO SHARE DATA	PRIMARY/METASTASIS/RECURRENCE	TISSUE HISTOLOGY	UNTREATED/TREATED	PDX ID	SITE
#0150	52	available to IRCCS only	metastasis/recurrence	HGS	treated	PDX#150	SC/IP
#0172	66	available to IRCCS only	metastasis/recurrence	HGS	treated	PDX#172	SC/IP
#0209	64	available to IRCCS only	metastasis/recurrence	clear cell	treated	PDX#209	SC/IP
#0474	73	available to IRCCS only	metastasis/recurrence	HGS	treated	PDX#474	SC/IP
#0475	75	available to IRCCS only	metastasis/primary	HGS	naive	PDX#475	SC/IP
#1622	72	available to IRCCS only	metastasis/recurrence	undifferentiated	treated	PDX#1622	SC/IP
#1658	65	available to IRCCS only	metastasis/recurrence	HGS	treated	PDX#1658	SC/IP
#1864	75	available to IRCCS only	metastasis/recurrence	HGS	treated	PDX#1864	SC/IP
#1897	67	available to IRCCS only	metastasis/recurrence	HGS	treated	PDX#1897	SC/IP
#1961	73	available to IRCCS only	primary	HG endometrioid	naive	PDX#1961	SC/IP
#1999	56	available to IRCCS only	primary	mucinous	naive	PDX#1999	SC/IP
#2085	66	available to IRCCS only	ascites/recurrence	HGS	treated	PDX#2085	IP
#2407	67	available to IRCCS only	ascites/primary	HGS	naive	PDX#2407	SC/IP
#2540	68	available to IRCCS only	primary	clear cell	naive	PDX#2540	SC/IP
#2547	56	available to IRCCS only	primary	HGS	treated NA-CHT	PDX#2547	SC/IP
#2699	52	available to IRCCS only	primary	HGS	naive	PDX#2699	SC
#2793	63	available to IRCCS only	primary	HGS	naive	PDX#2793	SC/IP
#2830	63	available to IRCCS only	metastasis/primary	HGS	treated NA-CHT	PDX#2830	SC/IP
#2834	59	available to IRCCS only	metastasis/primary	HGS	treated NA-CHT	PDX#2834	SC/IP
#2976	70	available to IRCCS only	metastasis/recurrence	HGS	treated	PDX#2976	SC/IP
#2991	55	available to IRCCS only	primary	HGS	treated	PDX#2991	SC/IP
#2995	54	available to IRCCS only	primary	LGS	treated NA-CHT	PDX#2995	SC
#3213	57	available to IRCCS only	metastasis/recurrence	HG pleiomorphic	treated	PDX#3213	IP
#3679	71	available to IRCCS only	metastasis/recurrence	HGS	treated	PDX#3679	SC
#3727	39	available to IRCCS only	metastasis/recurrence	borderline serous	treated	PDX#3727	SC
#3915	53	available to IRCCS only	primary	clear cell	treated NA-CHT	PDX#3915	SC
#3982	54	available to IRCCS only	metastasis/recurrence	HGS	treated	PDX#3982	SC
#SAN05	56	available to IRCCS only	primary	HG pleiomorphic	naive	PDX#SAN05	SC/IP
#SAN06	76	available to IRCCS only	primary	HGS	naive	PDX#SAN06	SC/IP
#SAN08	59	available to IRCCS only	primary	HGS	naive	PDX#SAN08	SC/IP
#SAN09	38	available to IRCCS only	primary	HG endometrioid	naive	PDX#SAN09	SC/IP
#SAN12	58	available to IRCCS only	primary	HGS	naive	PDX#SAN12	SC
#SAN20	76	available to IRCCS only	primary	HGS	treated NA-CHT	PDX#SAN20	SC/IP
#SAN21	67	available to IRCCS only	primary	HGS	naive	PDX#SAN21	SC/IP
#SAN24	70	available to IRCCS only	pleural effusion/recurrence	unknown	treated NA-CHT	PDX#SAN24	IP
#SAN25	57	available to IRCCS only	metastasis/primary	HGS	naive	PDX#SAN25	SC/IP
#SAN31	73	available to IRCCS only	metastasis/recurrence	undifferentiated	treated NA-CHT	PDX#SAN31	SC
#SAN37	57	available to IRCCS only	primary	HG endometrioid	naive	PDX#SAN37	SC/IP
#SAN40	75	available to IRCCS only	metastasis/primary	HGS	naive	PDX#SAN40	SC/IP
#SAN44	53	available to IRCCS only	metastasis/primary	undifferentiated	naive	PDX#SAN44	SC/IP
#SAN46	62	available to IRCCS only	primary	mucinous	naive	PDX#SAN46	SC/IP
#SAN47	69	available to IRCCS only	primary	clear cell	naive	PDX#SAN47	SC
#SAN60	78	available to IRCCS only	primary	clear cell	naive	PDX#SAN60	SC

Tab. 4.1.1: Patients' clinical information. Table shows the clinical information of the collected tumor samples. In the first column on the left is reported the ID of each samples according to the PROFILING protocol (see the Method section). In the last two columns on the right are reported the ID of each PDX line derived from the corresponding tumor and the site in which human samples were implanted in mice. Acronyms legend: SC= subcutaneous; IP= Intra-peritoneum; NA-CHT= Neo-adjuvant Chemotherapy

In particular figure 4.1.2 shows representative images of the IHC staining performed on TMA sections, whereas table 4.1.3 reports the histological characterization for all the 43 samples. In this table the expression of the above mentioned markers for each sample is indicated. All the morphological and genetic analyses were carried out within three passages of each PDX line. The maintenance of the phenotype of the source tumor during PDXs propagation was confirmed also by the analyses of further passages of the same PDX line. The genotypic characterization performed using T-NGS for *TP53* and *BRCA1* and *BRCA2* genes (Tab. 4.1.4) confirmed the presence of *TP53* mutation in all PDXs derived from HGS-EOCs according to the concept that *TP53* is a driver and trunk mutation in this tumor subtype. Moreover, T-NGS data of *BRCA1/2* genes showed that about 19% of our PDX lines carry mutations in *BRCA1/2* which is close to the expected frequency according to the *BRCA* mutation database (<http://arup.utah.edu/database/BRCA>). Table 4.1.4 refers to the specific mutations in *TP53* and *BRCA1/2* genes for each sample and the corresponding allele frequencies.

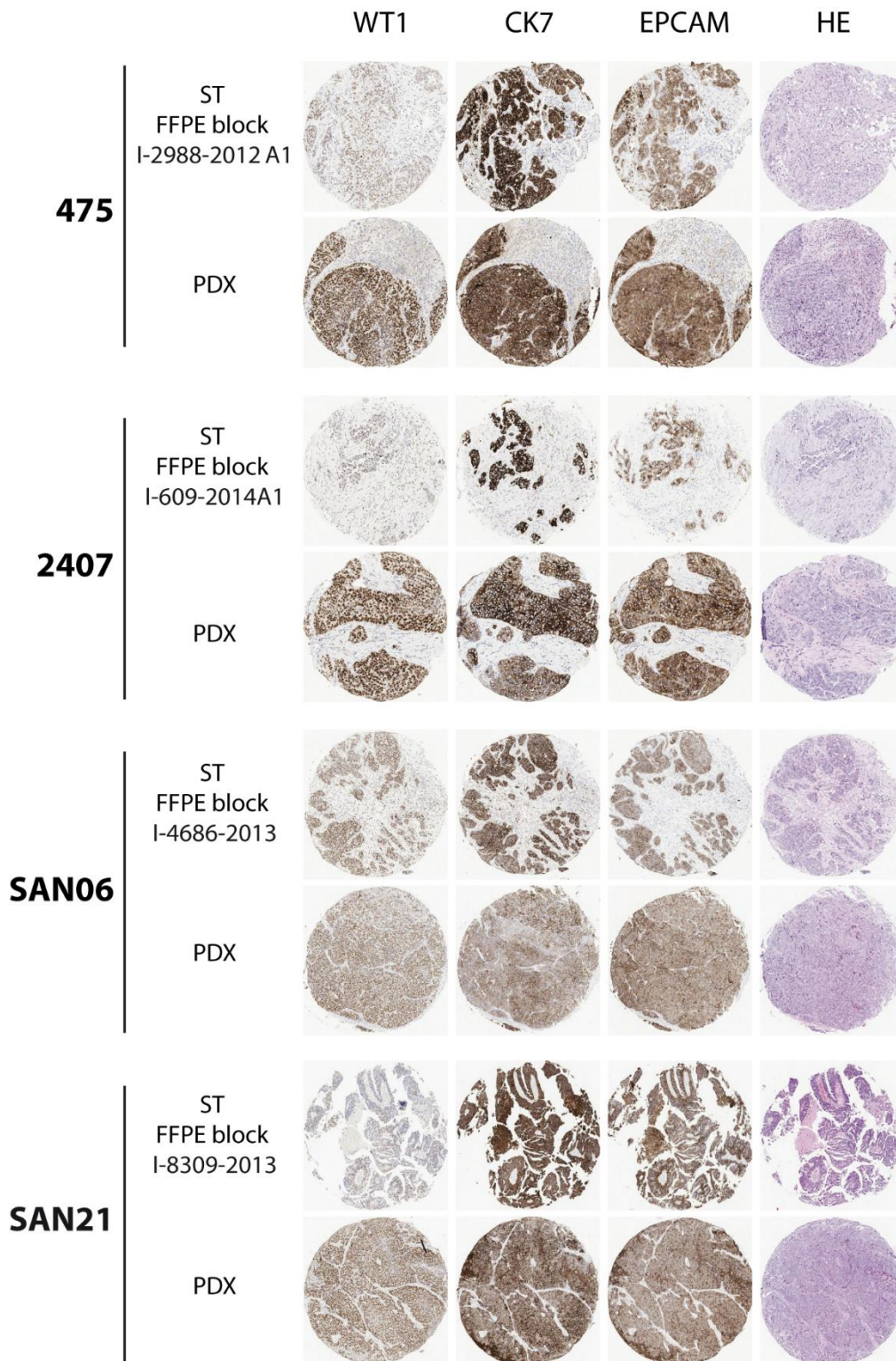


Fig. 4.1.2: Representative images of IHC analyses of TMAs. This figure shows the expression levels of the HGS-EOC markers in PDX and in the corresponding source tumors (ST). On the top are indicated the studied markers, whereas the numbers in bold on the left represent the ID assigned by PROFILING protocol to each PDX sample. For each corresponding ST, the ID number of the FFPE block is shown.

TMA characterization						
SAMPLE ID	PASSAGE QA PERFORMED	CK7	WT1	EPCAM	TP53	CD20
#0150	1	pos	pos	pos	pos	neg
#0172	1	pos	pos	pos	pos	neg
#0209	1	pos	ND	pos	ND	neg
#0474	2 (SC)	pos	pos	pos	pos	neg
#0475	1	pos	pos	pos	pos	neg
#1622	1	pos	pos	pos	pos	neg
#1658	2	pos	pos	pos	pos	neg
#1864	2	pos	pos	pos	pos	neg
#1897	2	pos	pos	pos	pos	neg
#1961	2 (SC)	pos	pos	pos	neg	neg
#1999	1	pos	neg	pos	neg	neg
#2085	2 (SC)	pos	pos	pos	pos	neg
#2407	2 (SC)	pos	pos	pos	pos	neg
#2540	1	pos	neg	pos	pos	neg
#2547	2	pos	pos	pos	pos	neg
#2699	1	neg	pos	neg	neg	neg
#2793	1	pos	pos	pos	pos	neg
#2830	2	pos	pos	ND	neg	neg
#2834	2	pos	pos	pos	pos	neg
#2976	1	pos	pos	pos	pos	neg
#2991	2	pos	neg	pos	neg	neg
#2995	2 (SC)	pos	pos	ND	pos	neg
#3213	2 (SC)	pos	ND	pos	ND	neg
#3679	1	pos	pos	pos	neg	neg
#3727	1	neg	ND	pos	ND	neg
#3915	1	pos	neg	pos	neg	neg
#3982	1	pos	pos	pos	neg	neg
#SAN05	3	pos	pos	pos	pos	neg
#SAN06	2	pos	pos	pos	pos	neg
#SAN08	1	pos	pos	pos	pos	neg
#SAN09	2	pos	neg	pos	pos	neg
#SAN12	1	pos	pos	pos	neg	neg
#SAN20	2 (SC)	pos	neg	ND	neg	neg
#SAN21	2 (SC)	pos	pos	pos	pos	neg
#SAN24	1	pos	pos	ND	pos	neg
#SAN25	2 (SC)	pos	pos	pos	pos	neg
#SAN31	2 (SC)	pos	pos	ND	pos	neg
#SAN37	1	pos	pos	pos	neg	neg
#SAN40	1	pos	pos	pos	pos	neg
#SAN44	1	pos	pos	pos	neg	neg
#SAN46	1	pos	neg	pos	pos	neg
#SAN47	1	pos	neg	pos	pos	neg
#SAN60	1	pos	ND	pos	ND	neg

Tab. 4.1.3: Histological characterization of 43 PDX lines of the platform. This table reports the results of the expression markers of HGS-EOCs and for CD20 scrutinized to rule out the growth of lymphomas in PDXs. ID number of each PDX line is reported on the first column on the left and the next column shows the PDX passage in which characterization has been performed.

Targeted-NGS (T-NGS) characterization

SAMPLE ID	TP53	TP53 AF	BRCA1	BRCA1 AF	BRCA2	BRCA2 AF
#0150	p.Y220C	0.997	VUS		WT	
#0172	p.R273C	0.999	WT		WT	
#0209	ND	ND	ND	ND	ND	ND
#0474	p.C238S	0.999	WT		WT	
#0475	p.V173L	0.988	WT		WT	
#1622	p.C141Y	0.999	WT		p.T219f; c.656CTG>G	1
#1658	p.I195T	0.998	WT		WT	
#1864	p.V173L	0.988	WT		WT	
#1897	c.990_993+16delTCAGGTACTAAGTCTTGG GA	1	WT		WT	
#1961	c.920-1G>A	0.986	WT		WT	
#1999	ND	ND	ND		ND	
#2085	p.R273H	0.996	WT		g. p.E1879f; c.5637GAATA>G	0.976
#2407	p.R273H	0.998	WT		WT	
#2540	ND	ND	ND	ND	ND	ND
#2547	p.C176W	0.998	WT		g. p.E1879f; c.5637GAATA>G	0.999
#2699	p.E198*	0.999	WT		WT	
#2793	p.G262D	0.998	WT		WT	
#2830	c.393-1GA>G	0.998	WT		WT	
#2834	p.Y126C	0.984	p.C24f	0.994	WT	
#2976	ND	ND	ND	ND	ND	ND
#2991	ND	ND	ND	ND	ND	ND
#2995	ND	ND	ND	ND	ND	ND
#3213	p.K132R	1	p.R1203*	1	WT	
#3679	ND	ND	ND	ND	ND	ND
#3727	WT		WT		WT	
#3915	WT		VUS		WT	
#3982	ND	ND	ND	ND	ND	ND
#SAN05	p.C275Y	1	WT		p.T219f; c.656CTG>G	0.999
#SAN06	p.Y234C	0.993	WT		VUS	
#SAN08	p.S127F	1	VUS		WT	
#SAN09	p.S127F	1	WT		WT	
#SAN12	c.97-2A>T	0.994	WT		WT	
#SAN20	p.R273H	0.923	VUS		WT	
#SAN21	p.Q167*	0.982	WT		WT	
#SAN24	p.R174S	0.996	WT		WT	
#SAN25	p.V173L	0.988	VUS		WT	
#SAN31	WT		VUS		WT	
#SAN37	c.1163_1170delAAGGGCCT	1	WT		WT	
#SAN40	p.I195T	0.962	WT		WT	
#SAN44	c.393-1GA>G	0.993	WT		VUS	
#SAN46	ND	ND	ND	ND	ND	ND
#SAN47	ND	ND	ND	ND	ND	ND
#SAN60	ND	ND	ND	ND	ND	ND

Tab. 4.1.4: Genotypic characterization of the 43 PDX lines. T-NGS analysis of *TP53* and *BRCA1/2*. For each sample the specific mutation of the analyzed genes and the allele frequency (AF) are reported. VUS= Variant of Unknown Significance.

4.2 WES and CNAs Analyses of Selected PDX Lines

Starting from the results obtained after sample characterization, 12 PDX lines derived from treatment naïve HGS-EOCs have been selected for further investigation. Table 4.2.1 lists the selected PDX lines with tumor characteristics and the patients' clinical information.

Patients Clinical Information												
ID PDX LINE	AGE	DISEASE STATUS AT SAMPLING	TREATMENT STATUS AT SAMPLING	SURGERY	BASELINE CA125 AT DIAGNOSIS	TUMOR RESIDUE	1st LINE CHEMO-THERAPY	RESPONSE TO 1st LINE TREATMENT	PFI	TOTAL CHE-MOTHERAPY LINES n°	OTHER LINES	CURRENT DI-SEASE STATUS
#475	75	primary	naive	ID ^a	unknown	≥1 cm	carboplatin	resistant	6 months	2	carboplatin + PLD ^b	deceased
#2407	67	primary	naive	ID ^a	1300	≥1 cm	carboplatin + paclitaxel	resistant	4 months	2	carboplatin + PLD ^b	deceased
#2547	56	primary	naive	ID ^a	1382	0	carboplatin + paclitaxel	sensitive	0	1	0	alive, no evidence of disease
#2699	52	primary	naive	upfront	1571,8	≥1 cm	carboplatin + paclitaxel	resistant	5 months	2	cyclophosphamide	deceased
#2793	63	primary	naive	upfront	88	0	carboplatin + cyclophosphamide	resistant	5 months	2	trabectedin, PLD ^b	deceased
#SAN05	56	primary	naive	upfront	468	0	Carboplatin + Cyclophosphamide	partially sensitive	11 months	3	etoposide	deceased
#SAN06	76	primary	naive	ID ^a	448	0	carboplatin + paclitaxel + trebananib	resistant	5 months	4	3 cycles PLD ^b + trabectedin	deceased
#SAN08	59	primary	naive	upfront	943	0	carboplatin + paclitaxel	partially sensitive	10 months	8	carboplatin-PLD ^b , carboplatin-paclitaxel, cisplatin, trabectedin, topotecan, etoposide	alive with disease
#SAN09	38	primary	naive	upfront	641	0	lost at follow-up	Unknown	Unknown	Unknown	Unknown	Unknown
#SAN12	58	primary	naive	upfront	1127	0	carboplatin + paclitaxel	resistant	4 months	lost at follow-up	Unknown	deceased
#SAN21	67	primary	naive	upfront	1988	≥1 cm	carboplatin + paclitaxel	resistant	4 months	2	PLD ^b + trabectedin	deceased
#SAN37	57	primary	naive	upfront	>10,000	≥1 cm	carboplatin + paclitaxel + bevacizumab	resistant	6 months	3	2 cycles PLD ^b	deceased

Tab. 4.2.1: Clinical information and clinical course of patients whose tumors have been propagated as the 12 PDX lines selected for in depth-analyses: patients' clinical information, therapy administered and patients' clinical course. All the PDX lines selected derived from HGS-EOCs naïve primary tumors.

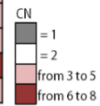
In order to identify possible drivers and actionable genetic aberrations in these 12 PDX lines, attention was focused on SNVs and copy number alterations (CNAs) affecting cancer-related genes reported in COSMIC ¹⁵⁶. Thus, Whole Exome Sequencing (WES) was performed which detected 2743 SNVs in 2314 genes. The results obtained using WES were compared with TCGA data and we found that 79% of mutated genes in our PDXs were reported to be mutated also in TCGA analysis of 523 HGS-EOCs. Moreover, the mutated genes which were not reported by TCGA (438/487), were listed as mutated genes in other cancer histotype according to Pan-

Cancer Atlas ^{157,158}. WES analysis showed that the only mutated gene across the all selected 12 PDX lines was *TP53* with an allele frequency approximately =1.0 according to the occurrence of loss of heterozygosity (LOH).

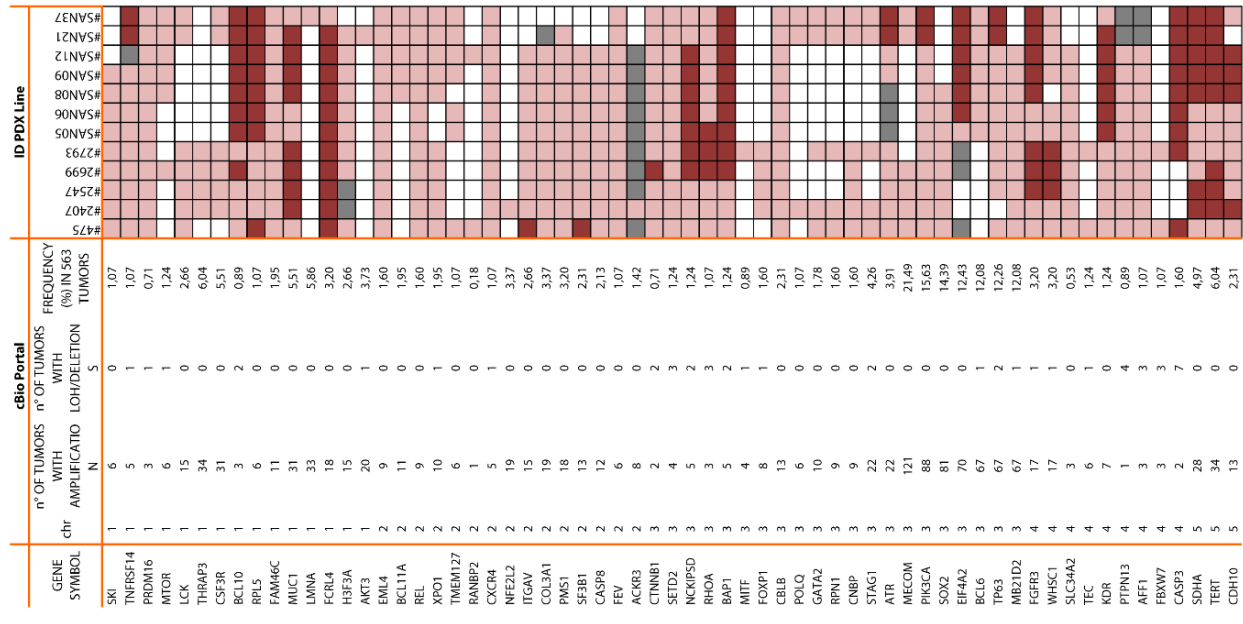
Analysis of Copy Number Alterations of the 12 selected PDXs showed that those detected in cancer genes corresponded to those reported in TCGA.

Interestingly, although only a small series was examined, the expected frequency of increased copy number of *CCNE1* (≈19%) and *PIK3CA* (≈20%) was found (Tab. 4.2.2). Furthermore, copy number alterations analyses confirmed the LOH of the *TP53* gene in each of the PDX lines (Tab. 4.2.3).

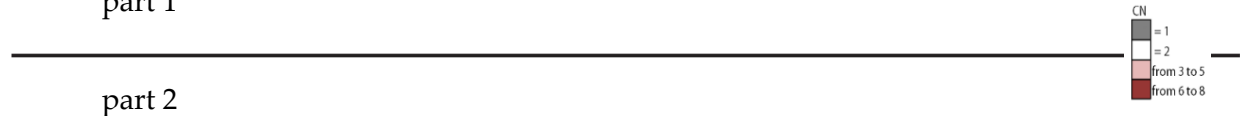
GENE SYMBOL	cBioPortal				ID PDX line											
	CYTOBAND	CNV	# SAMPLE	% FREQ	#475	#2407	#2547	#2699	#2793	#SAN05	#SAN06	#SAN08	#SAN09	#SAN12	#SAN21	#SAN37
MYC	8q24.21	AMP	190	33,22%	NA	NA	NA	NA	NA	NA	NA	NA	NA	NA	NA	NA
NDRG1	8q24.22	AMP	165	28,85%	NA	NA	NA	NA	NA	NA	NA	NA	NA	NA	NA	NA
AGO2	8q24.3	AMP	159	27,80%	NA	NA	NA	NA	NA	NA	NA	NA	NA	NA	NA	NA
MECOM	3q26.2	AMP	159	27,80%	NA	NA	NA	NA	NA	NA	NA	NA	NA	NA	NA	NA
PTK2	8q24.3	AMP	159	27,80%	NA	NA	NA	NA	NA	NA	NA	NA	NA	NA	NA	NA
EPPK1	8q24.3	AMP	155	27,10%	NA	NA	NA	NA	NA	NA	NA	NA	NA	NA	NA	NA
PLEC	8q24.3	AMP	155	27,10%	NA	NA	NA	NA	NA	NA	NA	NA	NA	NA	NA	NA
RECQL4	8q24.3	AMP	153	26,75%	NA	NA	NA	NA	NA	NA	NA	NA	NA	NA	NA	NA
PRKCI	3q26.2	AMP	139	24,30%	NA	NA	NA	NA	NA	NA	NA	NA	NA	NA	NA	NA
EXT1	8q24.11	AMP	132	23,08%	NA	NA	NA	NA	NA	NA	NA	NA	NA	NA	NA	NA
RAD21	8q24.11	AMP	122	21,33%	NA	NA	NA	NA	NA	NA	NA	NA	NA	NA	NA	NA
TBL1XR1	3q26.32	AMP	119	20,80%	NA	NA	NA	NA	NA	NA	NA	NA	NA	NA	NA	NA
PIK3CA	3q26.32	AMP	116	20,28%	NA	NA	NA	NA	NA	NA	NA	NA	NA	NA	NA	NA
CCNE1	19q12	AMP	112	19,58%	NA	NA	NA	NA	NA	NA	NA	NA	NA	NA	NA	NA
EPHB3	3q27.1	AMP	107	18,71%	NA	NA	NA	NA	NA	NA	NA	NA	NA	NA	NA	NA
SOX2	3q26.33	AMP	105	18,36%	NA	NA	NA	NA	NA	NA	NA	NA	NA	NA	NA	NA
DCUN1D1	3q26.33	AMP	104	18,18%	NA	NA	NA	NA	NA	NA	NA	NA	NA	NA	NA	NA
KLHL6	3q27.1	AMP	104	18,18%	NA	NA	NA	NA	NA	NA	NA	NA	NA	NA	NA	NA
MAP3K13	3q27.2	AMP	103	18,01%	NA	NA	NA	NA	NA	NA	NA	NA	NA	NA	NA	NA
ETV5	3q27.2	AMP	99	17,31%	NA	NA	NA	NA	NA	NA	NA	NA	NA	NA	NA	NA
FGF12	3q28-q29	AMP	97	16,96%	NA	NA	NA	NA	NA	NA	NA	NA	NA	NA	NA	NA
EIF4A2	3q27.3	AMP	94	16,43%	NA	NA	NA	NA	NA	NA	NA	NA	NA	NA	NA	NA
LPP	3q27.3-q28	AMP	94	16,43%	NA	NA	NA	NA	NA	NA	NA	NA	NA	NA	NA	NA
TFRC	3q29	AMP	93	16,26%	NA	NA	NA	NA	NA	NA	NA	NA	NA	NA	NA	NA
RPL35A	3q29	AMP	92	16,08%	NA	NA	NA	NA	NA	NA	NA	NA	NA	NA	NA	NA
TP63	3q28	AMP	91	15,91%	NA	NA	NA	NA	NA	NA	NA	NA	NA	NA	NA	NA
BCL6	3q27.3	AMP	90	15,73%	NA	NA	NA	NA	NA	NA	NA	NA	NA	NA	NA	NA
RSP02	8q23.1	AMP	90	15,73%	NA	NA	NA	NA	NA	NA	NA	NA	NA	NA	NA	NA
BRD4	19p13.12	AMP	69	12,06%	NA	NA	NA	NA	NA	NA	NA	NA	NA	NA	NA	NA
NOTCH3	19p13.12	AMP	68	11,89%	NA	NA	NA	NA	NA	NA	NA	NA	NA	NA	NA	NA
TPM4	19p13.12-p13.11	AMP	65	11,36%	NA	NA	NA	NA	NA	NA	NA	NA	NA	NA	NA	NA
DNAJB1	19p13.12	AMP	64	11,19%	NA	NA	NA	NA	NA	NA	NA	NA	NA	NA	NA	NA
TSHZ3	19q12	AMP	64	11,19%	NA	NA	NA	NA	NA	NA	NA	NA	NA	NA	NA	NA
LYL1	19p13.13	AMP	63	11,01%	NA	NA	NA	NA	NA	NA	NA	NA	NA	NA	NA	NA
COX6C	8q22.2	AMP	58	10,14%	NA	NA	NA	NA	NA	NA	NA	NA	NA	NA	NA	NA



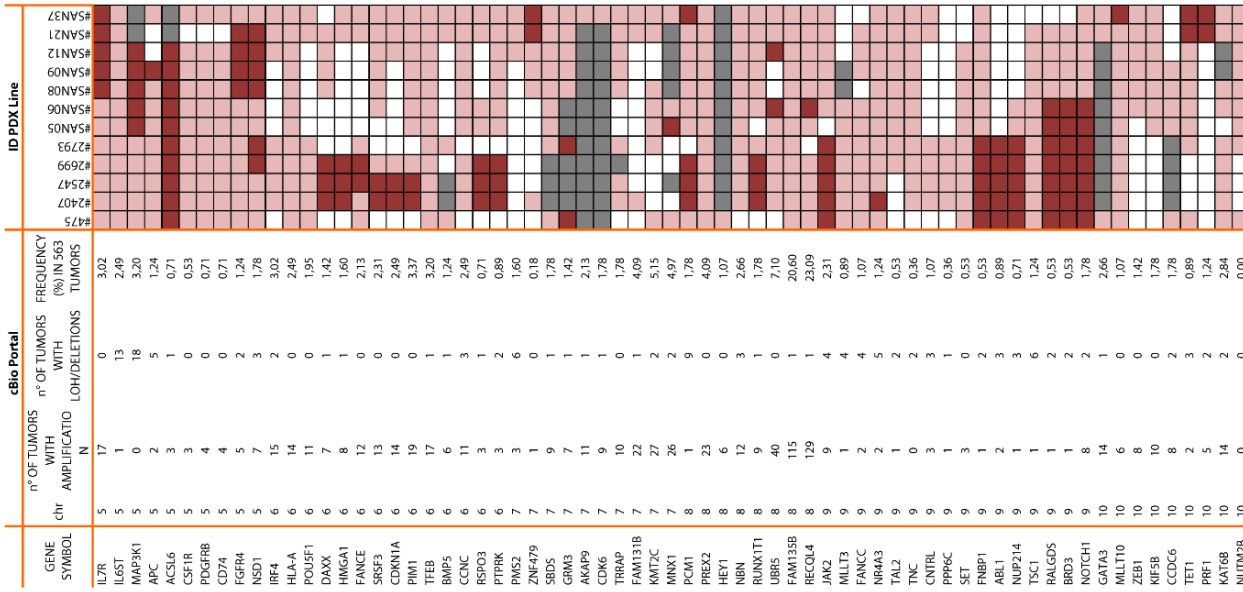
Tab. 4.2.2: CNAs detected in cancer genes in the 12 PDX lines selected. This table show the results of the CNAs analysis in the 12 PDX lines studied in-depth compared to CNAs of the genes found amplified in more than 10% of the HGS-EOCs reported in TCGA. On the bottom right color legend for copy number.



part 1



part 2



4.3 Identification of Possible Drivers and Actionable Mutations

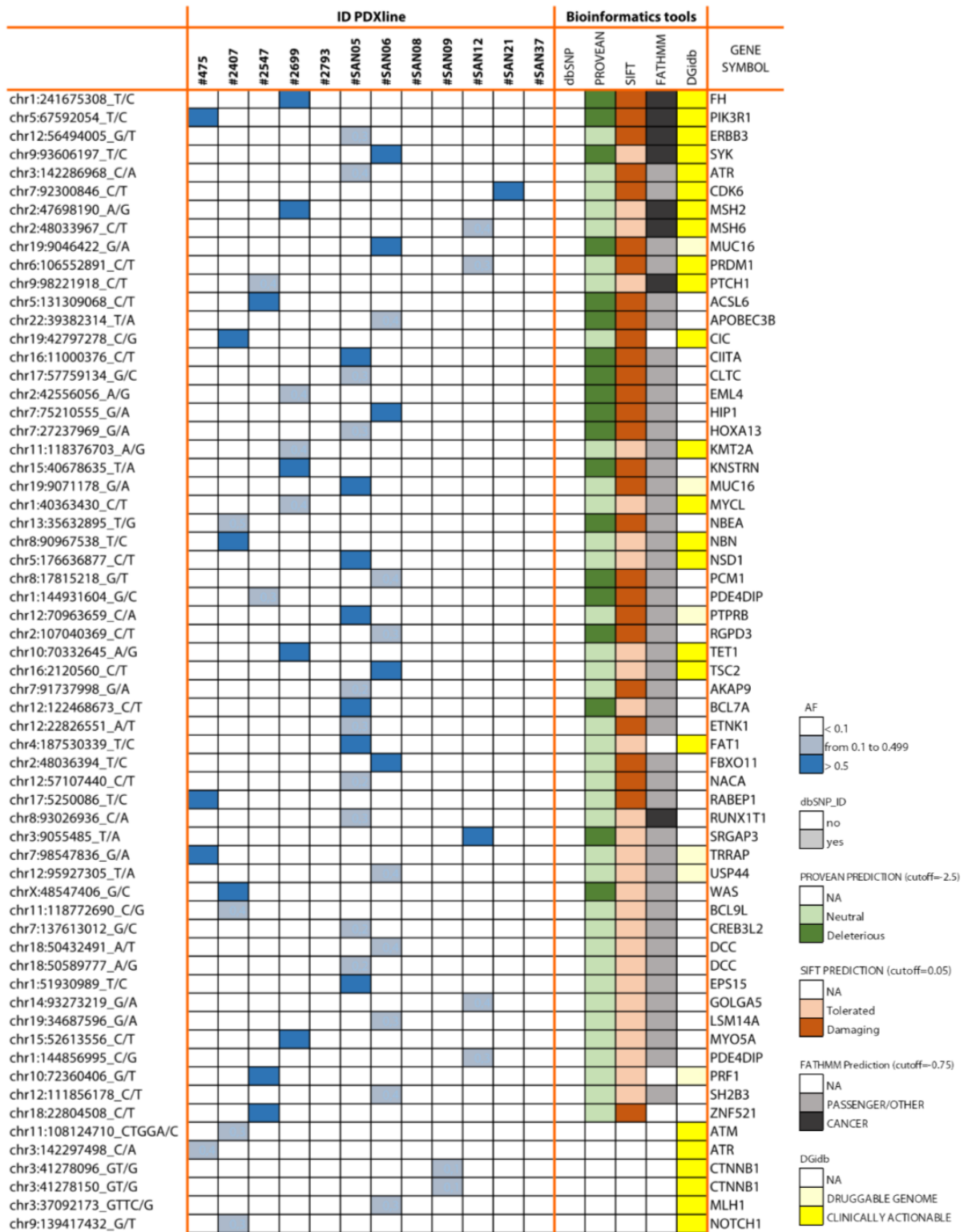
Among the SNVs identified by WES only the somatic ones, with an allele frequency equal or greater than 0.1, affecting cancer-related genes reported in COSMIC were taken into account and were analyzed using bioinformatics first:

- 1) SNPs were ruled out using a SNP database (dbSNP, <https://www.ncbi.nlm.nih.gov/snp>).
- 2) The possible impact of the selected SNVs on the function of the protein encoded by the relevant genes was carried out using the following bioinformatics tools: PROVEAN, SIFT and FATHMM¹⁵⁹. PROVEAN and SIFT are two aligned-based methods and predict the functional effects of amino-acid substitutions, insertions or deletions^{160,161}. FATHMM predicts the functional consequences of both coding and non-coding variants in the human genome exploiting the Hidden Markov Models¹⁶².
- 3) The actionability was considered using the Drug Genome Interaction database (DGidb, <http://dgidb.org/>)¹⁶³.

These analyses showed that in 3/12 PDX lines (#2793, #SAN08 and #SAN37) there were no mutations in cancer-related genes other than those detected in *TP53*; in the remaining 9/12 PDX lines only some somatic mutations have been predicted to be damaging and/or deleterious by PROVEAN, SIFT and FATHMM (Tab. 4.3.1).

In the #475 PDX line these analyses identified a possible driver and actionable point mutation in the *PIK3R1* gene, resulting in the W624R amino-acid residue substitution in the encoded protein p85 α , that is the regulatory subunit of the PI3K enzyme. Indeed, p85 α mutations might result in damages of physiological and pathological processes, through the activation of PI3K pathway *via* distinct molecular mechanisms. The *PIK3R1* mutation in the #475 PDX line has an allele frequency approximately =1.0, suggesting a loss of function mutation followed by LOH, in accordance with the oncosuppressor role of this gene. It is worth mentioning that the genetic analyses of PDXs allows the identification of genetic alteration in

pure human tissue, as the human stromal component of samples is fully substituted by the murine one no more than 3 passages.



	ID PDXline												Bioinformatics tools					GENE SYMBOL
	#475	#2407	#2547	#2699	#2793	#SAN05	#SAN06	#SAN08	#SAN09	#SAN12	#SAN21	#SAN37	dbSNP	PROVEAN	SIFT	FATHMM	DGidb	
chr3:121208936_A/C																		POLQ
chr8:145737068_GC/G																		RECQL4
chr17:78264463_AGAG/A																		RNF213
chr3:9106146_C/T																		SRGAP3
chr16:27414525_G/A																		IL21R
chr9:5522575_TG/T																		PDCD1LG2
chr7:91603264_G/T																		AKAP9
chr7:91670136_G/A																		AKAP9
chr8:1905131_C/T																		ARHGEF10
chr2:215593522_T/C																		BARD1
chr19:45260971_G/T																		BCL3
chr15:91326099_C/T																		BLM
chr15:91341520_G/A																		BLM
chr15:91354521_G/A																		BLM
chr7:2962848_G/A																		CARD11
chr2:202122956_T/C																		CASP8
chr3:105421032_C/G																		CBLB
chr19:45297479_C/T																		CBLC
chr19:42383351_G/A																		CD79A
chr13:28542699_C/A																		CDX2
chr9:123929920_G/A																		CNTRL
chr13:49281554_A/G																		CYSLTR2
chr22:41574383_A/C																		EP300
chr17:41606922_T/C																		ETV4
chr3:10081411_A/G																		FANCD2
chr13:28608473_C/T																		FLT3
chr13:28623587_C/T																		FLT3
chr5:180030221_C/T																		FLT4
chr14:93263964_C/T																		GOLGA5
chr15:45848153_C/T																		HMG2P46
chr2:176958235_A/G																		HOXD13
chr8:42174380_G/A																		IKBKB
chr7:151859683_G/A																		KMT2C
chr7:151879358_G/C																		KMT2C
chr5:56155618_A/G																		MAP3K1
chr3:185191196_G/A																		MAP3K13
chr19:9011412_C/T																		MUC16
chr19:9028306_C/G																		MUC16
chr19:9068374_A/G																		MUC16
chr19:9068458_A/T																		MUC16
chr19:9071562_C/T																		MUC16
chr22:36681797_C/T																		MYH9
chr13:36158038_A/G																		NBEA
chr8:90993640_C/T																		NBN
chr20:50092091_G/A																		NFATC2
chr20:50092185_T/C																		NFATC2
chr8:32621630_C/T																		NRG1
chr15:34648935_G/T																		NUTM1
chr7:6026607_T/A																		PMS2
chr7:6026865_T/C																		PMS2
chr12:133202740_C/T																		POLE
chr12:133202816_C/T																		POLE
chr20:41420095_T/C																		PTPRT
chr2:109356978_G/C																		RANBP2
chrX:47041666_G/C																		RBM10
chr3:181430391_T/G																		SOX2
chr2:37111123_G/A																		STRN
chr5:1254594_C/T																		TERT
chr9:135779052_G/A																		TSC1
chr15:50763945_T/A																		USP8
chr3:149374873_G/T																		WWTR1
chr19:54080067_T/C																		ZNF331
chr22:29444445_C/A																		ZNRF3

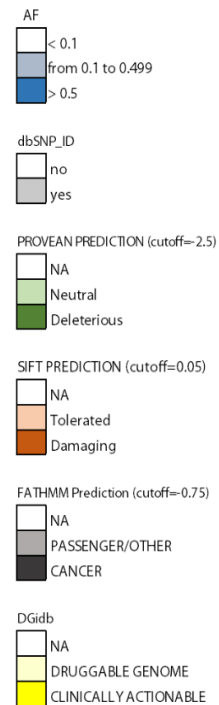


Fig. 4.3.1: SNVs in cancer-related genes found in the selected 12 PDX lines derived from naïve HGS-EOCs using WES. Table is divided in two pages. All mutations reported have an allele frequency ≥ 0.1 . On the left, the mutated sequence for each gene is indicated. On the right the results of the bioinformatics analyses performed with PROVEAN, SIFT and FATHMM, and the screening obtained with DGidb and dbSNP. Color legend is reported on the bottom right.

4.4 Study of PIK3R1^{W624R} Mutation Outcome: Structure-based Approach

As mentioned above, bioinformatics analysis (Tab. 4.3.1) showed that PIK3R1^{W624R} is predicted as deleterious and damaging by all three used software and possibly actionable by the DGIdb. As reported in literature and mentioned in the Introduction (see paragraph 1.5), the p85 subunit is not a kinase itself and its functions are mediated by the interaction with protein partners, among which the best known are the p110 PI3K subunits. The W624R amino acid substitution is in the cSH2 domain. The structure of p85 α consists in several domains which are differently involved in the interactions with protein partners. In particular, nSH2 and iSH2 are two domains involved in the interactions with p110 α ; BH domain is supposed to be involved in p85 α homodimerization and/or PTEN interactions; conversely the function of SH3 and cSH2 domains is still not completely understood (Fig 4.4.1).

Mutations in *PIK3R1* are very common across cancer lineages, but less common in ovarian cancer, and several hotspot regions have been identified. Among these, the most studied are those in domains involved in the binding with p110 α ¹¹². In figure 4.4.1 p85 α domains are depicted and the most frequent mutations detected in cancer are highlighted.

To better understand the potential role of PIK3R1^{W624R} as driver in the #475 PDX line and its role in protein function we decided to use a structure-based approach in collaboration with a crystallography expert. The possible role of the W624R mutation in the interaction between p85 α with p110 α was studied exploiting the known crystal structure of PI3K subunits (Fig 4.4.2). Regrettably, only the crystal structure of human p110 α in complex with nSH2 and iSH2 domains of p85 α is available in protein databank (PDB ID 4L1B) and not in complex with the cSH2 domain in which the W624R is located.

Hence, we explored the possible role of the amino-acid residue homologue to the W624 in mouse p85 being available the crystal structure of mouse p110 β isoform in complex with iSH2 and cSH2 domains of mouse p85 β isoform (PDB ID 2Y3A, Fig. 4.4.2 (C)). Structure superimposition showed that mouse p85 β shares common folds with the human p85 α

counterpart. Sequence alignments demonstrated that human p85 α and mouse p85 β display 73% homology and 59% identity, whereas human p110 α and mouse p110 β sequences have 57% homology and 40% identity, respectively.

According to sequence alignment (Fig. 4.4.2 (D)), the W624 in the human p85 α corresponds to W616 in the mouse cSH2 domain of p85 β . The comparison showed that the W616 in the cSH2 domain of mouse p85 β is not involved in the interaction between murine p85 β and p110 β . Thus, the structure-based approach did not help in predicting the possible role of the W624R mutation in PIK3R1.

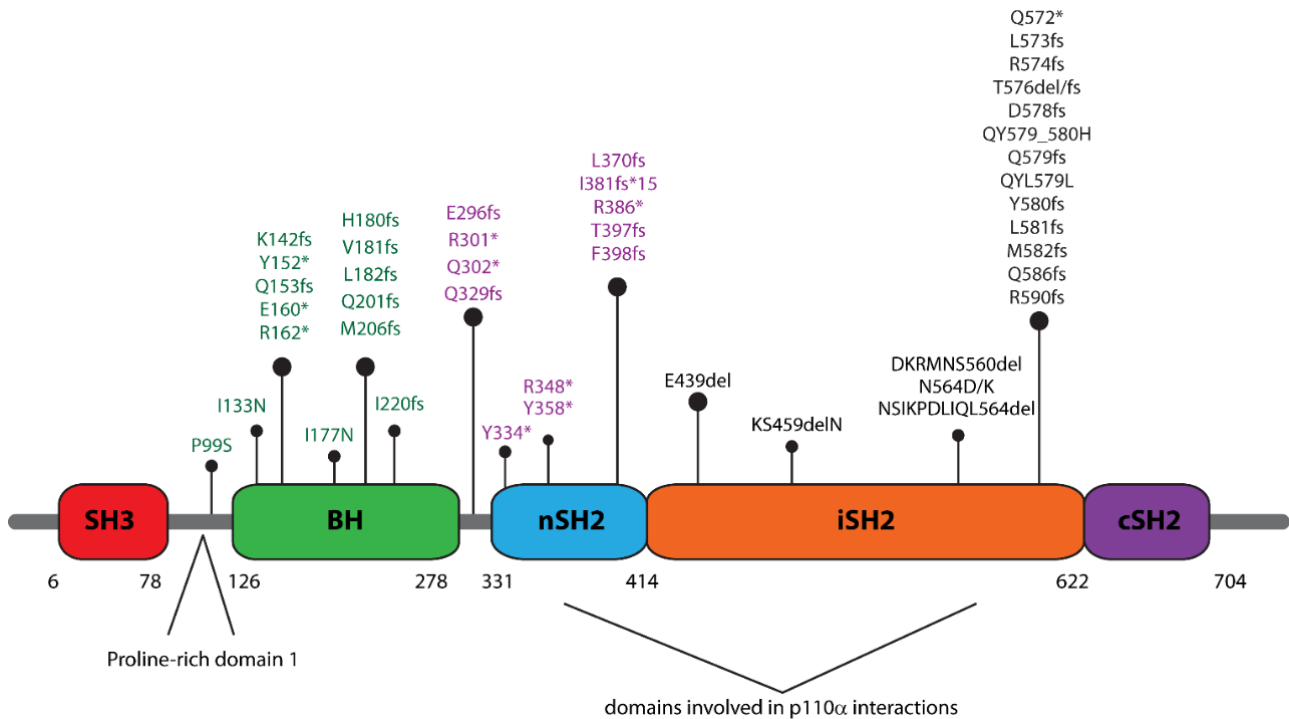


Fig. 4.4.1: PIK3R1 protein primary structures and domains. In this figure the domains of p85 α are depicted with the most frequent mutations detected in cancer. In green are reported mutations which could be involved in p85 α homodimerization and/or PTEN interactions; in purple are shown neomorphic mutations which could activate MAPK signaling pathway (see Introduction, paragraph 1.5); in black are mutations which impair the interactions with p110 α . For data about mutations localization see reference [11].

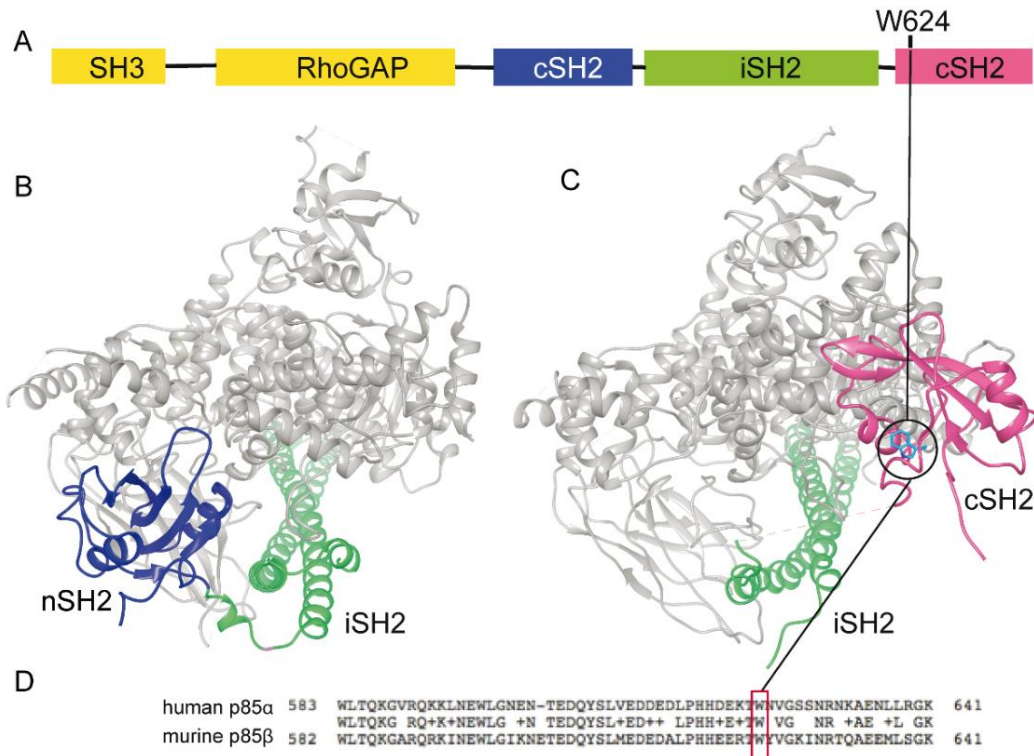


Fig. 4.4.2: Crystal structure of p110 α complexed with the p85 α subunit in human PI3K. (A) Domain organization of p85 α . (B) Available crystal structure (PDB ID 4L1B) of human p110 α isoform with catalytic activity (grey) complexed with nSH2 (blue) and iSH2 (green) domains of human p85 α ; (C) available crystal structure (PDB ID 2Y3A) of mouse p110 β in complex with iSH2 (green) and cSH2 (pink) domains of mouse p85 β ; (D) Alignment of the cSH2 domains of human p85 α and mouse p85 β ; homology is shown in the middle: W624 the human p85 α protein is conserved and corresponds to the W616 of the mouse p85 β protein (red box in D).

4.5 PIK3R1^{W624R} Results in the Activation of the PI3K Pathway

The detection of PIK3R1^{W624R} mutation with an allele frequency approximately =1.0 in PDX line #475, suggesting a potential role as trunk mutation, has prompted me to investigate in depth whether the PI3K/AKT pathway was activated in this PDX line. To this aim, IHC staining was performed on TMA sections of the selected 12 PDXs studied (Tab. 4.2.1) to detect the expression of phospho-S6 as a proxy of AKT activation, being the phosphorylation of S6 more reliably detectable using IHC than phospho-AKT. Figure 4.5.1 reports representative images of TMA staining, which shows that the level of phospho-S6 is considerably higher in PDX #475

in comparison with other PDX lines without mutations in gene involved in the PI3K/AKT/mTOR pathway, suggesting a likely activation of PI3K pathway in the #475 PDX line.

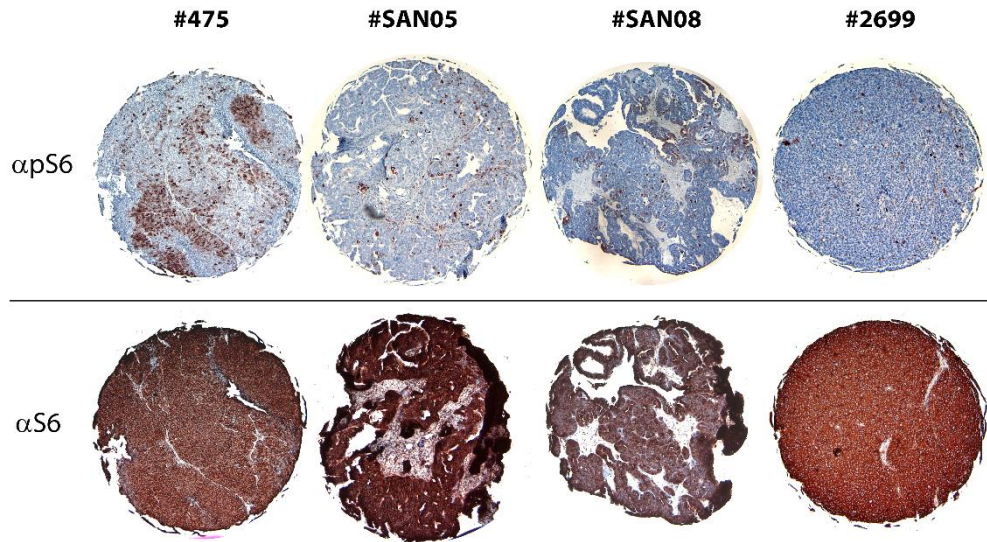


Fig. 4.5.1: Representative images of the expression of phospho-S6 as a proxy of PI3K activation in PDX samples. TMAs of PDX lines were stained with α pS6 (top) and α S6 antibodies (bottom) as a readout of PI3K/AKT/mTOR pathway activation. In the PDX line #475, carrying the $PIK3R1^{W624R}$ mutation, is visible a higher level of phospho-S6 compared to PDX lines without mutations of genes involved in this pathway. Numbers on the top are those of PDX lines as catalogued by the PROFILING approved protocol; on the left the antibodies used for detection are listed.

4.6 $PIK3R1^{W624R}$ is a Trunk Mutation in the #475 PDX Line and in the ST

Another hint of the possible driver function of the $PIK3R1^{W624R}$ could be its presence at similar allele frequency in consecutive passages of the #475 PDX line and also in the ST. WES analyses showed that the mutation in $PIK3R1$ was detectable in a number of serial and sequential passages of the #475 PDX line with an allele frequency of about 1.0 (Fig. 4.6.1 (A)). In addition, in these passages the same $TP53$ mutation was found with an allele frequency approximately = 1.0, in line with the role of trunk mutation of $TP53$ in HGS-EOCs. Interestingly, as also shown in figure 4.6.1 (A), most mutations were detected in all the examined passages

of this PDX line, whereas only a few of them were detected in a subset of passages. This demonstrated the genetic stability upon passages of the #475 PDX line.

To assess the presence of the same mutation in the patient's tumor we performed pyrosequencing using two distinct FFPE samples of the source tumor (Fig. 4.6.1 (B-E)). This analysis has revealed the presence of the *PIK3R1*^{W624R} in both samples. Moreover, in each FFPE sample the percentage of the *PIK3R1* mutation sequence was the same of the *TP53* allele found mutated in the PDX line (Fig. 4.6.1 (B-E)). As the percentage of the mutated *TP53* allele was considered a reliable proxy of the percentage of tumor cells in the source tumor specimens, data suggested that *PIK3R1*^{W624R} might be a trunk mutation also in the original patient's tumor.

Intriguingly, the *PIK3R1*^{W624R} was detected with the same AF in another but related PDX line, which was propagated from a sample of relapsed tumor of the same patient. This strengthened the possible importance of this mutation. The #475 PDX line carrying *PIK3R1*^{W624R} had been propagated from a biopsy sample taken at laparoscopy from a patient with a stage IIIc HGS-EOC (Tab. 4.2.1 and 4.1.1). This PDX line responded as well as the patient to platinum-based chemotherapy (for reference see ¹⁶⁴). Indeed, the patient received neo-adjuvant platinum-based chemotherapy followed by surgery. After six months the patient relapsed and received a second platinum-based chemotherapy line that unfortunately was limitedly effective. At the above mentioned post-chemotherapy surgery, another sample was taken and propagated to generate the PDX line #1864. This latter as well as the patient no longer responded to carboplatin (for reference see ¹⁶⁴). Clinical information about the patient's relapse and the corresponding PDX line #1864 is reported in table 4.1.1. Moreover, the #1864 PDX line belongs to the list of the 43 PDX lines fully characterized and the relevant information are reported in table 4.1.3 and 4.1.4. The #1864 PDXs displayed the same histological and genetics characteristics of the primary tumor from which the #475 PDX line has been propagated and of the #475 PDX line itself. WES demonstrated that the #1864 PDX line carried also the same *PIK3R1*^{W624R} mutation with an AF approximately = 1.0.

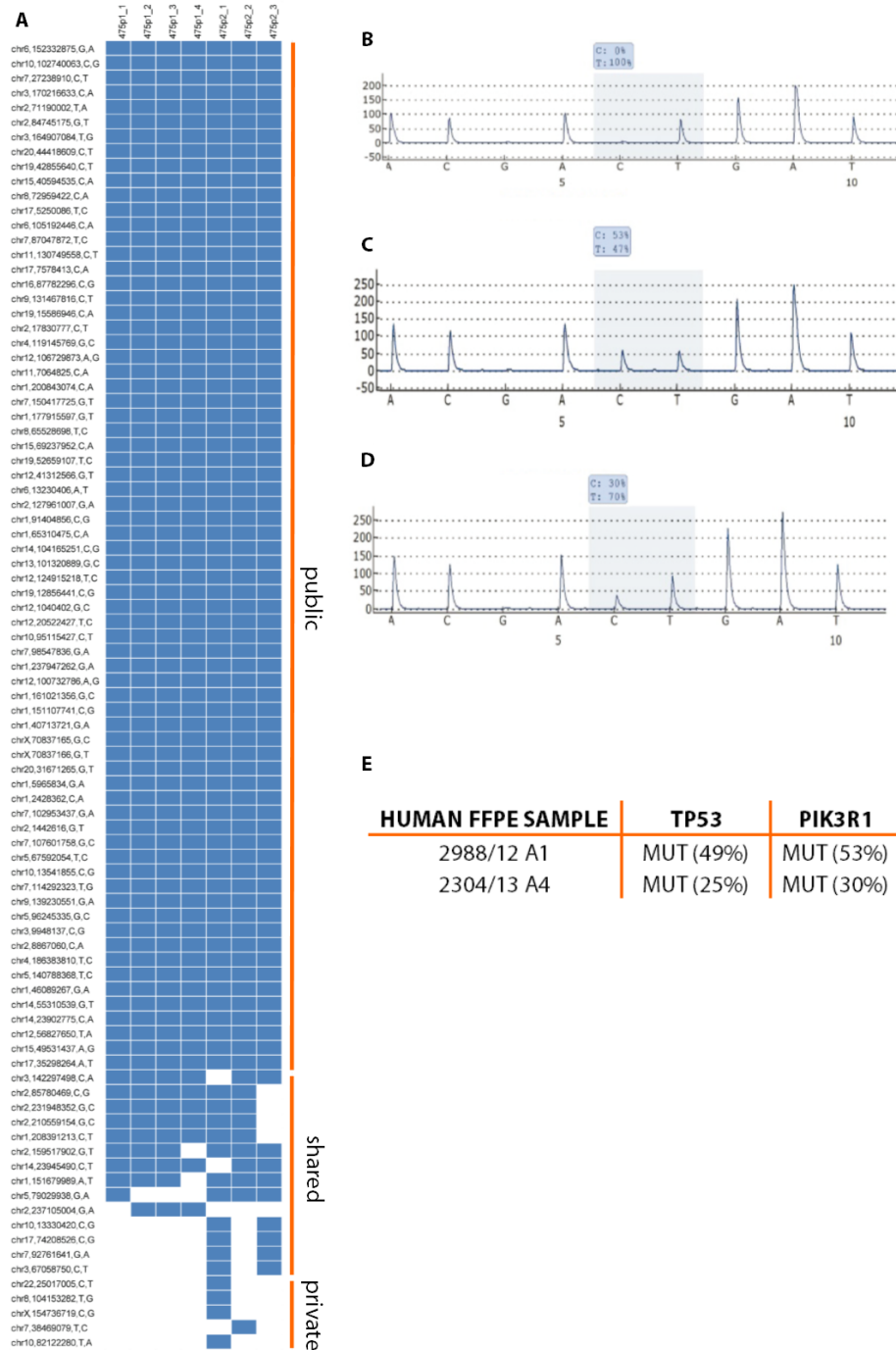


Fig. 4.6.1: Identification of the $PIK3R1^{W624R}$ mutation as trunk mutation in parallel and serial passages of the PDX line #475 and in the corresponding source tumor. (A) The $W624R$ mutation in $PIK3R1$ is one of several public mutations found in seven parallel and serial passages of the PDX line #475. (B–E) Pyrosequencing analysis of two FFPE samples from distinct blocks of the source tumor. The $TP53$ and the $PIK3R1$ mutated sequences showed the same allele frequency (AF) in each sample. The AF of the PDX line-specific $TP53$ mutation was considered as a proxy of the percentage of tumor cells in the human tumor samples. (B) Sequence of $PIK3R1$ in Control Reference Genome; (C) percentage of $PIK3R1^{W624R}$ in FFPE sample A1 from the paraffin block 2998 of the source tumor; (D) percentage of $PIK3R1^{W624R}$ in FFPE sample A4 from the paraffin block 2304 of the source tumor; (E) percentage of mutated sequences of $TP53$ and $PIK3R1$ in the two above FFPE samples.

4.7 *Ex Vivo* Assays of PIK3R1^{W624R} as a Driver and Actionable Mutation

As reported above, the structure-based approach to assay the function of the PIK3R1^{W624R} gave inconclusive results. On the other side, data showed that the PIK3R1^{W624R} was likely a trunk mutation in the PDX lines and the source tumor of the patient. Moreover, the activation of the PI3K/AKT pathway in the PDX line carrying this mutation has been shown (see above paragraph 4.5). Altogether, these data prompted me to perform functional assays *ex vivo* and *in vivo* of the PIK3R1^{W624R}, by challenging the susceptibility of PDXs and PDX derived tumor cells to inhibitors of the PI3K/AKT/mTOR pathway, because this pathway, as mentioned above, might be activated by the suppression of the p85 α regulatory subunit and fruitfully targeted for therapy. In the introduction (see paragraph 1.4) it was mentioned that primary cultures derived from patient's tumors represent an important tool in early phases of drug screenings. In this work the PDX derived tumor cells (PDTCs) have obtained by digesting PDX derived tumor pieces, as described in the Introduction and in detail in the Method section. Once optimized the protocol for PDTCs derivation, the reliability of PDTCs as experimental model was assayed by testing first the drug response correlation between PDTCs and tumors of origin, and then the capability of PDTCs to recreate tumors when inoculated in mice.

- 4.7.1 *Establishment and Quality Assessment of PDTCs as Ex Vivo Model Part 1: Carboplatin Sensitivity*

Once optimized the protocol for the establishment and the maintenance of the PDTCs (see the Method section), the first step for quality assessment was the comparison of drug responses of PDTCs and the corresponding source tumors. Therefore, the sensitivity of PDTCs to carboplatin was compared to that of the tumors of origin. CellTiter-Glo[®] viability assays were performed, treating PDCT lines with carboplatin for 72 hours as indicated in Methods section. Table 4.7.1 reports the clinical information of the patients from which we derived PDX lines and subsequently PDTCs cultures. Representative images of these PDTCs cultures are shown

in figure 4.7.2, which also shows the graph of the dose-response curves of each PDTCs lines treated with carboplatin. The comparison of carboplatin sensitivity of PDTC cultures to the clinical response to carboplatin of the corresponding patients showed that PDTCs reproduced patients' responses.

Patients Clinical Information							
PATIENT ID (PROFILING n.)	AGE	SAMPLE	TISSUE HISTOLOGY	TREATMENT STATUS AT SAMPLING	SAMPLE OBTAINED AT	1st LINE CHEMOTHERAPY	RESPONSE TO 1st LINE TREATMENT
#475	75	Primary	HGS	Naive	Laparoscopy	Carboplatin	Resistant
#SAN47	74	Metastasis	Undifferentiated	Treated	Interval debulking surgery	Carboplatin	Sensitive
#SAN96	58	Metastasis	HGS	Naive	Upfront surgery	Immunotherapy+ carboplatin+ bevacizumab	Ongoing

Tab. 4.7.1 Patients' information and clinical course. In this table are listed the clinical information of the patients from which have been derived PDX line and subsequently PDTCs used for the quality assessment I.

In the evaluation of these correlations we have taken into account the limitations of this model in predicting drug response in ovarian cancer patients. PDTCs are derived and maintained as short-term cultures, and therefore this model it is not suitable in predicting events of tumors recurrence and/or acquired resistance events. To overcome this limitation, we linked the drug response observed in PDTCs with the initial response of the patients to carboplatin. Indeed, as shown in table 4.2.1, patient #475 positively responded to carboplatin but relapsed after six months and for this she was regarded as eventually platinum resistant. However, we have propagated PDX from a sample collected before the chemotherapy regimen and the first response, although only for six months, of patient #475 came out to be predictable by PDTCs. Therefore, in the graph of figure 4.7.2 #475 PDTCs line is reported as Carboplatin sensitive. Conversely, PDX #SAN47 was propagated from a relapsed metastasis and thus it was not surprising to observe a partial response of the relevant PDTCs to the drugs. This is unrelated to the classification of the clinical course of the patient as partially sensitive to Carboplatin, who relapsed more than six months but within 1 year after treatment. Patient #SAN96 has been enrolled in a clinical trial and thus treated with carboplatin in combination with immunotherapy and bevacizumab; she is still under treatment with immunotherapy with

some response. #SAN96 PDTCs resulted resistant after *ex vivo* treatment with Carboplatin alone.

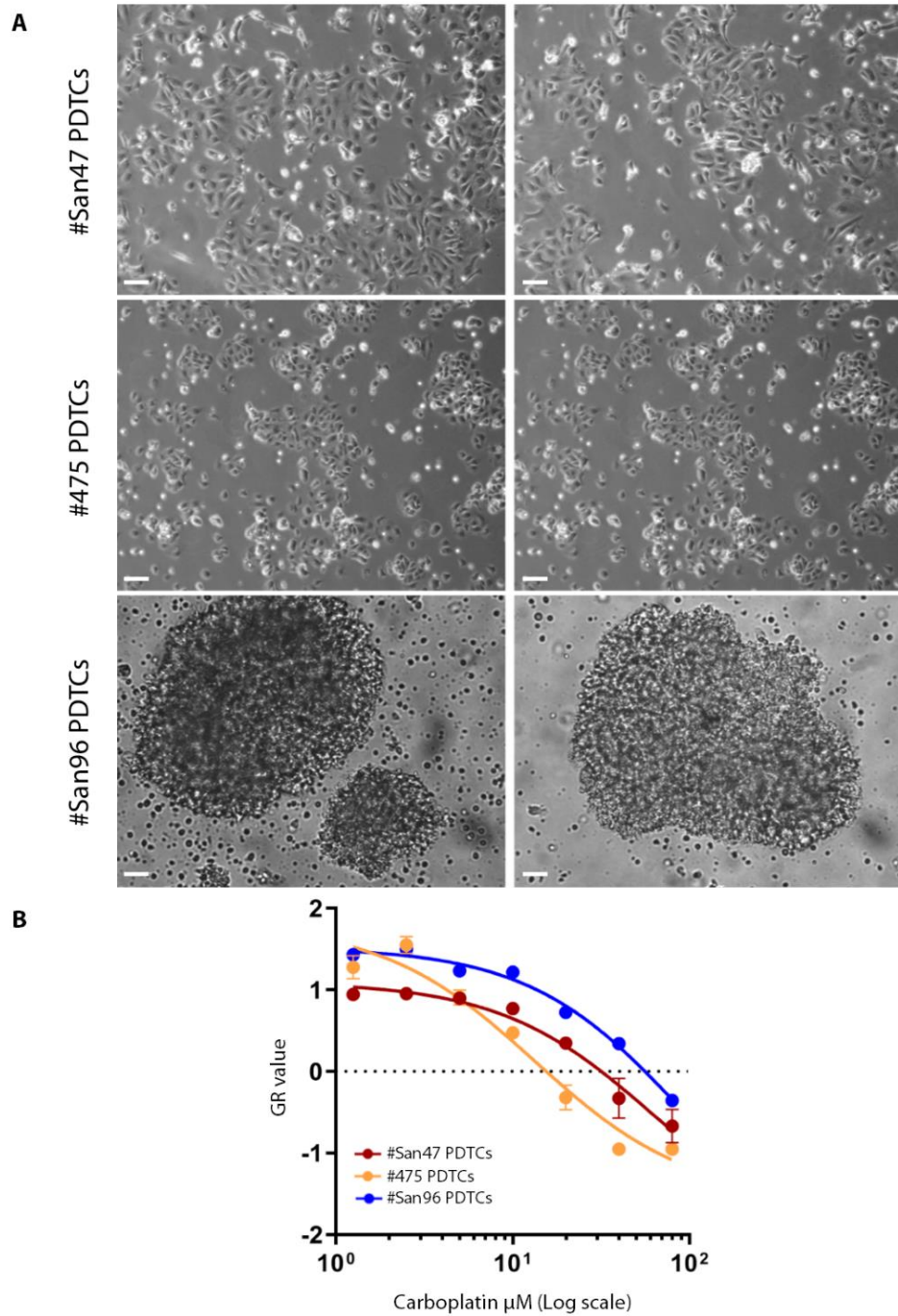


Fig. 4.7.2: Representative images of PDTCs cultures and Carboplatin drug response curves. (A) Representative images of PDTCs cell line cultures; (B) dose-response curves of the PDTCs short-term cultures treated with Carboplatin for 72 hours. Drug response data have been analyzed using GR metric. Numbers associated to PDTCs cultures correspond to that of the PDX line of origin, according to PROFILING protocol. Scale bar: $10\mu\text{m}$.

- *4.7.2 Establishment and Quality Assessment of PDTCs as Ex Vivo Model Part 2: Tumorigenicity of PDTCs*

Tumorigenicity of PDTCs was tested by reinjecting these cells in mice after culture establishment. Once derived, PDTCs were maintained in culture for 48 hours and then inoculated subcutaneously in mice. After 2-3 months the #475 PDTCs line generated tumors in mice, showing the tumorigenic potential of the cell cultures. Representative images of the HE staining performed on #475 PDX tumors and on #475 PDC-derived xenografts are reported in figure 4.7.2 which shows that tumors generated by PDTCs resume the histologic characteristics of the #475 PDX tumors from which PDTCs have been derived. Taken together, these results suggest that PDTCs are a reliable and suitable model for challenging the susceptibility of #475 PDX line to inhibitors of the PI3K/AKT/mTOR pathway.

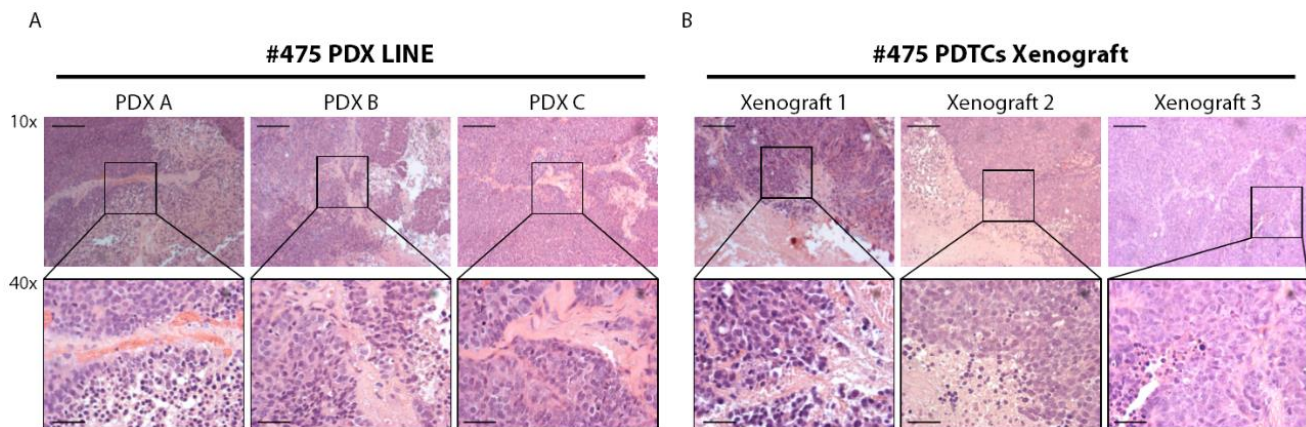


Fig. 4.7.2 Histology of #475 PDXs compared with #475 PDTCs xenograft. (A) Representative images of the HE staining on the PDX tumor sections; (B) HE staining of the tumor sections generated after #475 PDTCs injection in mice. On the left magnifications are indicated. 40x images represent the fields surrounded by the black squares of the corresponding images on the top. Scale bar 10x: 0.1 mm; scale bar 40x: 50 μ m.

- *4.7.3 Ex Vivo Assays of PI3K Pathway Inhibitors on #475 PDTCs*

SNVs identified in the #475 PDX, its paired #1864 PDX line and ST are numerous and thus it is important to define the possible role of PIK3R1^{W624R} as a driver and actionable target. As mentioned in Introduction (see paragraph 1.1 and 1.2), genomic studies on different cancer

types have led to the identification of specific genetic alterations as key oncogenic drivers, defined as mutations able to confer a selective advantage to a cell, through either increasing its survival or proliferation and, thus, able to cause clonal expansion of the carrier cell ¹⁶⁵. These findings have prompted the development of therapies targeting these mutations, which have provided demonstrable clinical benefit. Thus, a number of these mutations have also been defined as “actionable”, not only because their functional outcome makes carrier cells responsive to a targeted therapy, but also thanks to the availability of a specific targeted drug.

In order to evaluate the functional outcome of the PIK3R1^{W624R}, *ex vivo* cell susceptibility assays to drugs were performed. #475 PDX Derived Tumor Cells (#475 PDTCs) were depleted of mouse cells and propagated as short-term cultures as described above and in the Methods section. CellTiter-Glo[®] viability assays and Crystal Violet cytotoxic/cytostatic assays were carried out by exposing #475 PDTCs to inhibitors of the PI3K/AKT/MTOR pathway as described in Methods sections.

In these *ex vivo* experiments, PDTCs derived from another PDX line and commercial cell lines were used as controls. The following cell lines were selected, based on their known susceptibility to PI3K/AKT/mTOR pathway inhibitors and on their known mutation spectrum (Cancer Cell Line Encyclopedia (<https://portals.broadinstitute.org/ccle>), widely described in literature:

- A2780 ovarian carcinoma cells, carrying *PIK3CA*^{E365K} activating mutation and *PTEN* loss that make them highly susceptible to the pan-class I PI3K inhibitor Buparlisib (BKM120), to the p110 α specific inhibitor Alpelisib (BYL719) and to the dual PI3K/mTOR inhibitor Dactolisib (BEZ235).
- OVCAR8 ovarian carcinoma cells carrying wild-type *PIK3CA* and the *TP53* gene mutation, but known to be susceptible to the dual PI3K/mTOR inhibitor Dactolisib (BEZ235), as reported by the Genomic of Drug Sensitivity in Cancer Project (<https://www.cancerrxgene.org/>).

- LNCaP prostate carcinoma cells which are *PTEN*-mutated and are known to be exquisitely susceptible to the p110 β specific inhibitor GSK2636771.

- 4.7.4 *CellTiter-Glo*[®] Viability Assays of PI3K Pathway Inhibitors on #475 PDTCs

The first functional assay performed aimed at testing Buparlisib sensitivity of PIK3R1^{W624R} PDTCs in comparison with that of one PDTCs line without mutation in genes involved in PI3K/AKT/mTOR pathway. Thus, PDTCs were derived from the #2085 PDX line, which was propagated from a *bona fide* HGS-EOC carrying mutations of the *TP53* and *BRCA2* genes (for information see Tab. 4.1.1, 4.1.3, 4.1.4) but not in genes involved in the PI3K/AKT/mTOR pathway. #475 PDTCs and #2085 PDTCs were treated with Buparlisib for 72 hours and drug response data of this experiment are plotted in the graph of figure 4.7.4, which shows that #475 PDTCs carrying PIK3R1^{W624R}, are considerably more sensitive to Buparlisib in comparison to #2085 PDTCs.

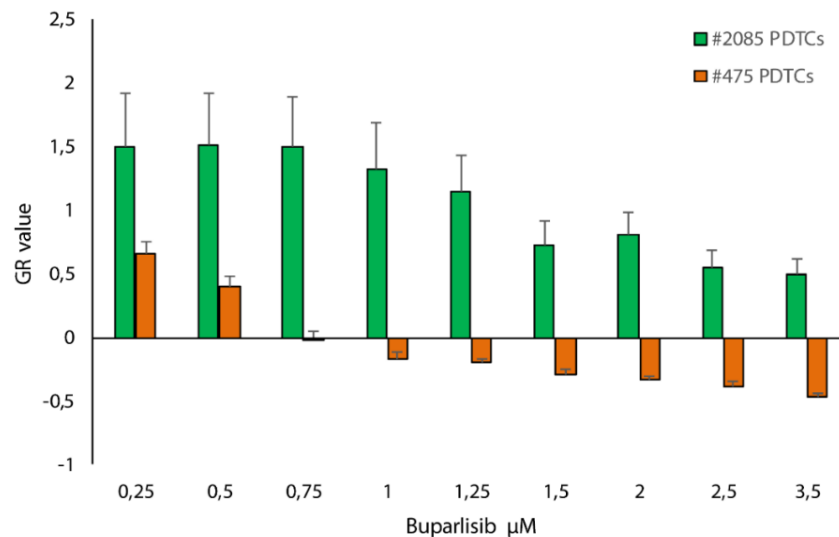


Fig 4.7.4: Comparison between the response of the PIK3R1^{W624R} carrying PDTCs and control #2085 PDTCs to the pan-class I PI3K inhibitor Buparlisib. In the graph the dose-response curves are reported of CellTiter-Glo[®] viability assays carried out for 72 hours. Data are the mean of three independent experiments with standard errors for each experimental point.

Drug response data were analyzed with GR metrics, which is able to normalize the drug response on cell doubling along the experiment (see Methods section for references).

Afterward, the sensitivity of #475 PDTCs to other PI3K inhibitors was tested. As previously mentioned, in this set of experiments we used as controls three different cell lines: A2780, OVCAR8 and LNCaP, whose mutation spectrum is described above. #475 PDTCs and the control cell lines were treated with Buparlisib, Dactolisib, Alpelisib and GSK2636771, whose specificity is also reported above (see paragraph 1.5), for 72 hours (Fig. 4.7.5 (A-D)).

The #475 PDTCs resulted highly susceptible to the pan-class I PI3K inhibitor Buparlisib, displaying a response curve similar to that of the positive control A2780 cells (Fig 4.7.5 (A)). Moreover, #475 PDTCs positively responded to the dual PI3K/mTOR inhibitor Dactolisib, and to Alpelisib, that is the p110 α specific inhibitor. Figure 4.7.5 (B) shows that #475 PDTCs susceptibility to Dactolisib was similar to that observed in the positive control OVCAR8. Similarly, the susceptibility to Alpelisib in #475 PDTCs is comparable to that of the most sensitive A2780 control cell line (Fig. 4.7.5 (C)). Conversely #475 PDTCs did not respond to treatment with GSK2636771, the p110 β selective inhibitor, displaying a response trend comparable to that of the resistant A2780 and OVCAR8 cells (Fig. 4.7.5 (D)).

The effects of these four PI3K pathway inhibitors have been evaluated also using Western blot. As indicated in Methods section, #475 PDTCs, A2780, OVCAR8 and LNCaP were treated with the inhibitors at different concentration for 24 hours and the phosphorylation *status* of AKT was evaluated as a proxy of PI3K pathway activation (Fig. 4.7.5 (E-H)). Treatments of #475 PDTCs with Buparlisib, Alpelisib and Dactolisib induced a strong dose-dependent down modulation of phospho-AKT (Fig. 4.7.5 (E-G)), which was poorly affected by GSK2636771 (Fig. 4.7.5 (H)).

The susceptibility of #475 PDTCs to dual PI3K/mTOR inhibitors was also challenged in another experiment using Gedatolisib (PKI587), which is currently under evaluation in a phase III trial¹³⁹. Data obtained in this experiment confirmed what observed with Dactolisib treatment as #475 PDTCs positively responded also to this dual PI3K/mTOR inhibitor (Fig. 4.7.6).

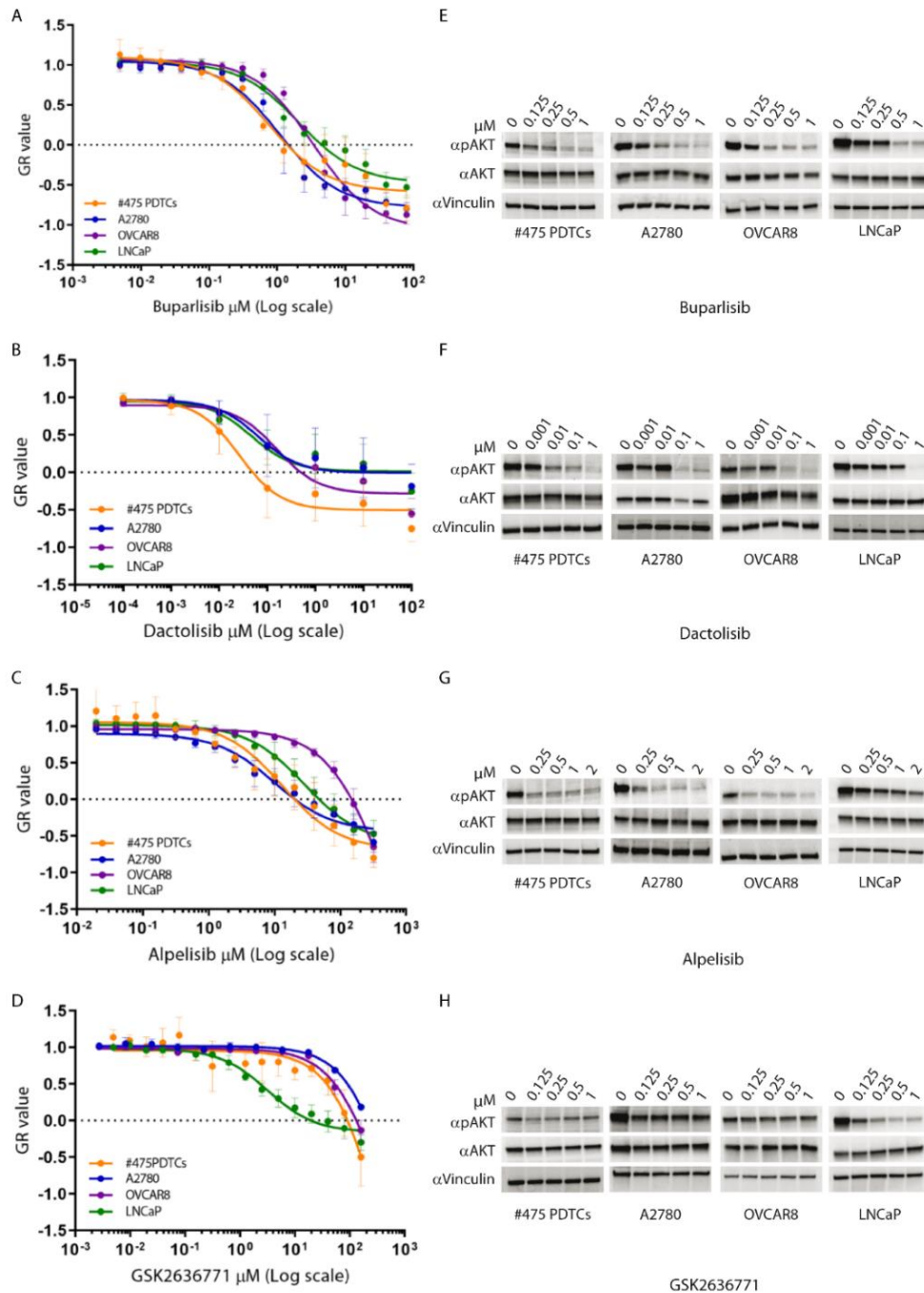


Fig. 4.7.5: Response of PIK3R1^{W624R} carrying PDTCs and control cell lines to inhibitors of the PI3K/AKT/mTOR pathway. (A-D): Dose-response curves after 72 hours of treatment in CellTiter-Glo[®] viability assays. Normalized growth rate (GR value) inhibition metrics of three replicate experiments are shown to take into account cell division rates, ± error bars for each experimental point. The sign of GR values relates directly to response phenotype: positive for partial growth inhibition, zero for complete cytostatic effect and negative for cytotoxicity. The x axis shows drug concentration on a log₁₀ (Log) scale. (E-H) Western blot analysis of AKT phosphorylation in response to drugs, as a proxy of PI3K pathway activation status.

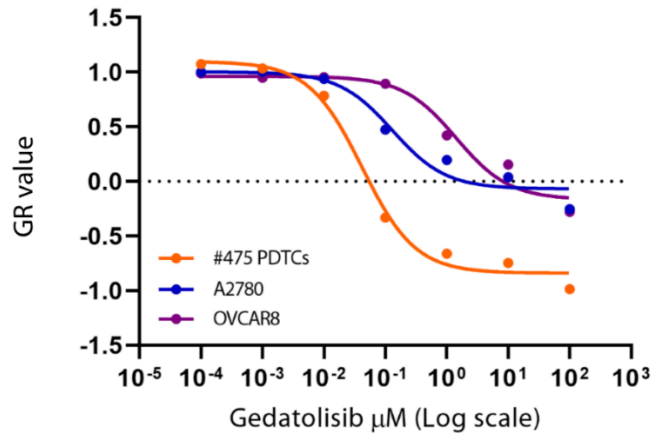


Fig. 4.7.6: Response to Gedatolisib (PKI587) of #475 PDXs, A2780 and OVCAR8 cells. Dose- response curves to Gedatolisib were assayed in CellTiter-Glo® viability assay for 72 hours at the same concentrations used for Dactolisib treatment of figure 4.7.5 (B).

As mentioned above the #475 PDX line carrying $\text{PIK3R1}^{\text{W624R}}$ had been propagated from a biopsy sample taken at laparoscopy from a patient with a stage IIIc HGS-EOC (Tab. 4.2.1 and 4.1.1). This PDX line responded as well as the patient to platinum-based chemotherapy (for reference see ¹⁶⁴). Indeed, the patient received neo-adjuvant platinum-based chemotherapy followed by surgery. After six months the patient relapsed and received a second platinum-based chemotherapy line that unfortunately was limitedly effective. At the above mentioned post-chemotherapy surgery, another sample was taken and propagated to generate the PDX line #1864. This latter as well as the patient no longer responded to carboplatin (for reference see ¹⁶⁴). In a previous work of Di Renzo's group, #1864 PDX line has been widely characterized. In particular, its susceptibility to other drugs used in clinic as second-line treatment, such as gemcitabine, trabectedin and pegylated liposomal doxorubicin, was assayed. The drug response of #1864 PDX line had been compared to that of #475: albeit #475 PDX line positively responded to the all treatments, #1864 PDX line no longer responded to trabectedin and gemcitabin, as well as carboplatin [165]. The #1864 PDX line was sequenced and found to carry the same $\text{PIK3R1}^{\text{W624R}}$ mutation of #475 with an AF of about 1.0. Thus here the susceptibility of #1864 PDXs derived from this PDX line to PI3K/AKT/mTOR pathway inhibitors is shown. In

these set of experiments, the #1864 PDTCs were treated with Buparlisib, Dactolisib, Alpelisib and GSK2636771 in CellTiter-Glo® assays for 72 hours and #475 PDTCs line was used as control. Figure 4.7.7 shows that the susceptibility of #1864 PDTCs to the four mentioned PI3K/AKT/mTOR inhibitors is comparable to that of #475 PDTCs, providing further evidence on the possible role of the PIK3R1^{W624R} as a driver and actionable mutation.

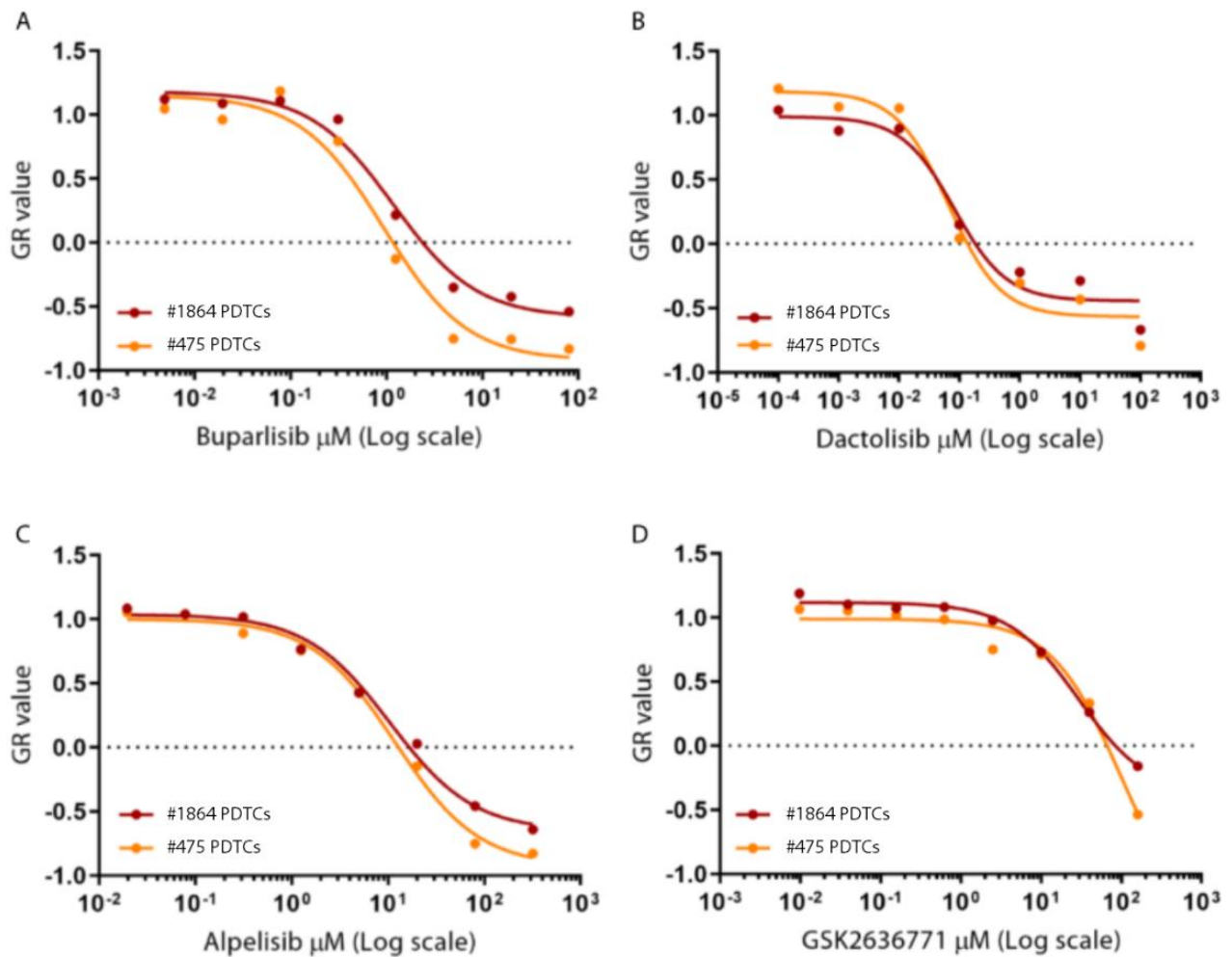


Fig. 4.7.7: Susceptibility to PI3K/AKT/mTOR pathway inhibitors of #1864 PDTCs. In this experiment #475 PDTCs used as control cell. In the figure are shown the responses of #1864 and #475 PDTCs to Buparlisib (A), Dactolisib (B), Alpelisib (C), GSK2636771(D) upon 72 hours of treatment in CellTiter-Glo® viability assay. Samples were treated with the same range of drug concentrations used in the experiments shown in figure 4.7.5 (A-D) but with less experimental point.

- 4.7.5 *Crystal Violet Cytotoxic/Cytostatic Assays of PI3K Pathway Inhibitors on #475 PDTCs*

In the introduction section (paragraph 1.5) it was mentioned that PI3K pathway is important not only in the regulation of cell proliferation but also in cell metabolism. CellTiter-Glo® viability assay measures the intracellular ATP production as read-out of cell viability. Several drugs, like PI3K pathway inhibitors, are known to impair cell metabolism and consequently ATP production; therefore, the effects of PI3Ki should not be solely estimated using CellTiter-Glo®. For this reason, also Crystal Violet cytotoxic/cytostatic assays were carried out.

#475 PDTCs and two control cell lines (A2780 and OVCAR8) have been exposed to Buparlisib, Dactolisib, Alpelisib and GSK2636771 for 72 hours at the same drug concentration ranges used in previous experiments. Afterwards, the drug response data have been analyzed with GR metrics similarly to the above experiments (for reference see Methods section). As shown in figure 4.7.8 (A-D)) the susceptibility of #475 PDTCs to these drugs, previously observed in CellTiter-Glo® assays (Fig. 4.7.5 (A-D)), was confirmed also by Crystal Violet cytotoxic/cytostatic assays (Fig 4.7.8 (A-D)). In particular, #475 PDTCs susceptibility to the pan-class I PI3K inhibitor Buparlisib (BKM120), to the p110 α specific inhibitor Alpelisib (BYL719) and to Dactolisib (BEZ235), was comparable to that of the positive controls (Fig. 4.7.8 (A-C)). Conversely, but not surprisingly, #475 PDTCs did not respond to the treatment with the p110 β selective inhibitor, GSK2636771 (Fig. 4.7.8 (D)) also in cytotoxic/cytostatic assays. Subsequently, the downstream effects onto the PI3K pathway of these four treatments were also evaluated with Western blot analyses of the phosphorylation *status* of AKT and S6 as proxy of PI3K pathway inhibition. Results of this analysis, shown in figure 4.7.9 (A-C) confirmed what observed in viability assays, being the AKT and S6 phosphorylation *status* modulated by drug treatments as expected.

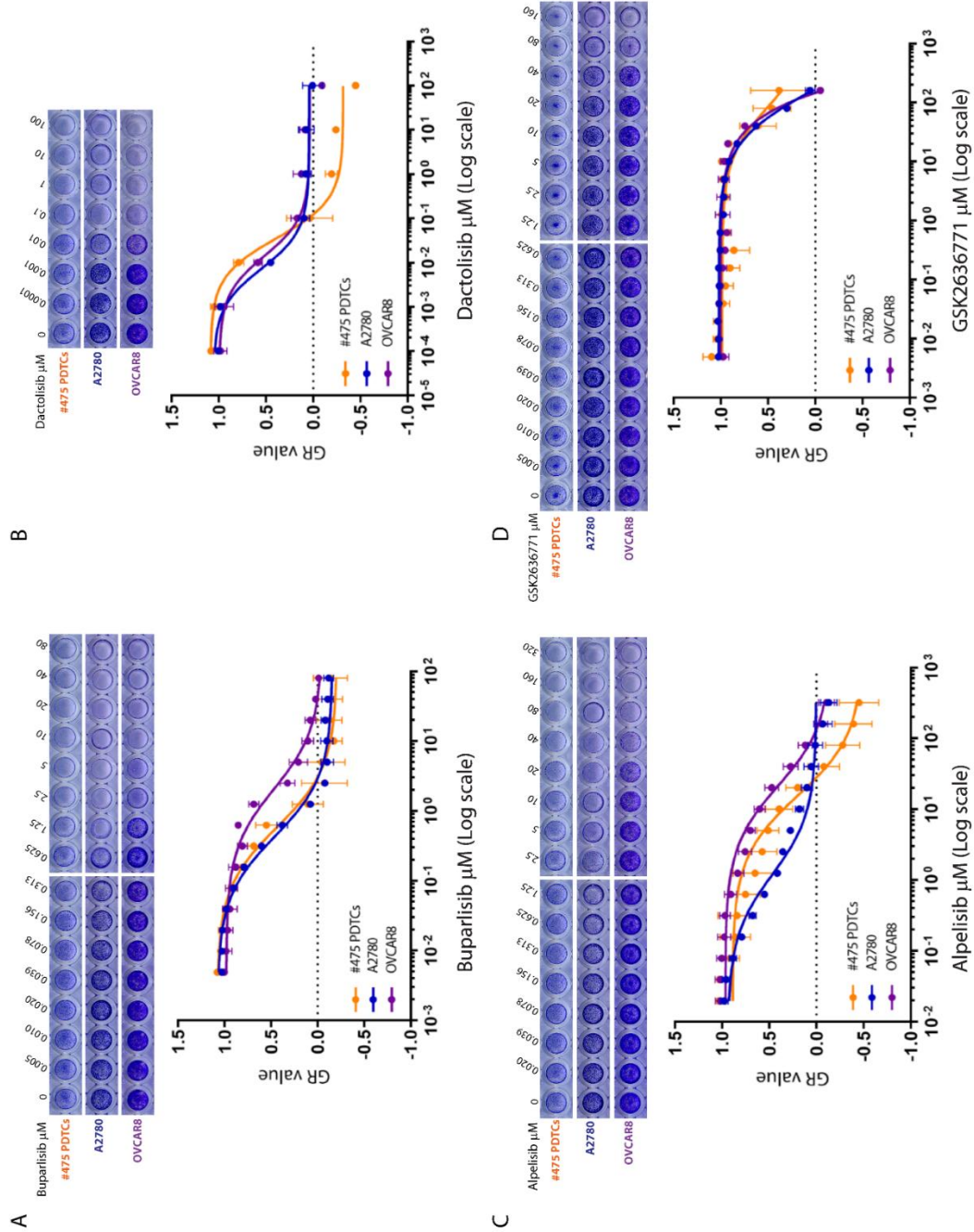


Fig. 4.7.8: Cytostatic/cytotoxic effect of PI3K pathway inhibitors on PI3K^{W624R} carrying PDTCs and control cell lines, evaluated with crystal violet staining. Control cell lines and the indicated drugs are described in the section 4.7.3. The effects were determined fixing and staining cells 72 hours after treatment and quantified as described in the Methods section. Representative images of #475 PDTCs and control cell lines stained with crystal violet are shown on the left of each graph in which the drug concentration used are also reported. Graphs show the quantification of the drug responses. Quantifications were carried out using the mean of three independent replicates \pm standard errors. (A-B) Treatments with Buparlisib and Dactolisib; (C-D) Treatments with the isoform-selective inhibitors for p100 α and p100 β , Alpelisib and GSK2636771, respectively.

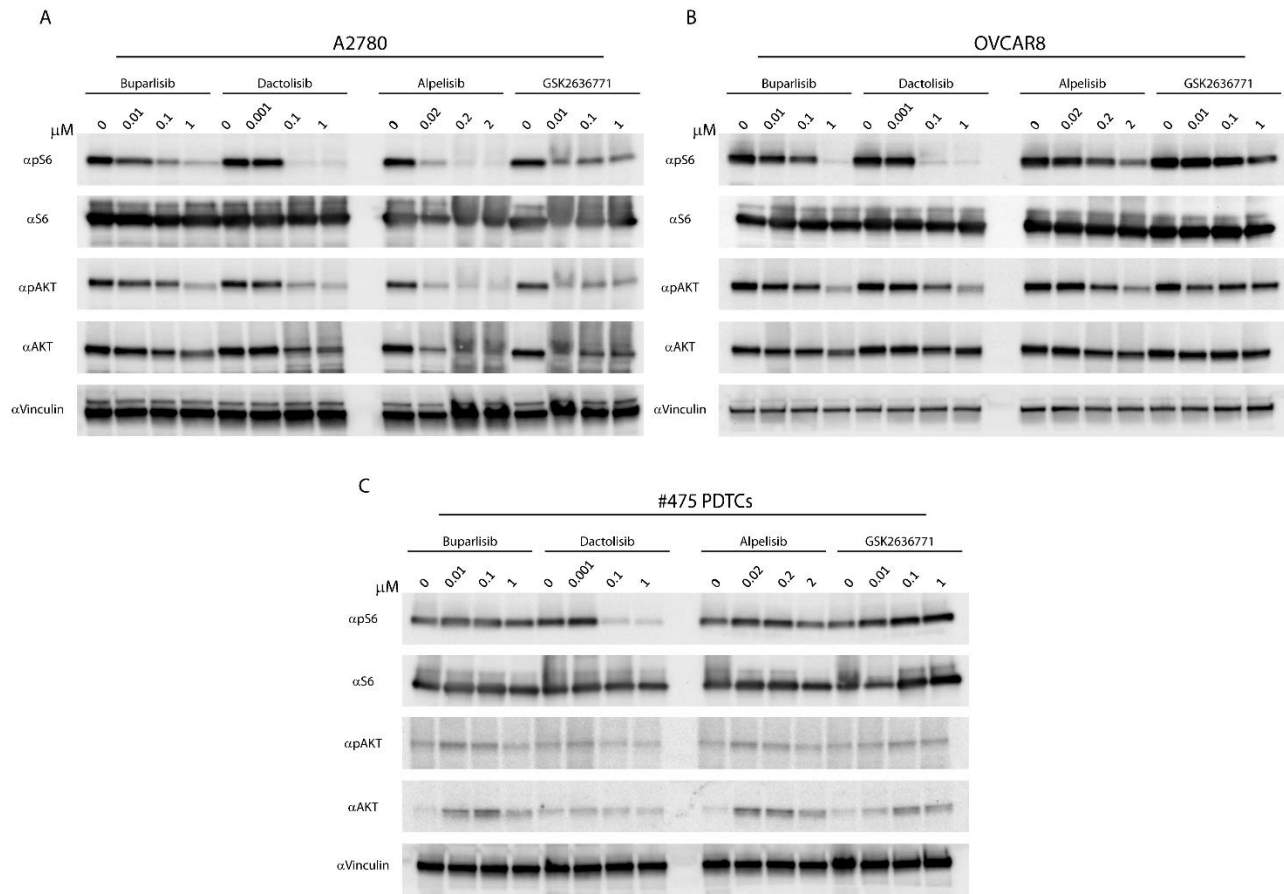


Fig. 4.7.9: Western blot analysis of S6 and AKT phosphorylation *status*. Western blot analyses were performed to assess the down-stream effects exerted by the treatments on the phosphorylation *status* of S6 and AKT as a proxy of PI3K pathway activation. Unlike the western blot experiments shown in fig. 4.7.5 (E-H), in these experiments different concentrations were used of Buparlisib, Dactolisib, Alpelisib and GSK2636771 in order to decrease the number of the experimental points and to fit all samples of the same cell line in the same gel. (A) A2780; (B) OVCAR8; (C) #475 PDTCs. Western blot analyses and cytostatic/cytotoxic assays were performed using the same cells, at the same passages used in fig 4.7.8.

4.8 *In Vivo* Assays of PIK3R1^{W624R} Actionability

Since Buparlisib acts on all the isoforms of Class I PI3K and the *ex vivo* experiments have shown that #475 PDTCs are exquisitely susceptible to this drug, response to Buparlisib of the #475 PDX line carrying the PIK3R1^{W624R} was assayed also *in vivo*.

For *in vivo* experiments #475 PDXs have been propagated in mice in order to get two cohorts: one for treatment with Buparlisib and one for control treatment with vehicle. In figure 4.8.1 is

reported a schematic representation of the schedule followed in these experiments (for details see Methods section, paragraph 3.2).

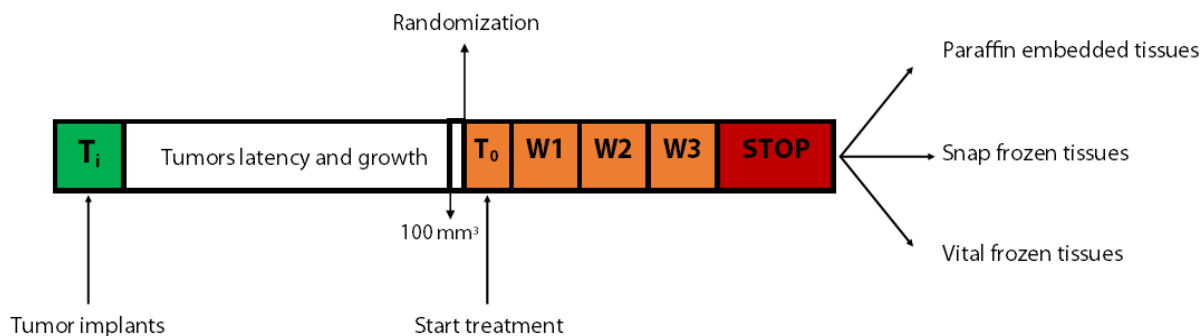


Fig. 4.8.1: Schematic representation of the treatment schedule used in the *in vivo* experiments. Treated mice received Buparlisib at 20mg/Kg whereas control mice were treated with vehicle alone. Mice were treated for 3 weeks, five days a week and at the end of experiment xenograft samples were processed for further analyses.

For the *in vivo* experiments, after the growth of xenograft to approximately 100 mm³, animals were randomized using the LAS suite¹⁴⁹ and divided in two cohorts made of 6 mice each: one for treatment with Buparlisib at 20mg/Kg and one for controls that received vehicle alone. The dose of 20 mg/kg has been chosen because it has been already reported in literature to be effective in PDX models of other cancer histotypes¹⁶⁶⁻¹⁶⁸. Moreover, treatment with doses higher than 30 mg/kg resulted in mice toxicity¹⁶⁹. Tumor volumes were measured twice a week along the experiment and data of tumor growth were analyzed to estimate the *in vivo* effects of Buparlisib treatment. Figure 4.8.2 shows that Buparlisib considerably delayed tumor growth in treated mice in comparison to the controls.

Since the total decrease of tumor volumes could not allow a proper estimation of possibly cytostatic agents, immunohistochemistochemical detection of Ki67 has been carried out in order to evaluate the proliferation index in all tumors of the control and treated cohorts (Fig. 4.8.3 (A-B)). Ki67 staining showed that treatment with Buparlisib significantly decreased the number of Ki67 positive cells in treated compared to control PDXs (Fig. 4.8.3 (A-B)).

Moreover, in order to evaluate the PI3K pathway inhibition by drug administration, immunohistochemistry with phospho-S6 antibody was performed (for details see Methods). Buparlisib was also able to induce a significant decrease of phospho-S6 positive cells in treated PDXs compared to control PDXs. (Fig. 4.8.4 (A-B)). As mentioned above, the phosphorylation of S6 is more reliably detectable using IHC than phospho-AKT and thus this is a suitable proxy of PI3K activation in IHC experiments. These data further highlighted the impairment of PI3K/AKT/mTOR pathway exerted by Buparlisib treatment of cells carrying the PIK3R1^{W624R}.

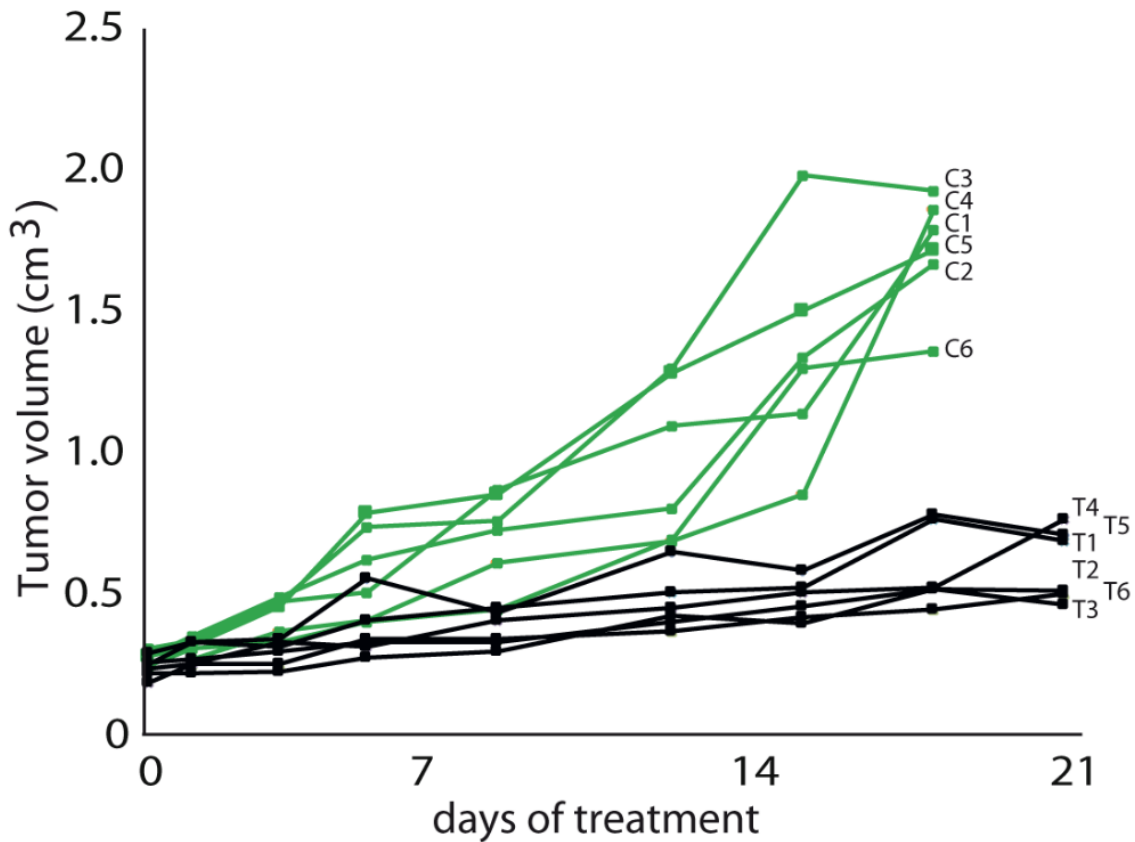


Fig. 4.8.2: *In vivo* response of the PIK3R1^{W624R} carrying PDXs to Buparlisib. Randomized mice were divided into two cohorts and treated with 20 mg/kg Buparlisib, administered as described in the Methods section. (A) Growth curves of treated (black lines) and control (green lines) animals.

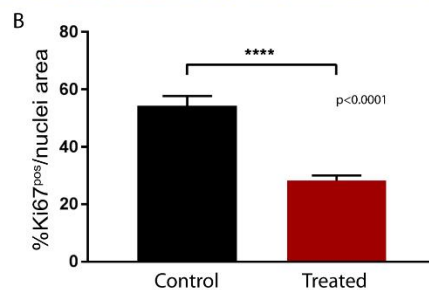
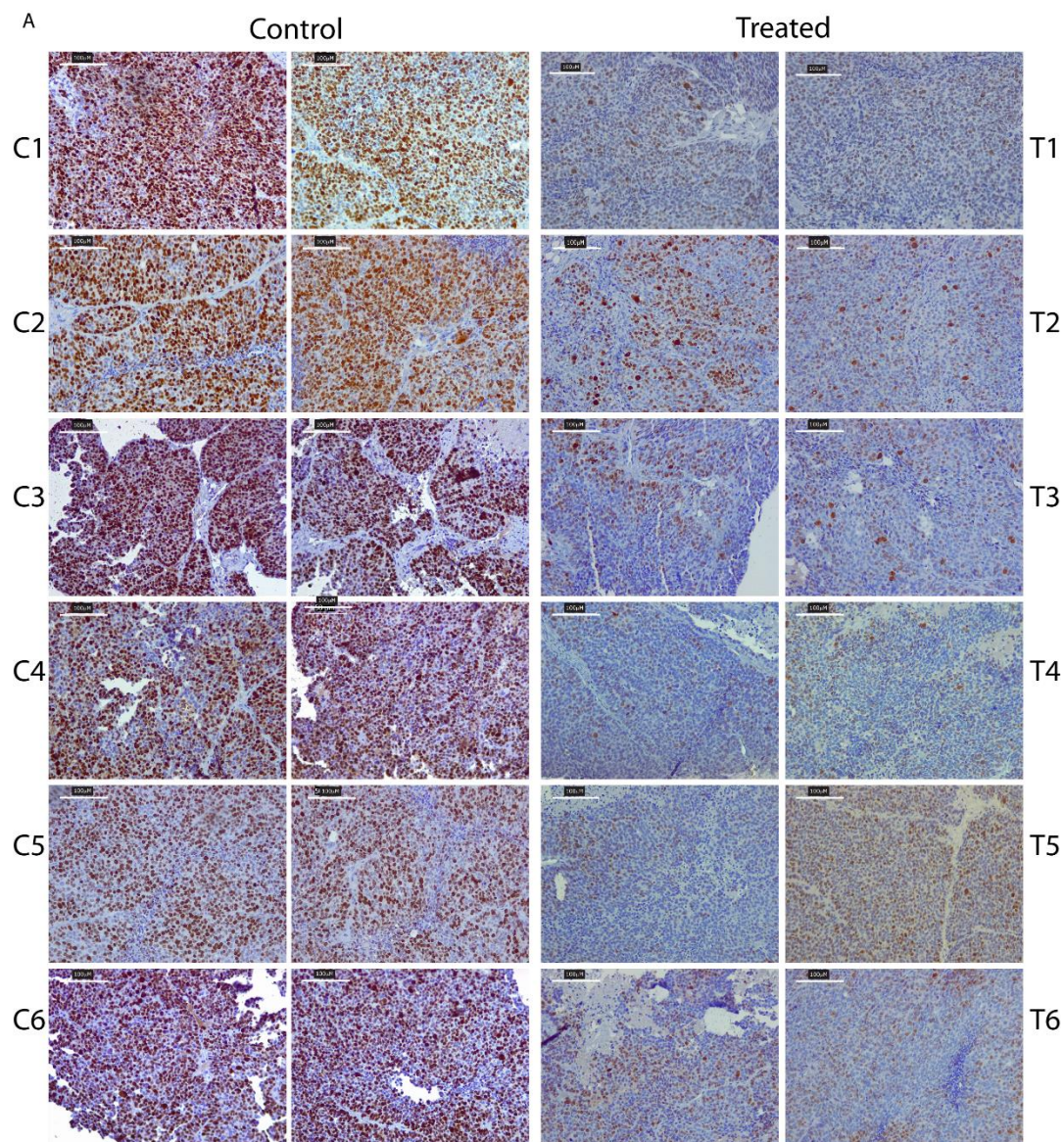


Fig. 4.8.3: Immunohistochemical detection of proliferation index in #475 PDXs, treated with Buparlisib. (A) Representative images of Ki67 positive cells detected in control and treated PDXs: C1-C6 stand for control mice 1-6, T1-T6 stand for treated mice 1-6 (indicated also in figure 4.8.2); (B) Quantification of Ki67 positive nuclei evaluated as the mean of the percentage of positive area versus total nuclei area estimated in all fields of each PDX of the *in vivo* experiment. The p value has been calculated using unpaired t-Student test.

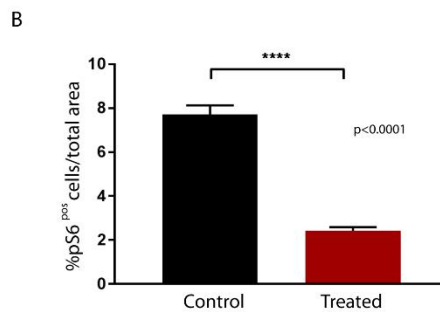
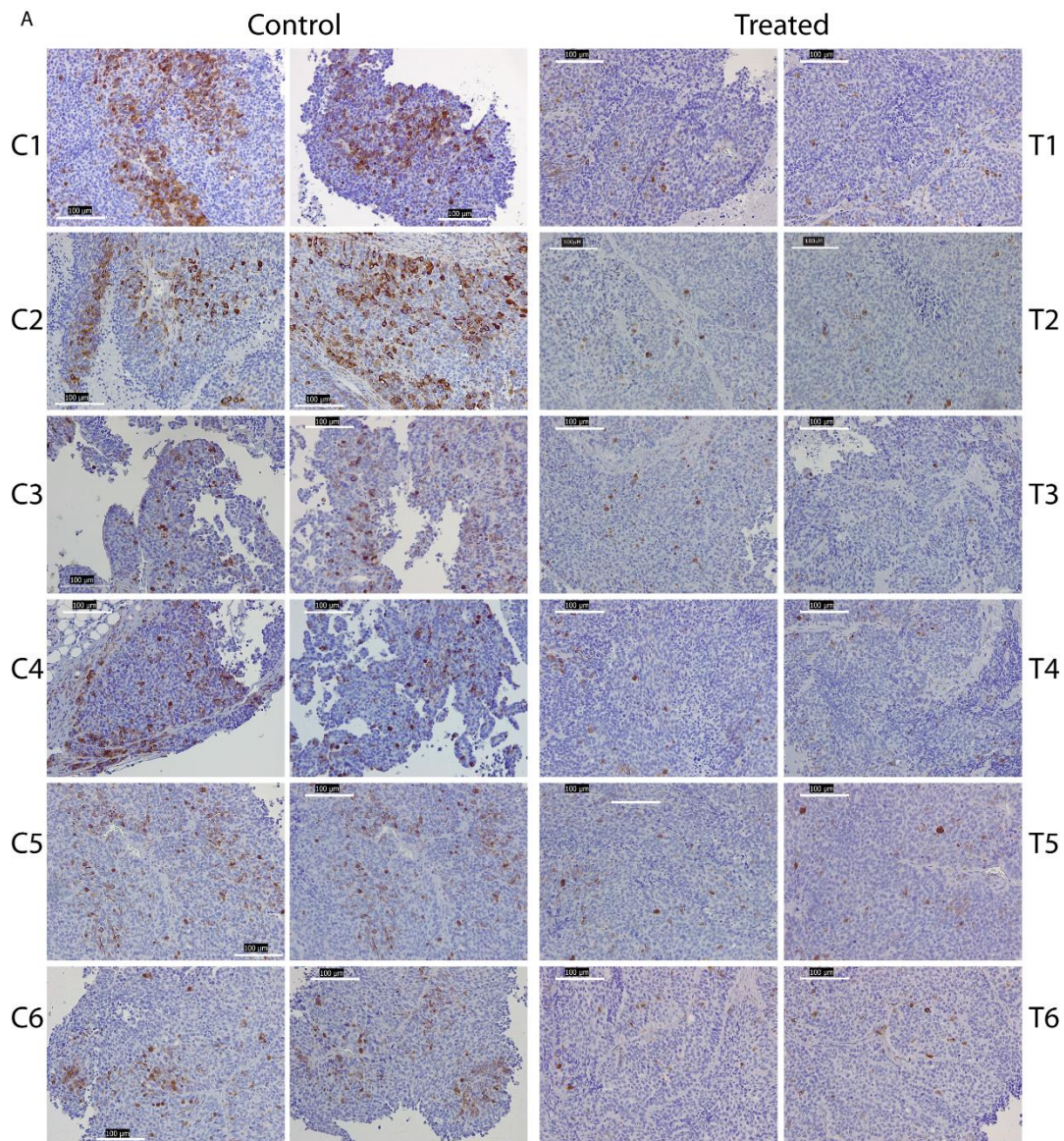


Fig. 4.8.4: Immunohistochemical detection of phospho-S6 as proxy of the decreased activation of PI3K pathway in #475 PDXs treated with Buparlisib. (A) Representative images of phospho-S6 positive cells detected in treated and control PDXs: C1-C6 stand for control mice 1-6, T1-T6 stand for treated mice 1-6 (indicated also in figure 4.8.2). (B) Quantification of phospho-S6 positive cells, evaluated as a percentage of positive area versus total area estimated in all fields of each PDX of the *in vivo* experiment. The p value has been calculated using unpaired t-Student test.

5. DISCUSSION

Molecular and genetics studies performed on HGS-EOCs have highlighted the profound genomic instability of this kind of tumor, unraveling the presence of the so-called long tail of mutation distribution (see paragraph 1.2) in which only a handful of cancer-related genes are mutated at low frequency ($\approx 1\%$)⁶. The role in carcinogenesis of genes located in the tail of this distribution is still unclear and needs to be investigated in order to understand their potential clinical impact^{1,6}.

In this thesis attention was focused in elaborating a pipeline to explore this tail and identify putative driver and actionable cancer-genes in HGS-EOCs.

The pipeline proposed in this thesis is based on Patients' derived models (PDXs and PDTCs) A number of PDX lines was analyzed first identify mutations and secondly to investigate on the biological impact of these mutations in protein functions. Thanks to these analyses we have detected the presence of a rare mutation in the *PIK3R1* tumor suppressor gene, consisting in an amino-acid substitution (W624R) in the cSH2 domain of the encoded protein p85 α .

Although the results of our bioinformatics analyses have suggested the potential deleterious/damaging impact of the W624R substitution in protein function it was difficult to predict its actual role on ovarian cancer. Then a structure-based approach was endeavored, as it is considered more specific in predicting driver mutation than the sequence-based one¹⁷⁰.

However, the analysis of the available crystal structures of the human p110 α and p85 α did not help in improving our comprehension in *PIK3R1*^{W624R} role, prompting the idea to use functional approaches using patient derived models.

The results obtained have shown that *PIK3R1*^{W624R} confers susceptibility to pathway inhibition being the *PIK3R1*^{W624R} PDTCs highly sensitive to the pan-class I PI3K and to the dual PI3K/mTOR inhibitors. The *ex vivo* assays on PDTCs model have also demonstrated that this mutation confers susceptibility to the p110 α specific inhibitor but not to the p110 β inhibitor

GSK2636771, although it had been postulated that the cSH2 domain of the human p85 α in oncogenesis could interact and inhibit the p110 β isoform of the PI3K¹⁷¹.

The *in vivo* experiments using PDX cohorts treated with the pan-class I PI3K inhibitor have confirmed the *ex vivo* assays results, providing a further evidence of the invaluable importance of the PDMs in preclinical research.

As mentioned in paragraph 1.5, *PIK3R1* is the 12th most commonly mutated gene across diverse cancer lineages, among which uterine carcinomas and carcinosarcomas, glioblastoma, breast and colorectal cancers, with the notable exception of HGS-EOC^{52,112}. In this latter cancer the aberrations in *PIK3R1* mainly consist in copy number alterations rather than mutations in gene sequence which account only about 3%^{125,128,132,133}. Most of the mutations detected so far in *PIK3R1* generally involve the nSH2 and iSH2 domain of the protein p85 α , which are required for the binding with the catalytic subunit.

The *PIK3R1*^{W624R} here described, is located in cSH2 domain. Little is known about those mutations located 'outside' to the hot spot regions. In particular, the same amino-acid substitution W624R has been previously detected but not characterized in one case of colorectal cancer, whereas another substitution in this amino-acid residue (W624C) has been found in one case of non-small cell lung carcinoma (NSCLC)^{172,173}. Moreover, a nucleotide change in the same codon, leading a non-sense mutation, has been detected in one stomach cancer sample and in one endometrial carcinoma^{174,175}. Other rare mutations in the cSH2 of the *PIK3R1* gene are reported in COSMIC and TumorPortal^{156,176}. The potential role of the mutations in *PIK3R1* gene has been discussed in paragraph 1.5. Particularly it has been focused on the oncogenic potential of those mutations located in the hot spot regions because unfortunately in the cSH2 domain of p85 α only two mutations have been proposed as likely involved in oncogenesis and tumor growth¹⁷⁷.

Data obtained not only have confirmed the requirement of proper functional assays for the evaluation of driving oncogenic effect of any given mutation but, more importantly, have demonstrated the importance to understand the potential clinical impact of the mutations in

the cancer genes mutated at low frequency. As well as HGS-EOCs, many tumor types are characterized by a long tail distribution of mutations. Moreover, some of the genes which are mutated at low frequencies in some cancers could be more frequently and significantly mutated in other cancer types. On one hand this evidence could suggest that almost all driver genes have been already identified. However, on the other hand the fact that many driver genes may occur at low frequency could suggest the possibility that most of these genes are unknown yet and needs to be identified. Notably, in preclinical studies of human samples there are many technical difficulties in identification of low frequency mutations, because of the tumor stroma contamination ⁶.

The present work has demonstrated, that, using patient derived models, it is possible to identify low frequency events which can act as drivers in carcinogenesis and play a key role in tumor maintenance. More importantly using this PDX-based pipeline we also have demonstrated that among the low frequency mutations, actionable targets could be found.

Several observations had suggested that the impact of any mutation, as well as its actionability, could be better studied in patient-derived models and in the actual tissue affected. As underlined in the introduction of this thesis, the genetics and molecular studies in cancer research, together with the traditional system of anatomic cancer classification, have greatly enlarged the knowledge in cancer. Unfortunately, in ovarian cancer, gene abnormalities other than homologous recombination defects are even more difficult to pair with an approved or investigational drug ¹⁷⁸.

In this work it has been shown that PIK3R1^{W624R} carries mutation in a domain which was not expected to be involved in oncogenesis, but nevertheless it came ut as a driver and actionable mutation in HGS-EOC, able to make tumors susceptible to the treatment with PI3K/mTOR pathway inhibitors. The PI3K/AKT/mTOR signaling pathway is one of the most frequently dysregulated ones in human cancers. More than 40 inhibitors of this pathway have reached various stages of clinical development, but only a few have been approved by FDA and EMA

¹⁷⁹. In clinical studies, inhibitors of the pathway have shown limited efficacy and/or manageability, while p110 isoform-specific inhibitors appear more promising in trials ^{110,143–148}. Altogether, the data show that, to assess the function of mutant alleles, assays in patient-derived models of the relevant cancer, such as PDXs and short-term PDTCs, are extremely important. Long-term cultures of patients' samples ¹⁸⁰ are useful for drug screening. Patient-derived tumor cells ^{89–92}, patient-derived tumor organoids (PDTOs) ^{97,98} and other 3D organotypic models ^{99,100} have been shown as a valuable model for rapid drug testing and thus for co-clinical trials, but their application may be limited by the modest take and throughput. Therefore, all the patient-derived experimental models should be considered complementary and not alternative, as every model system is imperfect but suitable in its own way with an accurate knowledge of its limitations.

REFERENCES

1. Lisio MA, Fu L, Goyeneche A, Gao ZH, Telleria C. High-grade serous ovarian cancer: Basic sciences, clinical and therapeutic standpoints. *International Journal of Molecular Sciences*. 2019;20(4). doi:10.3390/ijms20040952
2. Matulonis UA, Sood AK, Fallowfield L, Howitt BE, Sehouli J, Karlan BY. Ovarian cancer. *Nature Reviews Disease Primers*. 2016;2:1-22. doi:10.1038/nrdp.2016.61
3. Vaughan S, Coward JI, Bast RC, et al. Rethinking ovarian cancer: Recommendations for improving outcomes. *Nature Reviews Cancer*. 2011;11(10):719-725. doi:10.1038/nrc3144
4. Bell D, Berchuck A, Birrer M, et al. Integrated genomic analyses of ovarian carcinoma. *Nature*. 2011;474(7353):609-615. doi:10.1038/nature10166
5. Goringe KL, Jacobs S, Thompson ER, et al. High-resolution single nucleotide polymorphism array analysis of epithelial ovarian cancer reveals numerous microdeletions and amplifications. *Clinical Cancer Research*. 2007;13(16):4731-4739. doi:10.1158/1078-0432.CCR-07-0502
6. Garraway LA, Lander ES. Lessons from the cancer genome. *Cell*. 2013;153(1):17-37. doi:10.1016/j.cell.2013.03.002
7. Reid BM, Permuth JB, Sellers TA. Epidemiology of ovarian cancer: a review. *Cancer Biology and Medicine*. 2017;14(1):9-32. doi:10.20892/j.issn.2095-3941.2016.0084
8. Jayson GC, Kohn EC, Kitchener HC, Ledermann JA. Ovarian cancer. *The Lancet*. 2014;384(9951):1376-1388. doi:10.1016/S0140-6736(13)62146-7
9. Gao. cBioPortal for Cancer Genomics. 2013:2014-2016. https://www.cbioportal.org/study/summary?id=ov_tcga%2Cov_tcga_pub%2Cov_tcga_pan_can_atlas_2018%2Cscco_mskcc. Accessed March 18, 2020.
10. Stack MS, Fishman DA. Ovarian Cancer - Google Libri. https://books.google.it/books?id=LRqsBAAAQBAJ&pg=PT459&lpg=PT459&dq=Baiocchi+G+ovarian+cancer&source=bl&ots=cEtwdYq0--&sig=ACfU3U1rBgxRhAVr-myCPF8SFjod2x5kjQ&hl=it&sa=X&ved=2ahUKEwj4L_mqqHoAhVTasAKHaz_C7MQ6AEwBXoECAoQAQ#v=onepage&q=Baiocchi G ovarian can. Published 2002. Accessed March 17, 2020.
11. Lheureux S, Braunstein M, Oza AM. Epithelial ovarian cancer: Evolution of management in the era of precision medicine. *CA: A Cancer Journal for Clinicians*. 2019;69(4):caac.21559. doi:10.3322/caac.21559
12. Torre LA, Trabert B, DeSantis CE, et al. Ovarian cancer statistics, 2018. *CA: A Cancer Journal for Clinicians*. 2018;68(4):284-296. doi:10.3322/caac.21456
13. Wentzensen N, Poole EM, Trabert B, et al. Ovarian Cancer Risk Factors by Histologic Subtype:

An Analysis From the Ovarian Cancer Cohort Consortium. *Journal of clinical oncology : official journal of the American Society of Clinical Oncology*. 2016;34(24):2888-2898.
doi:10.1200/JCO.2016.66.8178

14. Kurman RJ, Shih IM. Molecular pathogenesis and extraovarian origin of epithelial ovarian cancer - Shifting the paradigm. *Human Pathology*. 2011;42(7):918-931.
doi:10.1016/j.humpath.2011.03.003
15. *Ovarian Cancers: Evolving Paradigms in Research and Care*. National Academies Press; 2016.
doi:10.17226/21841
16. Kurman RJ, Shih I-MM. The Origin and Pathogenesis of Epithelial Ovarian Cancer: A Proposed Unifying Theory. *The American Journal of Surgical Pathology*. 2010;34(3):433-443.
doi:10.1097/PAS.0b013e3181cf3d79
17. Kurman RJ, Shih IM. The dualistic model of ovarian carcinogenesis revisited, revised, and expanded. *American Journal of Pathology*. 2016;186(4):733-747. doi:10.1016/j.ajpath.2015.11.011
18. Piek JMJ, Verheijen RHM, Kenemans P, Massuger LF, Bulten H, Van Diest PJ. BRCA1/2-related ovarian cancers are of tubal origin: A hypothesis [1]. *Gynecologic Oncology*. 2003;90(2):491.
doi:10.1016/S0090-8258(03)00365-2
19. Piek JMJ, Van Diest PJ, Zweemer RP, et al. Dysplastic changes in prophylactically removed Fallopian tubes of women predisposed to developing ovarian cancer. *Journal of Pathology*. 2001;195(4):451-456. doi:10.1002/path.1000
20. Lee Y, Miron A, Drapkin R, et al. A candidate precursor to serous carcinoma that originates in the distal fallopian tube. *Journal of Pathology*. 2007;211(1):26-35. doi:10.1002/path.2091
21. Kindelberger DW, Lee Y, Miron A, et al. Intraepithelial carcinoma of the fimbria and pelvic serous carcinoma: Evidence for a causal relationship. *American Journal of Surgical Pathology*. 2007;31(2):161-169. doi:10.1097/01.pas.0000213335.40358.47
22. Howitt BE, Hanamornroongruang S, Lin DI, et al. Evidence for a dualistic model of high-grade serous carcinoma: BRCA mutation status, histology, and tubal intraepithelial carcinoma. *American Journal of Surgical Pathology*. 2015;39(3):287-293. doi:10.1097/PAS.0000000000000369
23. Woolas R, Jacobs I, Prys Davies A, et al. What is the true incidence of primary fallopian tube carcinoma? *International Journal of Gynecological Cancer*. 1994;4(6):384-388. doi:10.1046/j.1525-1438.1994.04060384.x
24. Reade CJ, McVey RM, Tone AA, et al. The Fallopian Tube as the Origin of High Grade Serous Ovarian Cancer: Review of a Paradigm Shift. *Journal of Obstetrics and Gynaecology Canada*. 2014;36(2):133-140. doi:10.1016/S1701-2163(15)30659-9
25. Lee Y, Medeiros F, Kindelberger D, Callahan MJ, Muto MG, Crum CP. Advances in the recognition of tubal intraepithelial carcinoma: Applications to cancer screening and the pathogenesis of ovarian cancer. *Advances in Anatomic Pathology*. 2006;13(1):1-7.
doi:10.1097/01.pap.0000201826.46978.e5

26. Roh MH, Kindelberger D, Crum CP. Serous tubal intraepithelial carcinoma and the dominant ovarian mass: Clues to serous tumor origin? *American Journal of Surgical Pathology*. 2009;33(3):376-383. doi:10.1097/PAS.0b013e3181868904
27. Callahan MJ, Crum CP, Medeiros F, et al. Primary fallopian tube malignancies in BRCA-positive women undergoing surgery for ovarian cancer risk reduction. *Journal of Clinical Oncology*. 2007;25(25):3985-3990. doi:10.1200/JCO.2007.12.2622
28. Shih IM, Kurman RJ. Ovarian Tumorigenesis: A Proposed Model Based on Morphological and Molecular Genetic Analysis. *American Journal of Pathology*. 2004;164(5):1511-1518. doi:10.1016/S0002-9440(10)63708-X
29. Kurman RJ, Carcangiu ML, Harrington CS, Young RH. WHO classification of tumours of female reproductive organs. *IARC Press (Lyon)*. 2014:170-206. <https://www.iarc.fr/news-events/iarc-publications-who-classification-of-tumours-of-female-reproductive-organs-fourth-edition/>. Accessed March 19, 2020.
30. Prat J. New insights into ovarian cancer pathology. *Annals of Oncology*. 2012;23(SUPPL. 10):x111-x117. doi:10.1093/annonc/mds300
31. Roy R, Chun J, Powell SN. BRCA1 and BRCA2: Different roles in a common pathway of genome protection. *Nature Reviews Cancer*. 2012;12(1):68-78. doi:10.1038/nrc3181
32. Budiana ING, Angelina M, Pemayun TGA. Ovarian cancer: Pathogenesis and current recommendations for prophylactic surgery. *Journal of the Turkish-German Gynecological Association*. 2019;20(1):47-54. doi:10.4274/jtgga.galenos.2018.2018.0119
33. Kuhn E, Kurman RJ, Vang R, et al. TP53 mutations in serous tubal intraepithelial carcinoma and concurrent pelvic high-grade serous carcinoma-evidence supporting the clonal relationship of the two lesions. *Journal of Pathology*. 2012;226(3):421-426. doi:10.1002/path.3023
34. Bowtell DD, Böhm S, Ahmed AA, et al. Rethinking ovarian cancer II: Reducing mortality from high-grade serous ovarian cancer. *Nature Reviews Cancer*. 2015;15(11):668-679. doi:10.1038/nrc4019
35. Call KM, Glaser T, Ito CY, et al. Isolation and characterization of a zinc finger polypeptide gene at the human chromosome 11 Wilms' tumor locus. *Cell*. 1990;60(3):509-520. doi:10.1016/0092-8674(90)90601-A
36. Manocha A, Jain S. WT1 in astrocytomas: Comprehensive evaluation of immunohistochemical expression and its potential utility in different histological grades. *Indian Journal of Cancer*. 2019;56(3):197-201. doi:10.4103/ijc.IJC_51_18
37. WT1 transcription factor [Homo sapiens (human)] - Gene - NCBI. <https://www.ncbi.nlm.nih.gov/gene/7490>. Accessed March 21, 2020.
38. Chu P, Wu E, Weiss LM. Cytokeratin 7 and Cytokeratin 20 expression in epithelial neoplasms: A survey of 435 cases. *Modern Pathology*. 2000;13(9):962-972. doi:10.1038/modpathol.3880175
39. Li X, Beihua K. PAX8 is a novel marker for differentiating between various types of tumor,

particularly ovarian epithelial carcinomas (review). *Oncology Letters*. 2013;5(3):735-738. doi:10.3892/ol.2013.1121

40. Nonaka D, Chiriboga L, Soslow RA. Expression of Pax8 as a useful marker in distinguishing ovarian carcinomas from mammary carcinomas. *American Journal of Surgical Pathology*. 2008;32(10):1566-1571. doi:10.1097/PAS.0b013e31816d71ad
41. Yoon N, Yoon G, Park CK, Kim HS. Stromal p16 expression is significantly increased in malignant ovarian neoplasms. *Oncotarget*. 2016;7(40):64665-64673. doi:10.18632/oncotarget.11660
42. Sallum, Andrade L, Ramalho S, et al. WT1, p53 and p16 expression in the diagnosis of low- and highgrade serous ovarian carcinomas and their relation to prognosis. *Oncotarget*. 2018;9(22):15818-15827. doi:10.18632/oncotarget.24530
43. O'Neill CJ, McBride HA, Connolly LE, Deavers MT, Malpica A, McCluggage WG. High-grade ovarian serous carcinoma exhibits significantly higher p16 expression than low-grade serous carcinoma and serous borderline tumour. *Histopathology*. 2007;50(6):773-779. doi:10.1111/j.1365-2559.2007.02682.x
44. Beirne JP, Mcart DG, James JA, Salto-Tellez M, Maxwell P, McCluggage WG. p16 as a prognostic indicator in ovarian/tubal high-grade serous carcinoma. *Histopathology*. 2016;68(4):615-618. doi:10.1111/his.12777
45. Cai Y, Zhai JJ, Feng BB, Duan XZ, He XJ. Expression of glucose transporter protein 1 and p63 in serous ovarian tumor. *Journal of Obstetrics and Gynaecology Research*. 2014;40(7):1925-1930. doi:10.1111/jog.12447
46. Mirsadraei L, Hodkoff A, Jones K, et al. Serous carcinoma mimicking primary urothelial carcinoma on clinical evaluation and pathology a potential diagnostic pitfall. *Archives of Pathology and Laboratory Medicine*. 2018;142(2):168-177. doi:10.5858/arpa.2017-0004-OA
47. McDermott JE, Arshad OA, Petyuk VA, et al. Proteogenomic Characterization of Ovarian HGSC Implicates Mitotic Kinases, Replication Stress in Observed Chromosomal Instability. *Cell Reports Medicine*. 2020:100004. doi:10.1016/j.xcrm.2020.100004
48. Hatano Y, Hatano K, Tamada M, et al. A comprehensive review of ovarian serous carcinoma. *Advances in Anatomic Pathology*. 2019;26(5):329-339. doi:10.1097/PAP.0000000000000243
49. Ahmed N, Abubaker K, Findlay J, Quinn M. Cancerous ovarian stem cells: Obscure targets for therapy but relevant to chemoresistance. *Journal of Cellular Biochemistry*. 2013;114(1):21-34. doi:10.1002/jcb.24317
50. Kuhn E, Wang TL, Doberstein K, et al. CCNE1 amplification and centrosome number abnormality in serous tubal intraepithelial carcinoma: Further evidence supporting its role as a precursor of ovarian high-grade serous carcinoma. *Modern Pathology*. 2016;29(10):1254-1261. doi:10.1038/modpathol.2016.101
51. Marquez RT, Baggerly KA, Patterson AP, et al. Patterns of gene expression in different histotypes of epithelial ovarian cancer correlate with those in normal fallopian tube,

- endometrium, and colon. *Clinical Cancer Research*. 2005;11(17):6116-6126. doi:10.1158/1078-0432.CCR-04-2509
52. Chang MT, Bhattarai TS, Schram AM, et al. Accelerating discovery of functional mutant alleles in cancer. *Cancer Discovery*. 2018;8(2):174-183. doi:10.1158/2159-8290.CD-17-0321
 53. Gadducci A, Guarneri V, Peccatori FA, et al. Current strategies for the targeted treatment of high-grade serous epithelial ovarian cancer and relevance of BRCA mutational status. *Journal of Ovarian Research*. 2019;12(1). doi:10.1186/s13048-019-0484-6
 54. Perren TJ, Swart AM, Pfisterer J, et al. A Phase 3 Trial of Bevacizumab in Ovarian Cancer. *New England Journal of Medicine*. 2011;365(26):2484-2496. doi:10.1056/nejmoa1103799
 55. Burger RA, Brady MF, Bookman MA, et al. Incorporation of bevacizumab in the primary treatment of ovarian cancer. *Obstetrical and Gynecological Survey*. 2012;67(5):289-290. doi:10.1097/OGX.0b013e3182547170
 56. Freimund AE, Beach JA, Christie EL, Bowtell DDL. Mechanisms of Drug Resistance in High-Grade Serous Ovarian Cancer. *Hematology/Oncology Clinics of North America*. 2018;32(6):983-996. doi:10.1016/j.hoc.2018.07.007
 57. Icon T, Collaborators AGO. Paclitaxel plus platinum-based chemotherapy versus conventional platinum-based chemotherapy in women with relapsed ovarian cancer: The ICON4/AGO-OVAR-2.2 trial. *Lancet*. 2003;361(9375):2099-2106. doi:10.1016/S0140-6736(03)13718-X
 58. Raja FA, Counsell N, Colombo N, et al. Platinum versus platinum-combination chemotherapy in platinum-sensitive recurrent ovarian cancer: A meta-analysis using individual patient data. *Annals of Oncology*. 2013;24(12):3028-3034. doi:10.1093/annonc/mdt406
 59. Pfisterer J, Plante M, Vergote I, et al. Gemcitabine plus carboplatin compared with carboplatin in patients with platinum-sensitive recurrent ovarian cancer: An intergroup trial of the AGO-OVAR, the NCIC CTG, and the EORTC GCG. *Journal of Clinical Oncology*. 2006;24(29):4699-4707. doi:10.1200/JCO.2006.06.0913
 60. Pujade-Lauraine E, Wagner U, Aavall-Lundqvist E, et al. Pegylated liposomal doxorubicin and carboplatin compared with paclitaxel and carboplatin for patients with platinum-sensitive ovarian cancer in late relapse. *Journal of Clinical Oncology*. 2010;28(20):3323-3329. doi:10.1200/JCO.2009.25.7519
 61. Salomon-Perzyński A, Salomon-Perzyńska M, Michalski B, Skrzypulec-Plinta V. High-grade serous ovarian cancer: the clone wars. *Archives of Gynecology and Obstetrics*. 2017;295(3):569-576. doi:10.1007/s00404-017-4292-1
 62. Sottoriva A, Spiteri I, Piccirillo SGM, et al. Intratumor heterogeneity in human glioblastoma reflects cancer evolutionary dynamics. *Proceedings of the National Academy of Sciences of the United States of America*. 2013;110(10):4009-4014. doi:10.1073/pnas.1219747110
 63. Williams MJ, Werner B, Barnes CP, Graham TA, Sottoriva A. Identification of neutral tumor evolution across cancer types. *Nature Genetics*. 2016;48(3):238-244. doi:10.1038/ng.3489

64. Taylor KN, Eskander RN. PARP inhibitors in epithelial ovarian cancer. *Recent Patents on Anti-Cancer Drug Discovery*. 2017;13:145-158. doi:10.2174/1574892813666171204094822
65. Kaelin WG. The concept of synthetic lethality in the context of anticancer therapy. *Nature Reviews Cancer*. 2005;5(9):689-698. doi:10.1038/nrc1691
66. Lord CJ, Ashworth A. PARP inhibitors: Synthetic lethality in the clinic. *Science*. 2017;355(6330):1152-1158. doi:10.1126/science.aam7344
67. Pujade-Lauraine E, Ledermann JA, Selle F, et al. Olaparib tablets as maintenance therapy in patients with platinum-sensitive, relapsed ovarian cancer and a BRCA1/2 mutation (SOLO2/ENGOT-Ov21): a double-blind, randomised, placebo-controlled, phase 3 trial. *The Lancet Oncology*. 2017;18(9):1274-1284. doi:10.1016/S1470-2045(17)30469-2
68. Kaye SB, Lubinski J, Matulonis U, et al. Phase II, open-label, randomized, multicenter study comparing the efficacy and safety of olaparib, a poly (ADP-ribose) polymerase inhibitor, and pegylated liposomal doxorubicin in patients with BRCA1 or BRCA2 mutations and recurrent ovarian cancer. *Journal of Clinical Oncology*. 2012;30(4):372-379. doi:10.1200/JCO.2011.36.9215
69. Ledermann J, Harter P, Gourley C, et al. Olaparib maintenance therapy in patients with platinum-sensitive relapsed serous ovarian cancer: A preplanned retrospective analysis of outcomes by BRCA status in a randomised phase 2 trial. *The Lancet Oncology*. 2014;15(8):852-861. doi:10.1016/S1470-2045(14)70228-1
70. Ledermann J, Harter P, Gourley C, et al. Olaparib Maintenance Therapy in Platinum-Sensitive Relapsed Ovarian Cancer. *New England Journal of Medicine*. 2012;366(15):1382-1392. doi:10.1056/nejmoa1105535
71. Oza AM, Cibula D, Benzaquen AO, et al. Olaparib combined with chemotherapy for recurrent platinum-sensitive ovarian cancer: A randomised phase 2 trial. *The Lancet Oncology*. 2015;16(1):87-97. doi:10.1016/S1470-2045(14)71135-0
72. Coleman RL, Oza AM, Lorusso D, et al. Rucaparib maintenance treatment for recurrent ovarian carcinoma after response to platinum therapy (ARIEL3): a randomised, double-blind, placebo-controlled, phase 3 trial. *The Lancet*. 2017;390(10106):1949-1961. doi:10.1016/S0140-6736(17)32440-6
73. Mirza MR, Monk BJ, Herrstedt J, et al. Niraparib maintenance therapy in platinum-sensitive, recurrent ovarian cancer. *New England Journal of Medicine*. 2016;375(22):2154-2164. doi:10.1056/NEJMoa1611310
74. Norquist B, Wurz KA, Pennil CC, et al. Secondary somatic mutations restoring BRCA1/2 predict chemotherapy resistance in hereditary ovarian carcinomas. *Journal of Clinical Oncology*. 2011;29(22):3008-3015. doi:10.1200/JCO.2010.34.2980
75. Tothill RW, Tinker A V., George J, et al. Novel molecular subtypes of serous and endometrioid ovarian cancer linked to clinical outcome. *Clinical Cancer Research*. 2008;14(16):5198-5208. doi:10.1158/1078-0432.CCR-08-0196

76. Zhang AW, McPherson A, Milne K, et al. Interfaces of Malignant and Immunologic Clonal Dynamics in Ovarian Cancer. *Cell*. 2018;173(7):1755-1769.e22. doi:10.1016/j.cell.2018.03.073
77. Thorsson V, Gibbs DL, Brown SD, et al. The Immune Landscape of Cancer. *Immunity*. 2018;48(4):812-830.e14. doi:10.1016/j.immuni.2018.03.023
78. Ledermann JA. Front-line therapy of advanced ovarian cancer: New approaches. *Annals of Oncology*. 2017;28(Supplement 8):viii46-viii50. doi:10.1093/annonc/mdx452
79. Maru Y, Hippo Y. Current Status of Patient-Derived Ovarian Cancer Models. *Cells*. 2019;8(5):505. doi:10.3390/cells8050505
80. Domcke S, Sinha R, Levine DA, Sander C, Schultz N. Evaluating cell lines as tumour models by comparison of genomic profiles. *Nature Communications*. 2013;4. doi:10.1038/ncomms3126
81. Beaufort CM, Helmijr JCA, Piskorz AM, et al. Ovarian cancer cell line panel (OCCP): Clinical importance of in vitro morphological subtypes. *PLoS ONE*. 2014;9(9):103988. doi:10.1371/journal.pone.0103988
82. Coscia F, Watters KM, Curtis M, et al. Integrative proteomic profiling of ovarian cancer cell lines reveals precursor cell associated proteins and functional status. *Nature Communications*. 2016;7. doi:10.1038/ncomms12645
83. Dong R, Qiang W, Guo H, et al. Histologic and molecular analysis of patient derived xenografts of high-grade serous ovarian carcinoma. *Journal of Hematology and Oncology*. 2016;9(1). doi:10.1186/s13045-016-0318-6
84. Liu JF, Palakurthi S, Zeng Q, et al. Establishment of patient-derived tumor xenograft models of epithelial ovarian cancer for preclinical evaluation of novel therapeutics. *Clinical Cancer Research*. 2017;23(5):1263-1273. doi:10.1158/1078-0432.CCR-16-1237
85. Byrne AT, Alférez DG, Amant F, et al. Interrogating open issues in cancer precision medicine with patient-derived xenografts. *Nature Reviews Cancer*. 2017;17(4):254-268. doi:10.1038/nrc.2016.140
86. Guenot D, Guérin E, Aguilon-Romain S, et al. Primary tumour genetic alterations and intra-tumoral heterogeneity are maintained in xenografts of human colon cancers showing chromosome instability. *Journal of Pathology*. 2006;208(5):643-652. doi:10.1002/path.1936
87. Cho YB, Hong HK, Choi Y La, et al. Colorectal cancer patient-derived xenografted tumors maintain characteristic features of the original tumors. *Journal of Surgical Research*. 2014;187(2):502-509. doi:10.1016/j.jss.2013.11.010
88. Liu Y, Chanana P, Davila JI, et al. Gene expression differences between matched pairs of ovarian cancer patient tumors and patient-derived xenografts. *Scientific Reports*. 2019;9(1). doi:10.1038/s41598-019-42680-2
89. Mukhopadhyay A, Elattar A, Cerbinskaite A, et al. Development of a functional assay for homologous recombination status in primary cultures of epithelial ovarian tumor and correlation with sensitivity to poly(ADP-ribose) polymerase inhibitors. *Clinical Cancer Research*.

2010;16(8):2344-2351. doi:10.1158/1078-0432.CCR-09-2758

90. O'Donnell RL, McCormick A, Mukhopadhyay A, et al. The use of ovarian cancer cells from patients undergoing surgery to generate primary cultures capable of undergoing functional analysis. *PLoS ONE*. 2014;9(3). doi:10.1371/journal.pone.0090604
91. Dunfield LD, Shepherd TG, Nachtigal MW. Primary culture and mRNA analysis of human ovarian cells. *Biological Procedures Online*. 2002;4(1):55-61. doi:10.1251/bpo34
92. Thériault BL, Portelance L, Mes-Masson AM, Nachtigal MW. Establishment of primary cultures from ovarian tumor tissue and ascites fluid. *Methods in Molecular Biology*. 2013;1049:323-336. doi:10.1007/978-1-62703-547-7_24
93. Kar R, Chawla D, Gupta B, Mehndiratta M, Wadhwa N, Agarwal R. Establishment of primary cell culture from ascitic fluid and solid tumor obtained from epithelial ovarian carcinoma patients. *International Journal of Gynecological Cancer*. 2017;27(9):2000-2005. doi:10.1097/IGC.0000000000001087
94. D'Ambrosio C, Erriquez J, Arigoni M, et al. PIK3R1W624R Is an Actionable Mutation in High Grade Serous Ovarian Carcinoma. *Cells*. 2020;9(2):442. doi:10.3390/cells9020442
95. Shield K, Ackland ML, Ahmed N, Rice GE. Multicellular spheroids in ovarian cancer metastases: Biology and pathology. *Gynecologic Oncology*. 2009;113(1):143-148. doi:10.1016/j.ygyno.2008.11.032
96. Gao Q, Yang Z, Xu S, et al. Heterotypic CAF-tumor spheroids promote early peritoneal metastasis of ovarian cancer. *Journal of Experimental Medicine*. 2019;216(3):688-703. doi:10.1084/jem.20180765
97. Hill SJ, Decker B, Roberts EA, et al. Prediction of DNA repair inhibitor response in short-term patient-derived ovarian cancer organoids. *Cancer Discovery*. 2018;8(11):1404-1421. doi:10.1158/2159-8290.CD-18-0474
98. Kopper O, de Witte CJ, Löhmußaar K, et al. An organoid platform for ovarian cancer captures intra- and interpatient heterogeneity. *Nature Medicine*. 2019;25(5):838-849. doi:10.1038/s41591-019-0422-6
99. Aref AR, Campisi M, Ivanova E, et al. 3D microfluidic: Ex vivo culture of organotypic tumor spheroids to model immune checkpoint blockade. *Lab on a Chip*. 2018;18(20):3129-3143. doi:10.1039/c8lc00322j
100. Deng J, Wang ES, Jenkins RW, et al. CDK4/6 inhibition augments antitumor immunity by enhancing T-cell activation. *Cancer Discovery*. 2018;8(2):216-233. doi:10.1158/2159-8290.CD-17-0915
101. Carpenter CL, Cantley LC. Phosphoinositide 3-kinase and the regulation of cell growth. *Biochimica et Biophysica Acta - Reviews on Cancer*. 1996;1288(1). doi:10.1016/0304-419X(96)00018-2
102. Carpenter C, Cantley L. Phosphoinositide kinases and Lewis C Cantley. *Current Opinion in Cell Biology*. 1996;8(2):153-158.

103. Thorpe LM, Yuzugullu H, Zhao JJ. PI3K in cancer: Divergent roles of isoforms, modes of activation and therapeutic targeting. *Nature Reviews Cancer*. 2015;15(1):7-24. doi:10.1038/nrc3860
104. CANTLEY LC, WHITMAN M, CHAHWALA S, et al. Oncogenes and Phosphatidylinositol Turnover. *Annals of the New York Academy of Sciences*. 1986;488(1):481-490. doi:10.1111/j.1749-6632.1986.tb54426.x
105. Fruman DA, Chiu H, Hopkins BD, Bagrodia S, Cantley LC, Abraham RT. The PI3K Pathway in Human Disease. *Cell*. 2017;170(4):605-635. doi:10.1016/j.cell.2017.07.029
106. Cantley LC. The phosphoinositide 3-kinase pathway. *Science*. 2002;296(5573):1655-1657. doi:10.1126/science.296.5573.1655
107. Arafeh R, Samuels Y. PIK3CA in cancer: The past 30 years. *Seminars in Cancer Biology*. 2019;59(November 2018):36-49. doi:10.1016/j.semcan.2019.02.002
108. Liu P, Cheng H, Roberts TM, Zhao JJ. Targeting the phosphoinositide 3-kinase pathway in cancer. *Nature Reviews Drug Discovery*. 2009;8(8):627-644. doi:10.1038/nrd2926
109. Martini M, Ciralo E, Gulluni F, Hirsch E. Targeting PI3K in cancer: Any good news? *Frontiers in Oncology*. 2013;3 MAY:108. doi:10.3389/fonc.2013.00108
110. Dienstmann R, Rodon J, Serra V, Tabernero J. Picking the point of inhibition: A comparative review of PI3K/AKT/mTOR pathway inhibitors. *Molecular Cancer Therapeutics*. 2014;13(5):1021-1031. doi:10.1158/1535-7163.MCT-13-0639
111. Gulluni F, De Santis MC, Margaria JP, Martini M, Hirsch E. Class II PI3K Functions in Cell Biology and Disease. *Trends in Cell Biology*. 2019;29(4):339-359. doi:10.1016/j.tcb.2019.01.001
112. Cheung LW, Mills GB. Targeting therapeutic liabilities engendered by PIK3R1 mutations for cancer treatment. *Pharmacogenomics*. 2016;17(3):297-307. doi:10.2217/pgs.15.174
113. Carnero A, Blanco-Aparicio C, Renner O, Link W, Leal J. The PTEN/PI3K/AKT Signalling Pathway in Cancer, Therapeutic Implications. *Current Cancer Drug Targets*. 2008;8(3):187-198. doi:10.2174/156800908784293659
114. Luo J, Cantley LC. The negative regulation of phosphoinositide 3-kinase signaling by p85 and its implication in cancer. *Cell Cycle*. 2005;4(10):1309-1312. doi:10.4161/cc.4.10.2062
115. Noorolyai S, Shajari N, Baghbani E, Sadreddini S, Baradaran B. The relation between PI3K/AKT signalling pathway and cancer. *Gene*. 2019;698:120-128. doi:10.1016/j.gene.2019.02.076
116. Martini M, De Santis MC, Braccini L, Gulluni F, Hirsch E. PI3K/AKT signaling pathway and cancer: An updated review. *Annals of Medicine*. 2014;46(6):372-383. doi:10.3109/07853890.2014.912836
117. Kriplani N, Hermida MA, Brown ER, Leslie NR. Class I PI 3-kinases: Function and evolution. *Advances in Biological Regulation*. 2015;59:53-64. doi:10.1016/j.jbior.2015.05.002
118. Engelman JA. Targeting PI3K signalling in cancer: Opportunities, challenges and limitations. *Nature Reviews Cancer*. 2009;9(8):550-562. doi:10.1038/nrc2664

119. Samuels Y, Wang Z, Bardelli A, et al. High Frequency of Mutations of the PIK3CA Gene in Human Cancers. *Science*. 2004;304(5670):554. doi:10.1126/science.1096502
120. Hennessy BT, Smith DL, Ram PT, Lu Y, Mills GB. Exploiting the PI3K/AKT pathway for cancer drug discovery. *Nature Reviews Drug Discovery*. 2005;4(12):988-1004. doi:10.1038/nrd1902
121. Kandoth C, McLellan MD, Vandin F, et al. Mutational landscape and significance across 12 major cancer types. *Nature*. 2013;502(7471):333-339. doi:10.1038/nature12634
122. PIK3CA Gene - Somatic Mutations in Cancer. <https://cancer.sanger.ac.uk/cosmic/gene/analysis?ln=PIK3CA>. Published 2020. Accessed April 7, 2020.
123. Leary A, Auclin E, Pautier P, Lhomme C. The PI3K/Akt/mTOR Pathway in Ovarian Cancer: Biological Rationale and Therapeutic Opportunities. In: *Ovarian Cancer - A Clinical and Translational Update*. InTech; 2013. doi:10.5772/54170
124. Campbell IG, Russell SE, Choong DYH, et al. Mutation of the PIK3CA gene in ovarian and breast cancer. *Cancer Research*. 2004;64(21):7678-7681. doi:10.1158/0008-5472.CAN-04-2933
125. PIK3R1 Gene - Somatic Mutations in Cancer. <https://cancer.sanger.ac.uk/cosmic/gene/analysis?ln=PIK3R1>. Published 2020. Accessed April 7, 2020.
126. Cheung LWT, Walkiewicz KW, Besong TM, et al. Regulation of the PI3K pathway through a p85 α monomer-homodimer equilibrium. *eLife*. 2015;4(JULY 2015). doi:10.7554/eLife.06866
127. Luo J, Cantley LC. The negative regulation of phosphoinositide 3-kinase signaling by p85 and its implication in cancer. *Cell Cycle*. 2005;4(10):1309-1312. doi:10.4161/cc.4.10.2062
128. Cheung LWT, Hennessy BT, Li J, et al. High frequency of PIK3R1 and PIK3R2 mutations in endometrial cancer elucidates a novel mechanism for regulation of PTEN protein stability. *Cancer Discovery*. 2011;1(2):170-185. doi:10.1158/2159-8290.CD-11-0039
129. Cheung LWT, Yu S, Zhang D, et al. Naturally occurring neomorphic PIK3R1 mutations activate the MAPK pathway, dictating therapeutic response to MAPK pathway inhibitors. *Cancer Cell*. 2014;26(4):479-494. doi:10.1016/j.ccell.2014.08.017
130. Costa C, Engelman JA. The Double Life of p85. *Cancer Cell*. 2014;26(4):445-447. doi:10.1016/j.ccell.2014.09.011
131. Chagpar RB, Links PH, Pastor MC, et al. Direct positive regulation of PTEN by the p85 subunit of phosphatidylinositol 3-kinase. *Proceedings of the National Academy of Sciences of the United States of America*. 2010;107(12):5471-5476. doi:10.1073/pnas.0908899107
132. cBioPortal for Cancer Genomics: PIK3R1 in pediatric-cancers and 2 other studies. https://www.cbioportal.org/results/cancerTypesSummary?Action=Submit&RPPA_SCORE_THRESHOLD=2.0&Z_SCORE_THRESHOLD=2.0&cancer_study_list=msk_impact_2017%2Cnsclc_tcg_a_broad_2016%2Cmixed_pipseq_2017&case_set_id=all&data_priority=0&gene_list=PIK3R1&geneset_list=&profileFilter=0&tab_index=tab_visualize. Accessed April 7, 2020.

133. Mabuchi S, Kuroda H, Takahashi R, Sasano T. The PI3K/AKT/mTOR pathway as a therapeutic target in ovarian cancer. *Gynecologic Oncology*. 2015;137(1):173-179. doi:10.1016/j.ygyno.2015.02.003
134. Huang X, Liu G, Guo J, Su ZQ. The PI3K/AKT pathway in obesity and type 2 diabetes. *International Journal of Biological Sciences*. 2018;14(11):1483-1496. doi:10.7150/ijbs.27173
135. Madsen RR, Vanhaesebroeck B, Semple RK. Cancer-Associated PIK3CA Mutations in Overgrowth Disorders. *Trends in Molecular Medicine*. 2018;24(10):856-870. doi:10.1016/j.molmed.2018.08.003
136. Keppler-Noreuil KM, Rios JJ, Parker VER, et al. PIK3CA-related overgrowth spectrum (PROS): Diagnostic and testing eligibility criteria, differential diagnosis, and evaluation. *American Journal of Medical Genetics, Part A*. 2015;167(2):287-295. doi:10.1002/ajmg.a.36836
137. Martinez-Lopez A, Blasco-Morente G, Perez-Lopez I, et al. CLOVES syndrome: review of a PIK3CA-related overgrowth spectrum (PROS). *Clinical Genetics*. 2017;91(1):14-21. doi:10.1111/cge.12832
138. Avila M, Dymont DA, Sagen J V, et al. Clinical reappraisal of SHORT syndrome with PIK3R1 mutations: Toward recommendation for molecular testing and management. *Clinical Genetics*. 2016;89(4):501-506. doi:10.1111/cge.12688
139. Yang J, Nie J, Ma X, Wei Y, Peng Y, Wei X. Targeting PI3K in cancer: Mechanisms and advances in clinical trials. *Molecular Cancer*. 2019;18(1):1-28. doi:10.1186/s12943-019-0954-x
140. PI3K inhibitors - List Results - ClinicalTrials.gov. <https://clinicaltrials.gov/ct2/results?term=PI3K+inhibitors&Search=Search>. Accessed April 7, 2020.
141. Maira SM, Pecchi S, Huang A, et al. Identification and characterization of NVP-BKM120, an orally available pan-class I PI3-kinase inhibitor. *Molecular Cancer Therapeutics*. 2012;11(2):317-328. doi:10.1158/1535-7163.MCT-11-0474
142. Burger MT, Pecchi S, Wagman A, et al. Identification of NVP-BKM120 as a potent, selective, orally bioavailable class I PI3 kinase inhibitor for treating cancer. *ACS Medicinal Chemistry Letters*. 2011;2(10):774-779. doi:10.1021/ml200156t
143. André F, Ciruelos E, Rubovszky G, et al. Alpelisib for PIK3CA -Mutated, Hormone Receptor-Positive Advanced Breast Cancer. *New England Journal of Medicine*. 2019;380(20):1929-1940. doi:10.1056/nejmoa1813904
144. Markham A. Alpelisib: First Global Approval. *Drugs*. 2019;79(11):1249-1253. doi:10.1007/s40265-019-01161-6
145. Stirrups R. Alpelisib plus fulvestrant for PIK3CA-mutated breast cancer. *The Lancet Oncology*. 2019;20(7):e347. doi:10.1016/S1470-2045(19)30372-9
146. Gobin B, Huin MB, Lamoureux F, et al. BYL719, a new α -specific PI3K inhibitor: Single administration and in combination with conventional chemotherapy for the treatment of

- osteosarcoma. *International Journal of Cancer*. 2015;136(4):784-796. doi:10.1002/ijc.29040
147. Kim HJ, Lee SY, Oh SC. The inositide signaling pathway as a target for treating gastric cancer and colorectal cancer. *Frontiers in Physiology*. 2016;7(MAY). doi:10.3389/fphys.2016.00168
 148. Mateo J, Ganji G, Lemech C, et al. A first-time-in-human study of GSK2636771, a phosphoinositide 3 kinase beta-selective inhibitor, in patients with advanced solid tumors. *Clinical Cancer Research*. 2017;23(19):5981-5992. doi:10.1158/1078-0432.CCR-17-0725
 149. Baralis E, Bertotti A, Fiori A, Grand A. LAS: a software platform to support oncological data management. *Journal of medical systems*. 2012;36 Suppl 1(1):81-90. doi:10.1007/s10916-012-9891-6
 150. Kononen J, Bubendorf L, Kallioniemi A, et al. Tissue microarrays for high-throughput molecular profiling of tumor specimens. *Nature Medicine*. 1998;4(7):844-847. doi:10.1038/nm0798-844
 151. Sapino A, Marchiò C, Senetta R, et al. Routine assessment of prognostic factors in breast cancer using a multicore tissue microarray procedure. *Virchows Archiv*. 2006;449(3):288-296. doi:10.1007/s00428-006-0233-2
 152. Butler KA, Hou X, Becker MA, et al. Prevention of Human Lymphoproliferative Tumor Formation in Ovarian Cancer Patient-Derived Xenografts. *Neoplasia (United States)*. 2017;19(8):628-636. doi:10.1016/j.neo.2017.04.007
 153. Clark NA, Hafner M, Kouril M, et al. GRcalculator: an online tool for calculating and mining dose-response data. *BMC cancer*. 2017;17(1):698. doi:10.1186/s12885-017-3689-3
 154. Hafner M, Niepel M, Chung M, Sorger PK. Growth rate inhibition metrics correct for confounders in measuring sensitivity to cancer drugs. *Nature Methods*. 2016;13(6):521-527. doi:10.1038/nmeth.3853
 155. Meehan TF, Conte N, Goldstein T, et al. PDX-MI: Minimal information for patient-derived tumor xenograft models. *Cancer Research*. 2017;77(21):e62-e66. doi:10.1158/0008-5472.CAN-17-0582
 156. Hancock JM, Zvelebil MJ, Griffith M, Griffith OL. COSMIC (Catalogue of Somatic Mutations in Cancer). In: *Dictionary of Bioinformatics and Computational Biology*. ; 2004. doi:10.1002/9780471650126.dob0851
 157. TCGA. Welcome to the Pan-Cancer Atlas. <https://www.cell.com/pb-assets/consortium/pancanceratlas/pancani3/index.html>. Published 2020. Accessed May 12, 2020.
 158. Nawy T. A pan-cancer atlas. *Nature methods*. 2018;15(6):407. doi:10.1038/s41592-018-0020-4
 159. Hassan MS, Shaalan AA, Dessouky MI, Abdelnaiem AE, ElHefnawi M. Evaluation of computational techniques for predicting non-synonymous single nucleotide variants pathogenicity. *Genomics*. 2019;111(4):869-882. doi:10.1016/j.ygeno.2018.05.013
 160. Choi Y, Chan AP. PROVEAN web server: A tool to predict the functional effect of amino acid substitutions and indels. *Bioinformatics*. 2015;31(16):2745-2747.

doi:10.1093/bioinformatics/btv195

161. Sim NL, Kumar P, Hu J, Henikoff S, Schneider G, Ng PC. SIFT web server: Predicting effects of amino acid substitutions on proteins. *Nucleic Acids Research*. 2012;40(W1). doi:10.1093/nar/gks539
162. Shihab HA, Rogers MF, Gough J, et al. An integrative approach to predicting the functional effects of non-coding and coding sequence variation. *Bioinformatics*. 2015;31(10):1536-1543. doi:10.1093/bioinformatics/btv009
163. Wagner AH, Coffman AC, Ainscough BJ, et al. DGIdb 2.0: Mining clinically relevant drug-gene interactions. *Nucleic Acids Research*. 2016;44(D1):D1036-D1044. doi:10.1093/nar/gkv1165
164. Erriquez J, Olivero M, Mittica G, et al. Xenopatients show the need for precision medicine approach to chemotherapy in ovarian cancer. *Oncotarget*. 2016;7(18):26181-26191. doi:10.18632/oncotarget.8325
165. Hyman DM, Taylor BS, Baselga J. Implementing Genome-Driven Oncology. *Cell*. 2017;168(4):584-599. doi:10.1016/j.cell.2016.12.015
166. Koul D, Fu J, Shen R, et al. Antitumor activity of NVP-BKM120 - A selective pan class I PI3 kinase inhibitor showed differential forms of cell death based on p53 status of glioma cells. *Clinical Cancer Research*. 2012;18(1):184-195. doi:10.1158/1078-0432.CCR-11-1558
167. Brachmann SM, Kleylein-Sohn J, Gaulis S, et al. Characterization of the mechanism of action of the pan class i PI3K inhibitor NVP-BKM120 across a broad range of concentrations. *Molecular Cancer Therapeutics*. 2012;11(8):1747-1757. doi:10.1158/1535-7163.MCT-11-1021
168. Allegretti M, Ricciardi MR, Licchetta R, et al. The pan-class i phosphatidylinositol-3 kinase inhibitor NVP-BKM120 demonstrates anti-leukemic activity in acute myeloid leukemia. *Scientific Reports*. 2015;5. doi:10.1038/srep18137
169. Krepler C, Xiao M, Sproesser K, et al. Personalized preclinical trials in BRAF Inhibitor-resistant patient-derived xenograft models identify second-line combination therapies. *Clinical Cancer Research*. 2016;22(7):1592-1602. doi:10.1158/1078-0432.CCR-15-1762
170. Bailey MH, Tokheim C, Porta-Pardo E, et al. Comprehensive Characterization of Cancer Driver Genes and Mutations. *Cell*. 2018;174(4):1034-1035. doi:10.1016/j.cell.2018.07.034
171. Zhang X, Vadas O, Perisic O, et al. Structure of Lipid Kinase p110 β /p85 β Elucidates an Unusual SH2-Domain-Mediated Inhibitory Mechanism. *Molecular Cell*. 2011;41(5):567-578. doi:10.1016/j.molcel.2011.01.026
172. Giannakis M, Mu XJ, Shukla SA, et al. Genomic Correlates of Immune-Cell Infiltrates in Colorectal. *Cell Reports*. 2016;15(4):857-865. doi:10.1016/j.celrep.2016.10.009
173. Campbell JD, Alexandrov A, Kim J, et al. Distinct patterns of somatic genome alterations in lung adenocarcinomas and squamous cell carcinomas. *Nature Genetics*. 2016;48(6):607-616. doi:10.1038/ng.3564

174. Wang K, Yuen ST, Xu J, et al. Whole-genome sequencing and comprehensive molecular profiling identify new driver mutations in gastric cancer. *Nature Genetics*. 2014;46(6):573-582. doi:10.1038/ng.2983
175. Soumerai TE, Donoghue MTA, Bandlamudi C, et al. Clinical utility of prospective molecular characterization in advanced endometrial cancer. *Clinical Cancer Research*. 2018;24(23):5939-5947. doi:10.1158/1078-0432.CCR-18-0412
176. TumorPortal. <http://www.tumorportal.org/>. Accessed May 15, 2020.
177. Jaiswal BS, Janakiraman V, Kljavin NM, et al. Somatic Mutations in p85 α Promote Tumorigenesis through Class IA PI3K Activation. *Cancer Cell*. 2009;16(6):463-474. doi:10.1016/j.ccr.2009.10.016
178. Barroilhet L, Matulonis U. The NCI-MATCH trial and precision medicine in gynecologic cancers. *Gynecologic Oncology*. 2018;148(3):585-590. doi:10.1016/j.ygyno.2018.01.008
179. Hanker AB, Kaklamani V, Arteaga CL. Challenges for the clinical development of PI3K inhibitors: Strategies to improve their impact in solid tumors. *Cancer Discovery*. 2019;9(4):482-491. doi:10.1158/2159-8290.CD-18-1175
180. Crystal AS, Shaw AT, Sequist L V., et al. Patient-derived models of acquired resistance can identify effective drug combinations for cancer. *Science*. 2014;346(6216):1480-1486. doi:10.1126/science.1254721